Neuromagnetic Decomposition of Social Interaction

Inauguraldissertation zur Erlangung des Doktorgrades der Humanwissenschaftlichen Fakultät der Universität zu Köln nach der Promotionsordnung vom 10.05.2010 vorgelegt von

Denis-Alexander Engemann

aus

Kiel

September 2014

1. Gutachter Prof. Dr. Gary Bente

Department Psychologie
Universität Zu Köln
Richard-Strauss-Straße 2
50931, Köln

2. Gutachter Prof. Dr. Dr. Kai Vogeley

Abteilung für Psychiatrie und Psychotherapie
Universitätsklinikum Köln
Zentrum fir Neurologie und Psychiatrie
50924, Köln

Acknowledgement

This thesis would not have been possible without the enduring and patient support of my colleagues, my friends, and my family. First and foremost, I am deeply obliged to my thesis advisors Prof. Dr. Dr. Kai Vogeley and Prof. Dr. Gary Bente for the trust and the strong support that I received during this demanding and audacious dissertation project. I am also very grateful to Prof. Dr. Gereon Fink and Prof. Dr. Peter Weiss-Blankenhorn for the support that I enjoyed throughout my years at the Institute of Cognitive Neuroscience, Jülich Research Centre. I could not have received more intellectual and personal freedom. Importantly, without this unique experience, I would not have been able to develop and pursue my academic interests as I did.

I am especially grateful to my colleagues at the Institute of Cognitive Neuroscience, the Institute of Medical Imaging Physics, (both Research Centre Jülich), and, the Neuroimaging Group at the University-Hospital of Cologne for with whom I shared great times. I'm especially obliged to Ralf Tepest for his generous patience regarding my coffee bill, which I think I paid for the first time after having enjoyed his black strong magic potion already for at least three years. I am extremely obliged to Kai Vogeley and Leo Schilbach and Bert Timmermanns for our stimulating discussions on implicit mentalizing, we-modes, joint attention and other minds. I am deeply indebted to my MEG teachers, Frank Boers, Jürgen Dammers, and Alex Gramfort, who constantly ignited and guided my passion for biomagnetism, signal processing, statistical learning and computer science with unparalleled patience and encouragement. The same is true for all MNE-Python developers and the scikit-learn developers. Sharing the experience of developing scientific software with you deeply shaped my ideas of how approach scientific and data challenges. Thanks Alex Gramfort, Martin Luessi, Eric Larson, Christian Brodbeck, Mainak Jas, Teon Brooks, Roman Goj, Daniel Strohmeier, Lauri Parkonnen, Matti Hämäläinen. Thanks Gaël Varoquaux, Olivier Grisel and Lars Buitinck. I am much obliged to Alex Gramfort, Eric Larson, and Guillaume Dumas for the countless discussions on fundamentals of MEG analysis and appropriate treatment of cognitive science data. I am especially indebted to Alex Gramfort for helping me to better understand the mathematics behind covariance estimation and source localization using minimum-norm estimates on which study 1 relies. I am extremely obliged to Hannah Eckert, Alexander Geiger and Andrea Muren for assisting with collecting the data for the

experiments in study 2. I am extremely grateful to Frank Boers for programming the graphical stimulator in study 2, experiment 2. I am very obliged to Jürgen Dammers for assisting me with implementing his artifact rejection method in Python and for teaching me the basic principles of independent component analysis. I am deeply indebted to Silvia Maier, Martin Luessi and Danilo Bzdok for proof-reading parts of my thesis. I am amazingly obliged to my friends Silvia, Carl-Friedrich, David and Danilo (randomized order), the last years would not have been as much fun without you. Also to all my other close friends who were not hit as directly by this thesis. I am extremely grateful to my parents for their support, their unshakable trust, and their unparalleled sense of humor. I hope that I did not forget anyone.

Contents

List of Figures

List of Tables

Acronyms

ACC anterior cingulate cortex. 8

BCI brain computer interfaces. 20

BOLD blood-oxygen-level-dependent. 12, 46

CSP common spatial patterns. 20

DISC dynamic imaging of coherent sources. 15, 22

dMPFC dorsomedial prefrontal cortex. 8, 9, 88

dSPM dynamical statistical parametric mapping. 15, 22, 65

ECD equivalent current dipole. 24

ECG electrocardigram. 58, 60, 61

EEG electroencephalography. 1–3, 8, 10–12, 17, 20, 27, 28, 30, 31, 33, 90, 91

EOG electrooculogram. 58, 60

FA factor analysis. 20, 25–29, 31–36, 38, 40–43, 60

FDR false discovery rate. 16

FEF frontal eye fields. 7

FG fusiform gyrus. 7, 8, 38, 79, 81, 82, 84, 85

fMRI functional magnetic resonance imaging. 1–3, 8, 9, 16, 17, 87

GFP global field power. 28, 31, 37, 41

hMNS human mirror-neuron system. 9

ICA independent component analysis. 13, 28, 40, 43, 60, 61, 91

IFG inferior frontal gyrus. 8, 9, 88

IPS intraparietal sulcus. 7, 81, 83, 84

IQR inter-quartile range. 50, 69

ISI inter-stimulus-interval. 46, 47, 55, 56, 77, 78, 86, 87, 91

LCMV linear constrained minimum-variance. 15, 22, 26

LG lingual gyrus. 8

LW Ledoit-Wolf. 23, 24, 35

M/EEG magnetoencephalography and electroencephalography. vi, 14–17, 19, 20, 22–24, 27, 30–33, 35, 39–43, 90

MAD median absolute deviation. 51, 52

MAP maximum a posteriori. 21

MCE minimum-current estimates. 22

MCP multiple comparison problem. 16, 17

MEG magnetoencephalography. 1, 3, 9–14, 16, 17, 19, 27–30, 40, 41, 44, 56, 60, 78, 79, 81, 90–92

MNE minimum-norm estimates. 15, 21–23, 28, 30, 32, 33, 41, 43, 63, 64

MSR magnetically shielded room. 10, 57, 58

mSTS middle superior temporal sulcus. 9, 80, 83, 84

MT/V5 middle temporal area. 7, 77, 79, 82, 85

MxME mixed-norm estimates. 15, 22

OFC orbitofrontal cortex. 8

PCA principal component analysis. 13, 14, 25–28, 32–36, 40, 42, 43, 60, 61

PPCA probabilistic principal component analysis. 20, 25–29, 31, 33, 35, 40, 42, 43

pSTS posterior superior temporal sulcus. 8, 77, 80, 82, 83

ROI regions of interest. 16

SC shrunk covariance. 24, 29, 33–36, 38, 40

SEM standard error of the mean. 50–52, 54

sLORETA low resolution brain electromagnetic tomography. 15, 22

SMG supramarginal gyrus. 8, 80

SOA stimulus onset asynchrony. 30

SQUID superconducting quantum interference device. 10

SSP signal space projection. 24, 28, 43, 91

SSRC social stimulus response compatibility. 45–47, 50, 56, 57, 78, 86, 88

SSS signal space separation. 20, 28, 43

STG superior temporal gyrus. 8, 80

STS superior temporal sulcus. 6–8, 81–83, 85

SVD singular value decomposition. 27–29

TF-MxNE time-frequency mixed-norm estimates. 15

TMS transcranial magnetic stimulation. 1

TPJ temporo-parietal junction. 8, 77, 79, 80, 83, 84

vMPFC ventromedial prefrontal cortex. 9

1 Social interaction, gaze exchange and cortical dynamics

Social cognition has a long past for mankind but, as a science, it has a short history. Over the last decades, it has been studied with unprecedented conceptual and methodological granularity while involving a growing number of academic disciplines. Social cognition historically spawned from social psychology and cognitive psychology and focussed on social information processing (Fiske & Taylor, 2013), which includes impression formation, person perception, social attribution, and, Theory of Mind. Other central notions refer to implicit and automated versus explicit and deliberate processing and are commonly subsumed under dual mode theories (Frith & Frith, 2008). Over the last two decades, many influences from neighboring disciplines have been incorporated and shaped the social cognition discourse in multiple ways by contributing new conceptual tools, paradigms and data analysis methods.

Research on social cognition has extended to neuroscience. Classical social cognition constructs have been mapped to fluctuations in brain function using electrophysiology and neuroimaging techniques such as functional magnetic resonance imaging (fMRI), electroencephalography (EEG), magnetoencephalography (MEG), and transcranial magnetic stimulation (TMS). As a result, putative core-networks of brain regions implicated in social cognition have been identified (Lieberman, 2006; Saxe, 2006; Frith & Frith, 2008). At the same time, the repertoire of study protocols has been dramatically extended by interaction-centered techniques. New insights into the development of cooperation, normative understanding and Theory of Mind have been generated by abandoning classical interviewing techniques that relied on language mastery. Instead, nonverbal multi-person paradigms have been developed, backed by concepts from cognitive science and philosophy of mind (Warneken, Chen, & Tomasello, 2006; Rakoczy, 2008; Köymen et al., 2014). These were then used to study the emerging intentional structure of early social interactions. Based on cross-species comparisons, cross-cultural studies and principles of darwinian evolution, related findings argue in favor of an inherently cooperative structure of basic person perception (Tomasello, Carpenter, Call, Behne, & Moll, 2005; Callaghan et al., 2011). This view has been complemented by embodiment approaches that focussed on interpersonal coordination dynamics instead. Related experimental findings revealed implicit but systematic synchronization between interaction partners (Sebanz & Frith, 2004; Marsh, Richardson, & Schmidt, 2009). A successive translation of such interaction-based techniques to neuroscience can be

observed over the last decade. Social decision-making processes and social conflict have been studied in healthy and clinical populations using protocols backed by behavioral game theory, often involving multiple subjects acting simultaneously. Virtual-reality techniques have been employed in concert with fMRI recordings to study biological motion and gaze-processing during ongoing interactions (Bohil, Alicea, & Biocca, 2011). Such techniques often rely on dynamic presentation of virtual characters in a quasi-naturalistic manner (Schilbach et al., 2009; Vogeley & Bente, 2010; Pfeiffer, Timmermans, Bente, Vogeley, & Schilbach, 2011). Social interaction and related coordination dynamics have been investigated usingbrain signals EEG and fMRI studies (Saito et al., 2010; Dumas, Chavez, Nadel, & Martinerie, 2012; Nummenmaa et al., 2012). These experimental approaches are accompanied by recent theoretical developments that propose an interactive approach to social cognition and social cognitive neuroscience based on the notions of embodiment, entrainment and a 2nd-person perspective (Hari & Kujala, 2009; Schilbach et al., 2013). In this context, gaze-processing has been argued to glue together the diverse scientific approaches to studying social interaction, especially with respect to cooperation and collaboration (Engemann, Bzdok, Eickhoff, Vogeley, & Schilbach, 2012).

At the same time, these protocols call for more advanced signal processing and data analysis techniques to leverage the increased granularity of experimental protocols. To fully recognize the mathematical foundations of game theoretic paradigms, researchers started to pursue computational bayesian techniques which permit to model behavior and related physiological parameters (Yoshida, Dolan, & Friston, 2008; Behrens, Hunt, & Rushworth, 2009). Machine-learning techniques have recently been adopted by social cognition researchers to predict and categorize mental states, behavior and social perception in a data-driven fashion based on brain-signals (Said, Moore, Engell, Todorov, & Haxby, 2010; Redcay & Carlson, 2014). The theory of complex systems and dynamic coupled oscillators has been used to analyze inter-person synchronization (Dumas, de Guzman, Tognoli, & Kelso, 2014).

These developments also raise increased demands with regard to basic neuroimaging techniques and their usage. Interactive paradigms are challenging to implement in an neuroimaging environment and the choice of the imaging modality is associated with different trade-offs between spatial resolution, temporal resolution and the ecological validity that can be reached for a paradigm in a given imaging environment. EEG is available at a low cost, provides with high mobility that allows to setup hyper-scanning protocols in everyday situations, but suffers from poor spatial resolution. In contrast, fMRI-protocols benefit from mature signal processing procedures and high availability, but suffer from lower temporal resolution. Novel developments such as multimodal imaging based on combined EEG-fMRI protocols or fast sequences that sample the hemodynamic signal at about 0.1 Hz mitigate this limitation to some extent but are not yet very well established. The combination of such

data— beyond an inferential level— in data analyses often requires to make concessions to either modality's unique strengths. The benefits of increased temporal resolution of fMRI are limited by the inherent characteristics of the hemodynamic signal which updates at a second scale. As a consequence the researcher is left with the burden of designing sophisticated and optimized sampling protocols which may interfere with the experimental logic dictated by the phenomenon under investigation. In this context, MEG constitutes an interesting technique as it combines temporal resolution at a millisecond scale with moderate spatial resolution that can achieve up to 3-5 millimeter spatial precision, and, moreover, has become increasingly available across sites[1]. Bibliographic indices as well as the recent publication of the first two MEG-methods textbooks for experimental researchers (Hansen, Kringelbach, & Salmelin, 2010; Supek & Aine, 2014) indicate an increasing adoption of this method in cognitive sciences. In contrast to EEG, in both fMRI and MEG settings, hyperscanning techniques are costly and do not yet enjoy a wide adoption, despite recent advances.

These examples illustrate the following developmental trajectories in social cognition research.

1. Analysis of ongoing and multi-agent interactions.
2. The differentiation of qualities and contexts inherent to social interaction instead of contrasting social with nonsocial categories.
3. Advanced neuroimaging and data analysis techniques.

The present thesis follows these principles in selecting a scientific problem that emerges at their intersection: the neuromagnetic study of eye gaze during social interacVirtual realitytion. To unfold this problem, the next section will review research findings on eye gaze and and detail its social cognitive role, its evolutionary origins, and its neurobiological basis. The subsequent section will introduce MEG, followed by a concluding synthesis of the present research agenda.

1.1 Gaze exchange as paradigmatic social interaction

Facial interactions are a prominent behavioral feature in primates, including monkeys. During hominoid evolution, increasingly complex social environments created selective pressures on the evolution of social-cognitive capacities (Humphrey, 1976; Dunbar, 1993). In such environments it was beneficial to predict conspecifics' behavior. Visual awareness depends on foveal stimulation, which depends on the eye position. Therefore, looking

[1] see http://megcommunity.org/index.php/groups-jobs/groups

behavior indicates the attentional focus, hence, allows to generate predictions regarding an individual's behavior. During evolution organisms learned to leverage this link. Their capacities to discern other conspecifics' looking direction progressively advanced (Tomasello, Call, & Hare, 2003; Tomasello, 2008; Shepherd, 2010). This process was further promoted by anatomical evolution. The human sclera gives a paradigmatic example as it lacks pigmentation and therefore produces a strong intensity and color contrast relative to the skin and the iris (Kobayashi & Kohshima, 1997). As a consequence, gaze direction has become transparent among humans. This property then paved the way for the evolution of advanced forms of intentional communication and cooperation that require the understanding of goals and intentions (Kobayashi & Kohshima, 1997; Tomasello, 1999; Tomasello et al., 2005). Therefore, gaze has been argued to play a unique role in human social cognition (Tomasello et al., 2005; Engemann et al., 2012; Pfeiffer, Vogeley, & Schilbach, 2013; Schilbach et al., 2013).

This evolution is reflected in the prominent role of eye gaze across human lifespan. Newborns prefer images depicting faces that look at them (Farroni, Csibra, & Simion, 2002). At the age 5-7 weeks, infants exhibit a strong increase in fixations of the eye region of a face (Haith, Bergman, & Moore, 1977). About 2 years of month infants begin to engage with caregivers in structured interaction that involves precisely timed alternations of looking at each other and terminating eye contact (Field, 1981; Reddy, 2003). At 10 months of age, infants recognize whether other persons look at each other or not and begin to expect eye contact during conversations (Beier & Spelke, 2012). Between 12 and 18 months of age, toddlers start to follow and direct other's gaze to objects (Carpenter, Nagell, Tomasello, Butterworth, & Moore, 1998). At this age, they begin to learn that their caregiver's attentional focus, as expressed by eye gaze, acts as a constraint to successful social interaction. Later in ontogeny, gaze behavior serves to establish and regulate intimacy and social distance (Argyle & Dean, 1965; Argyle & Ingham, 1972; Argyle, Ingham, Alkema, & McCallin, 1973). Patterns of gaze behavior further indicate social structure, hierarchy as well as cultural norms (Blais, Jack, Scheepers, Fiset, & Caldara, 2008; McCall, Blascovich, Young, & Persky, 2009). These interdisciplinary findings highlight the constitutive role of eye gaze for social interaction, communication and culture.

The following passages will summarize operational definitions of gaze, central associated behavioral findings, and related neuroscientific evidence. The section concludes with an intermediate evaluation.

1.1.1 Scientific operationalization of gaze

Mutual and averted gaze Gaze research follows a coarse classification of gaze-related phenomena which distinguishes visuomotor elements of gaze and emerging dynamic-intentional contexts thereof. In a first approximation, mutual and averted gaze were often contrasted. This distinction was typically implemented using images or photographs that convey the impression of eye contact or its absence. *Mutual gaze*, at the level of stimulus-materials also commonly referred to as direct gaze, denotes situations in which two observers look into each other's eyes. *Averted gaze* refers to situations in which the observed individual does not look into the observer's eyes but focusses on something else instead. Sensitivity to both direct gaze and averted gaze has been demonstrated in macaques and chimpanzees at the behavioral level (Perrett et al., 1985; Emery & Lorincz, 1997; Sato & Nakamura, 2001; Kano & Tomonaga, 2010) and at the neuronal level respectively (Hoffman, Gothard, Schmid, & Logothetis, 2007), even after differentiating between head posture and gaze direction (Perrett et al., 1985). Reminiscent of human infants (Farroni et al., 2002), chimpanzee infants have recently been reported to preferentially fixate photographs of human faces displaying direct gaze (Myowa-Yamakoshi, Tomonaga, Tanaka, & Matsuzawa, 2003; Tomonaga et al., 2004). However, recent findings suggests that adult chimpanzees exhibit less complex fixation patterns when analyzing another individual's eye region than humans (Kano & Tomonaga, 2010) conforming to the cooperative eye hypothesis (Kobayashi & Kohshima, 1997). In humans, exposure to mutual gaze has been found to modulate a wide spectrum of physiological and cognitive process including perceived intimacy (Argyle & Dean, 1965), attribution of sympathy (Kuzmanovic et al., 2009), attractiveness (Mason, Tatkow, & Macrae, 2005), emotional arousal (Nichols & Champness, 1971), imitation Wang, Newport, and Hamilton, 2011 and visual search (von Grünau & Anston, 1995). In contrast, exposure to averted gaze has been found to reorient attention to peripheral targets, commonly referred to as spatial-cueing (Posner, 1980).

Gaze-following, gaze alternation and joint attention Additional insights have been generated based on *gaze-following* paradigms, or more generally, in tasks in which mutual and averted gaze were dynamically combined. When presented with peripheral targets and distractors, macaques have been shown to follow a human's gaze to the target, conforming to the attentional reorienting characterization of averted gaze. Chimpanzees have been shown to be sensitive to gaze shifts in such gaze-following tasks under certain conditions. Recent findings based on systematic comparison between head and gaze cues suggests that chimpanzees attribute more relevance to head posture as compared to direction of eye gaze, whereas human children preferentially respond to gaze. For example, in a study by Tomasello, Hare, Lehmann, and Call (2007) children at 12 months of age neglected the head cue if the experimenter closed her eyes before moving her head, whereas chimpanzees were not sensitive to eye gaze. Such tasks highlight the communicative role of mutual gaze

as an ostensive cue (Sperber, Wilson, & Ziran, 1986) which biases the interpretation of subsequent behavior as communicative and intentional. This point is further illustrated by the phenomenon of joint attention which commonly emerges from single or repeated episodes of gaze-following with interleaved mutual gaze and has often been characterized as triadic interaction in which social interaction is structured around objects (Bard & Vauclair, 1984; Tomasello et al., 2005; Call, 2009). Chimpanzees have been shown to read both their interaction partner's attentional state and intentions based on gaze behavior. However, given the current state of research, it can be stated that only humans share a unique propensity to share their attention and intentions with their conspecifics (Call & Tomasello, 1999; Call, 2009). Sometimes researchers therefore distinguish joint attention (coincidental or implicit correspondence of mental states) from shared attention (mutual manifestness of corresponding mental states) (Emery, 2000). The social cognitive impact of gaze-based interactions is illustrated by studies in which such triadic joint attention was experimentally varied to study collaborative behavior, suggesting eye contact and joint attention to strongly modulate cooperative commitment and the normative implications of the following social interaction (for example Gräfenhain, Behne, Carpenter, and Tomasello (2009)). Joint attention, moreover, has been suggested to be a developmental precursor of language and Theory of Mind (Mundy, Sigman, & Kasari, 1990; Charman et al., 2000; Aschersleben, Hofer, & Jovanovic, 2008). The latter refers to the ability to explain others' behavior in terms of (false) beliefs and desires (Premack & Woodruff, 1978; Wimmer & Perner, 1983), also commonly summarized as mentalizing.

1.1.2 Neuroscientific analysis of gaze

Neural circuitry concerned with processing other individuals' faces and eye gaze have, to date, only been extensively investigated in macaque monkeys and in humans (Yovel & Freiwald, 2013). Exposure to face stimuli elicits activation in specialized parts of the primate visual system that is concerned with object recognition (Tsao, Moeller, & Freiwald, 2008; Yovel & Freiwald, 2013), also referred to as ventral visual stream (Corbetta, Patel, & Shulman, 2008). In macaques, most face-sensitive areas have been detected inside the superior temporal sulcus (STS), and, based on anatomical landmarks, occupy relatively more dorsal locations of the temporal cortex as compared to human face sensitive areas (Tsao et al., 2008). Additional face-sensitive neurons have been found in the monkey's amygdala (Hoffman et al., 2007) and in the monkey's ventral prefrontal cortex (Tsao et al., 2008), both related to emotion processing. It has been suggested that macaque face areas have undergone massive expansion and anatomical reorganization during hominoid evolution (Van Essen & Dierker, 2007). However, recent research has proposed that macaque intra-STS patches can be mapped to the human face-sensitive system (Orban, Van Essen, & Vanduffel, 2004).

Interestingly, numerous tuning characteristics have been isolated for these face-selective patches inside the monkey STS (Freiwald, Tsao, & Livingstone, 2009). These include face aspect-ratio, face direction, eye size, gaze direction, but also various mouth and limb attributes as well as preferential discharge during observation of action. These findings suggest that macaques possess a wide array of specialized functional units concerned with the analysis of social stimuli. Therefore, primate cross-species differences in behavioral capacities and propensities regarding eye gaze are expected to reflect progressive structural and functional refinements of the face and gaze processing system.

In humans, three occipito-temporal regions have been identified that harbor one to multiple face-sensitive areas (Yovel & Freiwald, 2013), i.e., the lateral occipital cortex, the face-sensitive fusiform gyrus fusiform gyrus (FG), and the STS. It has been suggested that the lateral occipital cortex implements an early face-related visual feature processing node which passes information to the face-sensitive FG and the STS (Haxby, A., & Gobbini, 2002). Numerous studies based on mutual gaze and averted gaze have suggested that the face-sensitive fusiform gyrus is preferentially concerned with recognition, categorization, individuation and processing of invariant face features. In contrast, the face sensitive patches inside the STS are commonly related to processing dynamic features of faces, such as eye gaze and facial expressions. This is illustrated by frequent coactivation of STS patches with the middle temporal area (MT/V5) region that is motion sensitive, the intraparietal sulcus (IPS) and the frontal eye fields (FEF) which are commonly related to spatial-attentional reorienting (dorsal attention network) (Corbetta et al., 2008). Interestingly, intracranial recordings from the face-sensitive fusiform gyrus show that early and late components can be differentiated which dissociate between function typically ascribed to the FG and the STS (Pourtois, Spinelli, Seeck, & Vuilleumier, 2010; Kawasaki et al., 2012). Several face-sensitive neuromagnetic components have been differentiated (Linkenkaer-Hansen et al., 1998; Liu, Harris, & Kanwisher, 2002; Sato, Kochiyama, Uono, & Yoshikawa, 2008; Morel, Ponz, Mercier, Vuilleumier, & George, 2009; Meeren, de Gelder, Ahlfors, Hamalainen, & Hadjikhani, 2013; Cauchoix, Barragan-Jason, Serre, & Barbeau, 2014). Among these, the M170 component, commonly attributed to face-recognition and individuation (Xu, Liu, & Kanwisher, 2005; Deffke et al., 2007; Taylor, Bayless, Mills, & Pang, 2011), has been most consistently supported by the literature. It has been localized to different regions, including the face-sensitive fusiform gyrus (Sams, Hietanen, Hari, Ilmoniemi, & Lounasmaa, 1997; Linkenkaer-Hansen et al., 1998; Sato et al., 1999; Watanabe, Kakigi, Koyama, & Kirino, 1999; Halgren, Raij, Marinkovic, Jousmaki, & Hari, 2000; Watanabe, Kakigi, & Puce, 2003; Deffke et al., 2007; Henson et al., 2007; Okazaki, Abrahamyan, Stevens, & Ioannides, 2008; Corrigan et al., 2009; Hadjikhani, Kveraga, Naik, & Ahlfors, 2009; Henson, Mattout, Phillips, & Friston, 2009), the extrastriate occipital cortices (Itier, Herdman, George, Cheyne, & Taylor,

2006; Thierry et al., 2006; Henson et al., 2009; Dumas et al., 2013), the lateral occipito-temporal cortex (Schweinberger, Pickering, Jentzsch, Burton, & Kaufmann, 2002; Dumas et al., 2013), the STS (Watanabe et al., 2003; Itier & Taylor, 2004; Corrigan et al., 2009) and the lingual gyrus (LG) (Mnatsakanian & Tarkka, 2004). A recent fMRI-based connectivity analysis has targeted functional coupling between occipto-temporal face-sensitive cortices and other cortical networks during perception of eye gaze (Nummenmaa, Passamonti, Rowe, Engell, & Calder, 2010). Results suggested that both, the fusiform gyrus and the posterior superior temporal sulcus (pSTS) share modulations of connectivity induced by eye gaze with the superior temporal gyrus (STG) and the supramarginal gyrus (SMG) which are also often attributed to the temporo-parietal junction (TPJ) and stand in close relationship with attentional capture and orienting to relevant objects (ventral attention network) (Corbetta et al., 2008). These findings suggest that the commonly assumed regional model of face-related visual processing in which the STS and the FG are preferentially concerned with dynamic and static featurs of faces, respectively, might need to be extended. Therefore, more advanced investigation of differential gaze-related cortical dynamics is warranted, which considers a wider range of social cognitive contexts.

Somewhat reminiscent of the monkey's ventral prefrontal face patches (Tsao et al., 2008), additional human regions linked with face- and gaze-processing have been found in the amygdala, the orbitofrontal cortex (OFC), the inferior frontal gyrus (IFG) and the dorso-medial prefrontal cortex (dMPFC) (Akiyama et al., 2007; Vuilleumier & Pourtois, 2007; Nummenmaa & Calder, 2009). The amygdala has been suggested to be modulate cortical face-related activity, depending on saliency, relevance and emotion (Senju & Johnson, 2009; Bzdok et al., 2012; Dumas et al., 2013). The dMPFC has recently been linked Theory of Mind and gaze-processing. This was illustrated by recent neuroimaging studies on joint attention which were based on hyperscanning techniques (Saito et al., 2010; Lachat, Farroni, & George, 2012), virtual environments (Schilbach et al., 2009; Pfeiffer et al., 2014) or live-video feedback (Redcay et al., 2010). While electrophysiological findings are most sparse, let alone reports with respect to cortical dynamics, a recent dual- EEG hyperscanning experiment found modulations of spectral inter-person synchrony in the alpha and the mu band related to joint attention (Lachat et al., 2012). Findings based on fMRI have related the dMPFC, the anterior cingulate cortex (ACC) and the right TPJ to the experience of shared as compared to individual visual attention during social interaction (Schilbach et al., 2009; Redcay et al., 2010; Pfeiffer et al., 2014). These findings suggest that the putative human cortical mentalizing system is tuned by dynamic alternations of mutual and averted gaze during ongoing interactions and that ensuing computations concerned with mental state attribution might therefore rely on shared visual attention. At a subcortical level, joint attention has been reported to evoke activation of the ventral striatum (Schilbach et al.,

2009; Pfeiffer et al., 2014), a structure implicated in the human reward system. Such findings conform with the shared intentionality theory of human cognitive and cultural evolution which predicts that sharing mental states is rewarding for humans (Tomasello et al., 2005; Call, 2009). Less unequivocally, activation of the IFG, which is believed to be part of the putative human mirror neuron system, has been reported to be evoked by joint attention (Saito et al., 2010). Recent meta-analytic connectivity studies add to this findings in demonstrating task-related and resting-state connectivity between gaze-related networks and the dMPFC but not the ventromedial prefrontal cortex (vMPFC). This suggests that the dMPFC is preferentially involved in higher-order processing and top-down modulation of basic social perceptions ensuing from interaction with others (Bzdok et al., 2013a).

These findings demonstrate that the macaque and the human gaze-processing system possesses striking functional and structural similarities. The systems of both species possess differentiated temporal cortical networks concerned with visual processing of faces and eye gaze, possess patches which are related to emotional modulation of gaze-processing, and, possess frontally situated patches concerned with specialized and higher-order processing of faces. Naturally, the structural expansion and evolution of face-sensitive cortical areas in humans seems to reflect the more diverse human social propensities. It has recently been argued that the human mentalizing network or at least core elements thereof can be delineated from the macaque's middle superior temporal sulcus (mSTS) region, suggesting that the evolutionary origins of human social cognition are grounded in visual and post-visual face-, gaze- and body-processing. On the other hand, the diverse functional imaging and electrophysiology findings regarding the social cognitive role of human visual face-sensitive areas demonstrate that more fine-grained investigations thereof are warranted. Given the tempting view that human origins of social cognition are situated in gaze processing, novel insights are expected from investigating how visual face-sensitive cortical networks are tuned by ongoing, social interaction. Unfortunately, to date, virtually nothing is known about this subject matter. MEG studies have revealed various characteristic modulations of cortical activity in visual face areas related to perception of eye gaze in both the time and the frequency domain (for example Taylor, George, and Ducorps (2001), Dobel, Junghofer, and Gruber (2011)). Unfortunately, it remains unclear, how these gaze-related signals relate to ongoing social interaction. A few recent fMRI studies have addressed the question of how the putative human mirror-neuron system (hMNS) is tuned by eye gaze during ongoing social interactions and suggest that networks related to mentalizing and self-other distinction, i.e., the dMPFC closely interacts with the putative hMNS to quickly adjust ongoing action to social and intentional contexts (Schilbach, 2010; Wang, Ramsey, & De C Hamilton, 2011). However, these findings did not detail the cortical dynamics. I therefore propose to investigate how social interaction tunes gaze-related cortical dynamics using MEG. The

following sections will give a brief summary of basic biophysical and physiological facts, principles and practices regarding MEG. Where it is indicated, links between MEG and social cognitive neuroscience will be established.

1.2 Magnetoencephalography

MEG is a noninvasive neuroimaging technique which permits the analysis of cortical dynamics at submillisecond temporal resolution. The following sections introduce the method summarize basic physiological, biophysical and analysis related principles and issues.

1.2.1 Neural sources

MEG measures extracranial magnetic fields inside a magnetically shielded room (MSR) by using an array of sensors which are positioned inside a helmet. These sensors are commonly referred to as superconducting quantum interference device (SQUID)s. These magnetic fields are usually observed at a scale of femtotesla (1×10^{-15} Tesla). The primary neuronal sources of MEG signals have been shown to reflect post-synaptic potentials of neocortical layer V and layer II-III neurons located in the walls of the sulci (Murakami, Hirose, & Okada, 2003; Murakami & Okada, 2006). These neurons posses long apical dendrites oriented peripendicularly to the pial surface. On de- or hyper-polarization resulting from synaptic modulation, electric currents flow alongs these dendrites and generate electromagnetic fields, appearing as a dipolar pattern from the distance (Hämäläinen, Hari, Ilmoniemi, & Knuutila, 1993). Assuming a single current dipole moment magnitude of 0.29 to 0.90 pAm for cells of this type, a population of 50.000 synchronously active neurons is required to generate a current dipole moment of 10nAm (Murakami & Okada, 2006), which is the threshold above which signals can be detected by MEG given the volume conductor properties and Maxwell's equations (Hämäläinen et al., 1993) and the noise level of the sensors. Depending on the density of pyramidal neurons in a patch of cortex, a thin column of of roughly $1mm^2$ can already generate a detectable dipole moment (Murakami & Okada, 2006). However, due to field cancellation, larger areas may be required to generate a detectable MEG signal (Hämäläinen et al., 1993). To a lesser extent, and, depending on the geometry of their dendrites, stellate neurons may also contribute to the MEG signal (Murakami & Okada, 2006). In contrast, action potentials are unlikely to be detectable by MEG because large-scale synchronization of action potentials is highly unlikely under nonpathological conditions and, moreover, their field is rather described by a quadrupole (Hämäläinen et al., 1993; Murakami & Okada, 2006). Importantly, passive volume currents, also called secondary currents, lead to cancellation of radially oriented primary currents (Hämäläinen et al., 1993). This is why MEG is mainly sensitive to the tangential field components whereas EEG is

also sensitive to radial components oriented towards the skull (Hämäläinen et al., 1993; Ahlfors, Han, Belliveau, & Hämäläinen, 2010). Given the negligible magnetic resistance of the conducting medium and reference-free measurements of magnetic fields, MEG signals directly capture current magnitudes of a population of neurons and are, hence, less subject to spatial distortion than EEG signals. Second, because conductivities have a stronger impact on EEG signals, it is also more difficult to reliably estimate a forward solution. These properties allow to achieve a more accurate localization of MEG signals as compared to EEG. Depending on the signals, MEG inverse solutions reach a precision of 3-5mm (Hämäläinen et al., 1993). Importantly, MEG signals can be generated by sources that are not otherwise detectable because they are too transient to be reflected in fMRI-BOLD signals (Logothetis, Pauls, Augath, Trinath, & Oeltermann, 2001; Singh, Barnes, Hillebrand, Forde, & Williams, 2002; Logothetis, 2008; Muthukumaraswamy & Singh, 2009). Other sources possess spectral characteristics that EEG cannot clearly differentiate (Hari & Kujala, 2009). It has also been suggested that the orientation selectivity of MEG can improve the signal-to-noise ratio for certain sources (Ahlfors et al., 2010; Ahlfors et al., 2010). Against the background of the previous discussion, these properties suggest that MEG might play an important role in further differentiating gaze-related cortical dynamics.

1.2.2 Taxonomy of neuromagnetic signals

Research has converged on the following threefold classification of MEG and MEG signals.

Spontaneous oscillatory activity can occur in the absence of any stimulus or overt behavior, but can be modulated by various conditions. One prominent example of such spontaneous activity refers to oscillations in the alpha band (7–13 Hz), commonly observed at sensors over parietal and occipital brain areas while subjects are at rest (Berger, 1929; De Munck et al., 2007). These spontaneous oscillations are further modulated by context, for instance, when subject's have their eyes closed alpha-power usually increases (Ciulla, Takeda, & Endo, 1999).

Induced oscillatory activity is strictly task-related and is defined as response fluctuation over a series of repeated stimuli. An example of such induced oscillatory are task-related modulations of 40-90Hz gamma band responses in the visual cortex (Tallon-Baudry & Bertrand, 1999; Muthukumaraswamy & Singh, 2009; Brunet et al., 2014). Importantly, because this kind of activation is not strictly phase-locked to the stimuli, signals cannot be directly averaged across trials in the temporal domain, since such averaging would only preserve time-locked components (Tallon-Baudry & Bertrand, 1999).

Time-locked activity, also referred to as evoked response, is phase-locked to stimulus or motor events. Prominent examples of such responses are given by the M170 face-sensitive

component, a deflection with a peak around 170 milliseconds which becomes visible when averaging over multiple trials in which faces have been presented (Susac, Ilmoniemi, Ranken, & Supek, 2011; Taylor et al., 2011; Perry & Singh, 2014).

Oscillatory activity can be generated by thalamo-cortical modulation but can also emerge locally in a population of synchroneously discharging cortical neurons (Llinás, 1988; Ribary et al., 1991; Ikeda, Leyba, Bartolo, Wang, & Okada, 2002), and has been linked to numerous cognitive and behavioral phenomena including attention and awareness (Tallon-Baudry & Bertrand, 1999). Importantly, oscillations establish a link between MEG and EEG signals and hemodynamic responses as measured by the blood-oxygen-level-dependent (BOLD) signal (Logothetis et al., 2001; Singh et al., 2002; Logothetis, 2008; Muthukumaraswamy & Singh, 2009). Despite the exhaustive body of electrophysiology literature regarding time-locked activity, no unequivocal physiological explanation of the phenomena has been been achieved so far (Hanslmayr et al., 2007; Sauseng et al., 2007; Mazaheri & Jensen, 2010). The classical additive model suggests the existence of weak potentials that are evoked by certain stimuli or events in a stereotype manner but are overshadowed by ongoing oscillatory brain activity. In this model, averaging across trials eliminates non-time-locked activity and ultimately reveals the weak evoked response by linear addition. Alternatively, it has been argued, that time-locked activity results from synchronous resetting of the phase in a population of neurons (Makeig et al., 2002; Sauseng et al., 2007). In this model, no weak component is assumed at the single trial, but averaging will lead to the deletion of non-time-locked activation and will preserve the first cycle of the waveform after the time-locked reset. While this debate is still not resolved it is noteworthy that the phase-resetting theory is more parsimonious since it explains composite phenomena in terms of basic oscillatory network dynamics and modulation instead of assuming a more complex ontology of intrinsic brain responses. A more recent proposal also pursued an oscillatory explanation of time-locked activity but focussed on rhythmic properties required to explain sustained evoked responses which the phase-resetting theory falls short of (Mazaheri & Jensen, 2008, 2010).

1.2.3 Principles of MEG data analysis

To process MEG data such that accurate descriptions of active neural sources can be obtained is both challenging and resource consuming (Gramfort et al., 2013a). It involves removal of noise and artifacts from the measurements, extracting anatomical models from MRI-scans, a numerical solution of the biomagnetic forward problem, and a plausible, constrained solution to the inverse problem (von Helmholtz, 1853). The following passage gives a brief overview on MEG data processing which follows the summaries provided by Gramfort et al. (2013a, 2014).

1.2.3.1 Signal extraction

MEG recordings cannot be meaningfully analyzed without any preprocessing. The common steps related to preprocessing are concerned with reducing interference from endogenous (biological) and exogenous (environmental) sources.

Often the signal of interest and interferences thereof occupy different frequency bands, and, hence can be filtered accordingly. Filtering approaches can be regarded as settled, but still, the characteristics of a filter and the exact choices of parameters should be considered carefully against the background of the scientific question and the signal of interest. Some filters may induce phase or frequency related artifacts, while, for example weak sustained evoked responses can be wiped out by inappropriate high-pass filter settings and too wide transition bandwidths.

When segmenting continuous recordings into observation windows organized around events of interest, commonly referred to as epochs, one simple but efficient option of artifact removal amounts to discarding contaminated epochs. Typically, peak-to-peak amplitude thresholds are defined based on the natural scale of the measurements and the expected amplitude of the signal of interest. Epochs in which one single sensor at a given sample exceeds the defined threshold are subsequently excluded. For MEG data this threshold depends on the sensor type, typically for magnetometers values between 2000 and 4000 fT can be considered meaningful choices. The resulting number of remaining trails is an important aspect to monitor. To avoid biased analysis when comparing conditions, after rejection of epochs the number of trials should be equalized for each condition.

Fine-grained post-hoc tuning of signal quality can be achieved by employing signal decomposition techniques, often resulting in more 'good' segments of data. The general principle behind such approaches consists in estimating a transformation on a subspace of the data in which noise and artifact related signal components are be separated based on their differential statistical features, as characterized by variance, skewness or kurtosis. Commonly used are procedures based on principal component analysis (PCA) or independent component analysis (ICA). One important aspect to be considered refers to the introduction of artificial correlations into the data due to rank reduction. The rank of the data refers to the system of linearly independent equations. Signal decomposition techniques typically project the data on a subsystem of independent components which has a lower rank than the number of observations. Each noise-related component which is removed, typically reduces the rank by the number of one. As long as the rank of the between-sensors noise covariance matches the rank of the data, and as long as the difference between the rank and the numbers of sensors is not too large, rank reduction does usually not pose a problem to subsequent analysis. One has to be certain, however, that the signals of interest are not described,

by low-variance components that would be excluded by excessive rank reduction. If one assumes for example preprocessing based on PCA, components would be orthogonal and sorted by variance in descending order. Often such procedures take into account the noise covariance, estimated from data acquired in the absence of a subject or from segments of data considered as irrelevant, also referred to as subject noise. If the scientific interest focusses on ongoing, task-free, or instantaneous single-trial activity, the separation of subject noise from the signals of interest is less probable, hence, estimators of the noise covariance based on empty room recordings are preferable.

1.2.3.2 Source localization

One fundamental challenge of MEG data refers to the fact that neuromagnetic signals are recorded outside and not inside of the head and it is necessary to solve an ill-posed inverse problem in order to localize the origin of the signals. Unfortunately, no mathematically unique solution exists to determine the exact origin of these signals (von Helmholtz, 1853). This problem is commonly addressed by choosing biophysically and anatomically plausible constraints to the space of feasible solutions. This step is commonly referred to as inverse solution. A particular method for source localization is also called inverse solver. Resulting estimated dynamics of cortical sources are often referred to as source estimates. As a direct consequence of the ill-posed nature of the inverse problem such estimates to some degree depend on model assumptions and parameter choices, which stands in sharp contrast to MRI data-acquisition which does not implicate such an ill-posed problem.

Based on Maxwell's equations it is possible to predict the extracranial magnetic fields based on a given cortical electric current at a given location in the brain (Hämäläinen et al., 1993; Gramfort et al., 2013a). To compute such a forward solution, which is an essential component of any source localization method, one needs to take into account tissue conductivities, the head geometry, and sensor arrangements (Gramfort et al., 2013a). Assuming a current dipole as source model and a constant conductivity per shell[2] (skin, skull, brain), a boundary element model (BEM) can be used to simplify the forward solution (Mosher, Leahy, & Lewis, 1999). Once an appropriate forward model has been estimated the remaining problem amounts to finding a transformation of the measured data which, given the forward model allows to reconstruct the measured sensor data with minimum error. This step is referred to as inverse solution.

The basic sources of M/EEG data are described as equivalent current dipoles. A classic source localization approach assumes that the signals observed can be explained by a small number of such dipoles. Such models can be compellingly parsimonious and easy to interpret, but

[2] described by so called piecewise constant functions.

the assumption of a small set of focal active sources is not always plausible. For example, complex cognitive processes and ongoing spontaneous or "resting-state" activity is likely to implicate activity in networks of brain regions and such activity may be too spatially extended to be properly accounted for by one or a few current dipoles. In addition, dipole models make more assumptions about the data and the fitting procedure is computationally demanding.

In contrast, distributed source models implicate thousands of dipolar sources which are positioned in a grid of predefined locations, based on anatomical information. The only parameters to be estimated for such source localization methods are the dipole amplitudes at a given time. The most popular distributed source localization models implement linear models with ℓ_2-norm constraints. For example models from the minimum-norm estimates (MNE) family, weighted MNE (Lin, Belliveau, Dale, & Hamalainen, 2006), low resolution brain electromagnetic tomography (sLORETA) (Pascual-Marqui, 2002), dynamical statistical parametric mapping (dSPM) (Dale et al., 2000), mixed-norm estimates (MxME) (Gramfort, Kowalski, & Hämäläinen, 2012), time-frequency mixed-norm estimates (TF-MxNE) (Gramfort, Strohmeier, Haueisen, Hämäläinen, & Kowalski, 2013b), or time domain, e.g. linear constrained minimum-variance (LCMV) (Veen, Drongelen, Yuchtman, & Suzuki, 1997), and frequency domain, beamformers, e.g. dynamic imaging of coherent sources (DISC) (Gross, Kujala, Hämäläinen, & Timmermann, 2001). It is important to note that some of these inverse solvers, i.e., TF-MxNE, LCMV, DISC, and MxME implement non-linear optimizations that cannot be expressed in a single matrix multiplication with a weight matrix. Moreover, beamformers implement adaptive spatial filters which not only depend on the forward model and the noise covariance but also on the covariance of the data[3]. Such Euclidean ℓ_2-norm constraints inherently assume Gaussian noise with zero mean and equal variance across sensors. While bandpass filtering can improve data with regard to these requirements it is usually preferred to implement a spatial whitening step that allows to suppress between-sensor correlations related to noise. More specifically, the spatial covariance of the additive noise is estimated from data and subsequently used for whitening. This transforms data into independent white noise vectors characterized by identical variances across channels. Importantly, in the statistical literature it is a commonly known fact that covariance estimators can be unstable if the number of samples is insufficient. The relevance of this problem has recently been demonstrated for source localization of M/EEG data and, to date, it is unknown to which extent this problem scales with decreasing signal-to-noise ratio, as common for high-level cognitive processes and related signal contrasts.

[3]For contextual completeness, the term beamformer refers to radar technology, which was the historical context in which such models have initially been developed

1.2.3.3 Statistical analysis

When identifying active neuronal sources based on MEG signals, the researcher not only faces challenges related to the high anatomical variability of the brain across subjects. The increased temporal granularity of MEG adds another layer of complexity once cortical sources are compared across subjects (Gramfort et al., 2013a). A group analysis of cortical source estimates over a time range of a few hundred milliseconds easily implicates millions of statistical variables and constitutes a severe multiple comparison problem (MCP). Common approaches to the MCP employed for fMRI research are often too conservative for M/EEG applications. For example, the false discovery rate (FDR) which counts as rather liberal in the fMRI domain is prohibitive for most meaningful whole brain analysis using MEG. This problem is specifically aggravated by domain-specific aspects of cognitive and social cognitive neuroscience. In particular, high variability between subjects, weak effect sizes or unstable effects add to this problem. In the following paragraphs, one recently developed approach to address the MCP in the context of M/EEG will be introduced.

To mitigate the MCP, many MEG researchers tend to analyze average time courses from regions of interest (ROI) instead of analyzing all source locations. Another variant of this approach coined 'mean amplitude analysis' compares signals averaged over all source locations and time samples in an ROI across conditions. While sensitivity is gained by reducing the number of multiple comparisons and, hence, the amount of correction, such averaging approaches may fail to detect effects of interest that are both sparse and transient. Moreover, this approach clearly abandons a data-driven perspective, that is desirable for scientific exploration, in favor of confirmatory analyses. This challenge recently stimulated methodological developments which adapt to the requirements imposed modern M/EEG analysis. One promising approach put forward by Maris and Oostenveld (2007) tackles the MCP by making use of clustering techniques in combination with a nonparametric permutation test. The output of an arbitrary test statistic, often a t-test or an ANOVA statistic is fed into a clustering procedure which ties together independent observations that exceed a threshold value of the test statistic, based on their adjacency in feature space, e.g. their spatial and temporal neighborhood. An initial clusterwise test statistic, also referred to as maximum statistic (Nichols & Holmes, 2002), is then obtained by summing the test statistic of each variable. Subsequently, this procedure is repeated multiple times on random partitions of the data where the samples are randomly assigned to conditions. The significance test is then obtained by analyzing the tails of the resulting distribution using the clusterwise test statistic. This approach alleviates the MCP as adjacent variables are combined into one score and the correction for multiple comparisons is carried out on a few observations, not on millions. The sensitivity of the test statistic can then be further increased by incorporating

prior knowledge such as the spatial adjacency between source location as a constraint for cluster formation. Other advanced options for treating the MCP refer to approaches based on random field theory (Kilner, Kiebel, & Friston, 2005) and recent studies suggest comparable results for both families of methods (Pantazis, Nichols, Baillet, & Leahy, 2005). It can be stated, however, that random field theory makes stricter assumptions about the data because it specifies smoothness and distribution parameters.

1.3 Structure and scientific agenda

The previous review suggests that, to date, cortical dynamics underlying gaze processing are not sufficiently understood. Interaction oriented experimental protocols have demonstrated extended but highly contextual brain responses to eye gaze. Combined with MEG such protocols are expected to extend the scientific understanding of human gaze-processing. However, for such applications, MEG is still less standardized than fMRI and poses particular data processing challenges to the researcher. These refer to the inverse problem and the high dimensionality of the dara, which both become more difficult to master if data suffer from a low signal-to-noise ratio. This is arguably the case for subtle social cognitive comparisons in the context of interaction oriented protocols.

The goal of this thesis is to advance the neuromagnetic study of social cognition. First, by developing new a new method which helps to process low signal-to-noise data and by evaluating it on domain specific data. Second, by developing and evaluating a novel experimental MEGprotocol that contextualizes gaze processing and its related cortical dynamics with regard to social interaction.

Study 1 set out to improve the general stability of neuromagnetic findings, both within and across studies and laboratories in replacing hand-set parameter choices by automatic and data-driven parametrization. To maximize efficiency, a problem was picked that is common to nearly all source localization methods and many preprocessing procedures, the estimation of M/EEG between-sensor covariance. As has been shown by previous work (Woolrich, Hunt, Groves, & Barnes, 2011a), estimates of the M/EEG between-sensor covariance can dramatically impact final analysis results. To address this challenge, study 1 exploited state-of-the-art machine-learning techniques to achieve an automatic solution for the estimation of MEG and EEG between-sensor covariance an. Besides domain general model validation, study 1 pursued a domain-specific and practically oriented validation which was based on a publicly available dataset from an experiment which examined cortical responses to human faces. The results of study-1 demonstrate the relevance of the problem and the generality of the solution.

The goal of **Study 2** was to investigate neuromagnetic underpinnings of gaze-processing during social interaction. The study comprised two experiments. Experiment 1 set out to develop a forefront gaze processing protocol. This protocol had the purpose of orchestrating two conflicting goals. Capturing gaze-processing during ongoing interaction in a maximum naturalistic way while producing controlled neuromagnetic recordings. The protocol focussed on continuous action-perception loops as a proxy for social interaction but made use of virtual characters to control the physical properties of the stimulation. To leverage the naturalistic potential of such virtual characters, the statistical structure of gaze behavior was explicitly designed to promote the subject's entrainment to the task. The social dimension was further contextualized by varying the participant's action intentions and the social relevance characteristics of stimuli. Based on this protocol, experiment 2 allowed to systematically evaluate time-locking properties of cortical dynamics supporting gaze processing during ongoing action-perception loops.

2 Automated model selection in covariance estimation and spatial whitening of MEG and EEG signals.

2.1 Introduction

At the current state of the art, MEG applications constitute inherent mathematical and statistical signal processing challenges. A modern M/EEG analysis workflow involves segmentation of anatomical MRI data, the computation of an electromagnetic forward model, multiple data-coregistration steps, extraction of signals of interest from the raw measurements and finally a numerical solution to the ill-posed biomagnetic inverse problem (Hämäläinen, Lin, & Mosher, 2010; Gramfort et al., 2013a). This study will focus on one common problem of M/EEG analysis pipelines which is the estimation of between-sensor covariance, also referred to as spatial covariance. Interest for such covariance estimates comes from the known physics of the problem and commonly used Gaussian assumptions. Thanks to the linearity of Maxwell's equations, M/EEG data are obtained by linear mixing of brain sources, which are corrupted by additive noise. Assuming the source amplitudes to be Gaussian, the measured data are also Gaussian due to linear mixing. The additive noise is also commonly assumed to be Gaussian. Under these assumptions, brain signals and noise can be fully characterized with a mean vector and a covariance matrix. In practice signals are high pass filtered or "baseline corrected", which allows us to assume the data to be zero mean. The only quantities to be estimated from data are therefore the spatial covariances.

The problem of estimating the covariance between an array of features from multivariate samples is a problem that has been widely studied in statistics and for which various models have been proposed. In one such approach (Ledoit & Wolf, 2004; Chen, Wiesel, Eldar, & Hero, 2010), optimal coefficients are computed for the shrinkage targeting the off-diagonal terms while other contributions propose structured models with reduced rank assumptions (Tipping & Bishop, 1999; Barber, 2012). In the context of M/EEG, noise can be biological (heart beat, eye blinks, muscle activity), environmental (line noise) and sensor-related. Purely sensor-related noise can be assumed to be independent across sensors.

It can hence be modeled with a diagonal covariance matrix. In contrast, most sources of noise are structured and induce strong correlations between sensors. When estimating the spatial covariance from signal of interest as done for beamformers (Veen, Drongelen, Yuchtman, & Suzuki, 1997) or brain computer interfaces (BCI) for common spatial patterns (CSP) (Ramoser, Müller-Gerking, & Pfurtscheller, 1998), strong between-sensor correlation occur and can be explained by the following fact. If one assumes a single active source in the brain without the presence of noise, the linearity of the forward problem guarantees that the measured data span a subspace of dimension one. If one now assumes that the source rotates over time, the subspace dimension increases to two in the case of MEG and three in the case of EEG. See for example Mosher and Leahy (1998) for discussions on this matter. Low rank hypotheses are also relevant for some MEG systems where the data are projected to a low rank signal subspace for denoising. This technique is known as signal space separation (SSS) (Taulu, Simola, & Kajola, 2005). Another peculiarity of modern MEG systems is the different sensor types used during recordings, i.e. magnetometers and planar gradiometers. These impose additional difficulties to the estimation because values differ by orders of magnitude between sensors while the sources captured only partially overlap.

This study therefore evaluates various strategies for the estimation of the spatial covariance of M/EEG data under Gaussian assumptions and develops a systematic approach of deciding between these alternatives. The study will focus on two particular kinds of approaches, shrinkage covariance estimators (Ledoit & Wolf, 2004; Chen et al., 2010) and on generative low rank models, also commonly referred to as latent variable models: probabilistic principal component analysis (PPCA) and factor analysis (FA) (Tipping & Bishop, 1999; Barber, 2012). In a first step, relevant statistical models and methods and their corresponding assumptions will be introduced and related to M/EEG data and the problem of covariance estimation. Subsequently, relevant implementation strategies will be detailed. Finally, a comprehensive quantified evaluation of two classical and four alternative approaches to covariance estimation is conducted based on simulations, on sensor space analyses of different M/EEG datasets, and, on source localizations of differentially face-related cortical activity based on a publicly available dataset.

2.2 Material and methods

2.2.1 Statistical methods

Before detailing the covariance estimation models, a motivating example will be considered: the problem of source reconstruction with ℓ_2 regularization, also known as MNE. The notations which will be used for that purpose are adopted from the MNE-manual[1].

2.2.1.1 Minimum-norm estimates (MNE)

MNE employ a distributed source model that consists of a large number of spatially fixed candidate dipoles whose amplitudes are estimated from the data (Hämäläinen et al., 2010; Gramfort et al., 2013a). For the present purpose N denotes the number of sensors, M the number of candidate dipoles and T the number of time samples in the data. Following the linearity of Maxwell's equation and the assumption of additive noise, the data matrix Y of size $N \times T$ is obtained by multiplication of the forward gain matrix G of size $N \times M$ by X, the unknown sources amplitudes of size $M \times T$, to which is added a noise term E of size $N \times T$. The model reads:

$$Y = GX + E \ . \tag{2.1}$$

According to Tarantola (1987), and Lin et al. (2006) the model can then be further specified as follows. Assuming that X and E have zero mean Gaussian distributions at each time sample t, i.e. $X_t \sim \mathcal{N}(0, R)$ and $E_t \sim \mathcal{N}(0, C)$. The matrices R and C, of size $M \times M$ and $N \times N$ respectively, refer to the source covariance and the noise covariance. Assuming C and R to be known, an estimate $\hat{X}$ of the amplitudes of the dipoles located on the cortical mantle is obtained by maximum a posteriori (MAP):

$$\hat{X} = \underset{X \in \mathbb{R}^{M \times T}}{\arg\min} \|Y - GX\|_C^2 + \|X\|_R^2 \tag{2.2}$$

where $\|A\|_B^2 = \text{Trace}(A^t B^{-1} A)$. This leads to:

$$\hat{X} = RG^t(GRG^t + C)^{-1}Y \ , \tag{2.3}$$

where G^t stands for the matrix transposition of G.

The noise is said to be white if the matrix C is the identity I. In the following $C^{\frac{1}{2}}$ denotes a square root matrix of C, such that $C^{\frac{1}{2}}C^{\frac{1}{2}} = C$. Note that there is no unique square root of a matrix which refers to the problem of invertibility. If C is invertible, so is $C^{\frac{1}{2}}$. If one denotes by $\tilde{Y} = C^{-\frac{1}{2}}Y$ and $\tilde{G} = C^{-\frac{1}{2}}G$ then (2.3) is equivalent to:

$$\hat{X} = R\tilde{G}^t(\tilde{G}R\tilde{G}^t + I)^{-1}\tilde{Y} \ . \tag{2.4}$$

[1] http://martinos.org/mne/stable/manual.html#manual

In other words, after introducing $\tilde{Y}$ and $\tilde{G}$, the noise can be modeled as white. One can observe that (2.4) resembles (2.3) after replacing C by I. The process of computing $C^{\frac{1}{2}}$ and subsequently $\tilde{Y}$ and $\tilde{G}$ is called spatial whitening. The matrix $\tilde{Y}$ contains the whitened data, and $\tilde{G}$ is referred to as the whitened gain matrix.

In practice the square root $C^{\frac{1}{2}}$ is obtained from the eigenvalue decomposition under symmetry constraints of the estimated covariance $C = U_C \Lambda_C^2 U_C^t$ where U_C is an orthonormal matrix, $U_C U_C^t = I$, and Λ_C is a diagonal matrix with non negative entries. Assuming C to be full rank, it is straight forward to verify that $C^{-\frac{1}{2}} = \Lambda_C^{-1} U_C^t$ is a valid square root of C.

To reduce redundancy: (2.4) reveals that MNE actually implements what is known as Tikhonov regularization (Tikhonov & Arsenin, 1977) or Ridge regression in the field of statistical learning (Hoerl & Kennard, 1970). As a consequence, if the gain matrix and the data are appropriately whitened, general conditions of statistical regression models apply to the M/EEG inverse problem. Minimum-norm estimates, therefore, rely on the specification of the noise covariance matrix that needs to be estimated from the data. Or in other words, the inverse solution is likely to be wrong if the covariance estimate is wrong. This also holds true for most other source localization including time-domain and frequency-domain beamformers such as LCMV (Veen et al., 1997) and DISC (Gross, Kujala, Hämäläinen, & Timmermann, 2001), respectively. It likewise applies to MNE variants such as dSPM (Litvak et al., 2011) or sLORETA (Pascual-Marqui, 2002), as well as other distributed models such as minimum-current estimates (MCE) (Uutela, Hämäläinen, & Somersalo, 1999), MxME (Gramfort, Kowalski, & Hämäläinen, 2012; Gramfort, Strohmeier, Haueisen, Hämäläinen, & Kowalski, 2013b). It therefore cannot be considered a local problem.

2.2.1.2 Model selection using cross-validation

The noise covariance estimator is typically applied to segments of M/EEG data that were not used to estimate the noise covariance and that typically include both, brain signals and noise. Its quality can hence be assessed by investigating how well the model describes new data. This idea of model quality assessment on unseen data is realized by aggregating results over random partitions of the data, and is referred to as cross-validation. Since M/EEG data are assumed to follow a multivariate Gaussian distribution, parametrized by a covariance matrix C, adapting Minka (2000) eq. 16, Barber (2012) eq. 21.2.20 and Tipping and Bishop (1999) eq. 4, the log-likelihood of some data Y can be expressed as

$$\mathcal{L}(Y|C) = -\frac{1}{2T}\mathrm{Trace}(YY^tC^{-1}) - \frac{1}{2}\log((2\pi)^N \det(C)) \ . \tag{2.5}$$

The higher this quantity on unseen data, the more appropriate the estimated noise covariance C and the higher its success at spatially whitening the data. The log-likelihood, hence, allows to select the best noise covariance estimators out of a given set of models using cross-validation on left out data. The following passage will discuss candidate strategies to estimate covariance matrices from M/EEG data.

2.2.1.3 Empirical covariance and regularization

The empirical covariance matrix can be computed by $C = \frac{1}{T}YY^t$, where Y contains the sensor data of size $N \times T$. With a sufficient number of observations (T large), the sample covariance, which can be derived from maximum likelihood, is a good estimator of the true covariance. Typically, a noise covariance is computed on baseline segments preceding stimulation or for MEG on empty room measurements during which no subject is present. Outlier samples, e.g., biological artifacts, often contaminate the data and sometimes the data statistics can change over time, e.g., changes in environmental noise or changes in head position. In such situations, a limited number of samples is available causing the empirical covariance to suffer from high variance. The estimate is noisy and unreliable for further analysis.

One typical way to reduce the variance of the covariance estimator is to apply *diagonal loading*. It consists in amplifying the diagonal with a hand-selected constant which attenuates the off-diagonal elements that correspond to inter-sensor covariance:

$$C' = C + \alpha I, \quad \alpha > 0 \ . \tag{2.6}$$

The value α is the regularization parameter. This diagonal weighting of the covariance stabilizes MNE-like estimates by reducing the variance. However, the introduced bias amounts to assuming a stronger noise level which leads to underestimated amplitudes in the source estimates. This especially applies to dSPM and sLORETA where the noise variance is used to rescale MNE estimates and convert them to statistical quantities such as F or T statistics. When used in beamformers, such a regularization of the data covariance matrices tends to increase the point spread function of the spatial filters and smear the estimates (Woolrich, Hunt, Groves, & Barnes, 2011b). In addition, hand-set regularization raises a new problem, which is how to choose the value of α.

2.2.1.4 Shrinkage models of covariance

An improvement of the hand-selected regularization or shrinkage approach is provided by the Ledoit-Wolf (LW) shrinkage model (Ledoit & Wolf, 2004). This covariance model

constitutes an optimal weighted average of the invariant identity matrix and the variable empirical covariance matrix (2.7). The LW covariance estimates C_{LW} takes the form of:

$$C_{LW} = (1 - \alpha)C + \alpha\mu I \ , \tag{2.7}$$

where I stands for the identity matrix, μ is the mean of the diagonal elements of C, and α is called the shrinkage parameter. The contribution of Ledoit and Wolf, 2004 is to provide a formula to compute the optimal value for α. The solution is derived from the values of N, the number of dimensions, and T, the number of samples. It is provided in closed form and minimizes the mean squared error between the estimator and the population covariance. The underlying assumptions of the LW estimator is that the data are independent identically distributed (i.i.d.) which, as will be seen below, is not a reasonable assumption for M/EEG data. However, Ledoit and Wolf (2004) have shown that the optimal shrinkage parameter guarantees C_{LW} to be well conditioned, i.e., matrix inversion is numerically stable, and more stable than the empirical covariance.

A data-driven extension to the Ledoit-Wolf estimator can be motivated by (2.7). Instead of using the Ledoit-Wolf formula to compute α, cross-validation and likelihood estimation on unseen data can be compared over a range of α values to select the optimal regularization parameter. The optimal α can then be determined as the one yielding a covariance estimator with the maximum likelihood on unseen data. Throughout the manuscript, models with data-driven shrinkage coefficient as in (2.7) will be referred to as shrunk covariance (SC). (for additional details on the SC estimator, see the related documentation and examples from the scikit-learn library for machine learning (Pedregosa et al., 2011)).

2.2.1.5 Latent variable models of covariance

2.2.1.5.1 Probabilistic principal component analysis (PPCA) M/EEG measurements are obtained by sensor recordings at various locations in space. They include signals from the brain but also artifacts. Such signals and artifacts yield spatially structured patterns on the sensor array. For example, a source in the brain that would be well modeled by an equivalent current dipole (ECD) produces a dipolar pattern on the sensors. If this dipole does not rotate, due to the physics of the forward problem, the signal space spanned by this ECD is of dimension one. The signal space is thus said to be of rank one. Both sources in the brain and artifacts share this property of generating low rank signals on the sensors. This is for example what justifies the use of signal space projection (SSP) (Uusitalo & Ilmoniemi, 1997). The idea behind SSP is that the noise subspace is of low rank and approximately orthogonal with the subspace spanned by the brain signals of interest. Therefore, projecting the data on the orthogonal of the noise subspace will remove artifacts and therefore denoise

the data. PCA is a statistical method that is built on this idea of low rank signal space. When using classical PCA, one needs to pre-specify the number of components, which matches the rank of the subspace. While PCA was historically introduced as a method to reduce the dimension of data, or to approximate a matrix with one of lower rank, Tipping and Bishop (1999) have explained how it can be reframed as a generative probabilistic model and coined the term PPCA.

According to this perspective, PPCA corresponds to a multivariate Gaussian model where a random vector can be expressed as a random weighted linear combination of components added to some independent noise. The covariance can be decomposed as the sum of a low rank matrix and a scaled identity matrix. This statistical model transforms standard PCA into a latent variable model such as FA.

To give a more formal description of the PCA model, let K represent the number of components and y a sample generated by the model. The N-dimensional vector y is then obtained from a K-dimensional random vector w which is linearly transformed by K latent factors forming a matrix H of size $N \times K$, to which is added a fixed N-dimensional vector m and a random noise vector e (cf. Tipping and Bishop (1999) and Minka (2000))

$$y = Hw + m + e \ . \tag{2.8}$$

Both w and e are independent random vectors obtained from spherical[2] multivariate Gaussian distributions, respectively of size K and N. Following Tipping and Bishop (1999) and (Minka, 2000), the covariance can be derived from the latent variable model as follows: Without loss of generality, the covariance of w is the identity I_K and the covariance of e is $\sigma^2 I_N$

$$e \sim \mathcal{N}(0, \sigma^2 I_N) \quad \text{and} \quad w \sim \mathcal{N}(0, I_K) \ . \tag{2.9}$$

It naturally follows that given H, m and σ, the vector y is Gaussian:

$$y|H, m, \sigma \sim \mathcal{N}(m, HH^t + \sigma^2 I_N) \ . \tag{2.10}$$

As a result, the covariance derived from the PCA model is given by:

$$C_{PCA} = HH^t + \sigma^2 I_N \ . \tag{2.11}$$

The natural question is then how to estimate m, H and σ from the data, and why the standard PCA method provides estimates of these quantities. In then following, $Y =$

[2] with identity covariance matrix

$\{y_1, \ldots, y_T\}$ denotes the observed data. According to the PPCA model (Minka, 2000) the likelihood of the data is expressed by:

$$p(Y|H, m, \sigma) = (2\pi)^{-\frac{TM}{2}} \det(HH^t + \sigma^2 I_N)^{-\frac{T}{2}} \exp\left(-\frac{1}{2}\text{Trace}((HH^t + \sigma^2 I_N)^{-1} S)\right) \ , \tag{2.12}$$

where

$$S = \sum_i (y_i - m)(y_i - m)^t \ . \tag{2.13}$$

The maximum-likelihood estimates of each parameter are given by (2.14).

$$\hat{m} = \frac{1}{T}\sum_{i=1}^{T} y_i \qquad \hat{\sigma}^2 = \frac{\sum_{j=K+1}^{M} \lambda_j}{M - K} \qquad \hat{H} = U(\Lambda - \hat{\sigma}^2 I_K)^{\frac{1}{2}} Q \ , \tag{2.14}$$

where U is the matrix formed by the K top eigenvectors of S, the diagonal matrix Λ contains the corresponding eigenvalues λ_1 to λ_N while Q is a random orthogonal matrix. Importantly, to recover the principal components given by standard PCA, this matrix Q needs to be an identity matrix. From this it naturally follows how C_PPCA can be derived from standard PCA estimates.

The latter results are obtained assuming the number of components K to be known. In order to estimate this number from the data, various strategies have been developed. In Bishop (1999), Bayesian PCA has been proposed as an extensions of PPCA in which hyperparameters control the number of dimensions. This technique was used in the context of LCMV beamformers to estimate the spatial covariance of the data and its rank (Woolrich et al., 2011b). In contrast, Minka (2000) proposed a Bayesian rank estimation technique based on Laplace approximation where inference is obtained from a variational Bayes approach. The resulting rank estimate will be referred to in the following as PCA Bayes. Finally, as detailed in (Minka, 2000), cross-validation can be used to obtain rank estimates using PPCA without using additional hyperparameters as used in Bayesian PCA. With this approach, PPCA models are estimated on a fraction of the data over all possible numbers of components while the Gaussian likelihood of left out data is used as a principled quantitative measure to evaluate how well the model fits the data. The estimated number of components, K, is the value that maximizes the Gaussian likelihood of the left out data. In the course of the study the focus will be put on the two latter approaches, Bayesian estimation with Laplace approximation and cross-validation.

2.2.1.5.2 Factor analysis FA is another latent variable model that can be regarded as extension of PPCA (Tipping & Bishop, 1999; Barber, 2012). The crucial difference to PPCA is that instead of assuming spherical noise, $e \sim \mathcal{N}(0, \sigma^2 I_N)$, it assumes a diagonal covariance, $w \sim \mathcal{N}(0, \Psi)$, where Ψ is diagonal with diagonal positive entries denoted by $\psi_1, \ldots, \psi_N$. In

contrast, PPCA is said to assume a homoscedastic noise: the noise variance is the same for all variables, here all sensors. Contrastingly, FA assumes a heteroscedastic noise: the noise variance differs between sensors.

Adapting (2.11), the covariance as delivered by FA is given by

$$C_{FA} = HH^t + \text{diag}(\psi_1, \ldots, \psi_D) \ . \tag{2.15}$$

Factor analysis therefore covers a richer class of models and can be more suitable for data such as M/EEG where the noise varies between sensors, for example, due to undetected bad channels, or when combining different sensor types, e.g. magnetometers and gradiometers. The consequence of this difference between PCA and FA models, is that the component matrix in FA differs from the principal components, also referred to as principal axes of the data (Tipping & Bishop, 1999). This practically implies that the FA model parameters cannot be inferred as easily as with PPCA. Indeed, no closed form solution is available for FA. It hence relies on an iterative algorithm.

The estimation of the FA model parameters is performed using expectation maximization (EM) as described in Barber (2012). In practice each iteration consists of a spatial whitening of the data using the present estimate of the data covariance followed by an update of the components. This later step is performed with an singular value decomposition (SVD), which is also commonly used to compute the standard PCA solution. Usually a minimum of 20 iterations is necessary to reach convergence of the FA estimation on M/EEG data. FA is therefore about 20 times slower to compute than a PCA. However, thanks to randomized numerical linear algebra (Martinsson, Rokhlin, & Tygert, 2011), SVD computation can be significantly sped up making FA estimation very tractable on full datasets, even when combining MEG and EEG. Such an efficient implementation is provided in the scikit-learn machine learning library (Pedregosa et al., 2011; Abraham et al., 2014).

2.2.2 Whitened evoked response

The whitened evoked response is a sensor-space metric which is obtained by computing a matrix multiplication between the whitener and the array of sensor measurements:

$$C^{-1/2}Y \tag{2.16}$$

The resulting signal amplitudes are expected to be situated between -1.96 and 1.96 for baseline segments from which the covariance was estimated, following a standard-normal distribution.

2.2.3 Whitened global field power

After having applied the whitener, the noise can assumed to be white. The global field power (GFP) is a sensor space metric that quantifies variability over the sensor array at a given time sample. It assumes χ^2 random variable that is normalized by the number of channels. Should the dimensionality of the data have been previously reduced, the χ^2 random variable does not have N degrees of freedom but $P < N$ where P is the size of the subspace the data belong to. This typically happens when ICA, SSP or SSS has been applied to the data and its rank is reduced as a consequence thereof. This yields the following expression for computing the rank-adjusted GFP.

$$\frac{\sum_{i=1}^{P} x_i^2}{P}. \tag{2.17}$$

The resulting signals are expected to have a value of one for baseline segments from which the covariance was estimated.

2.2.4 General data analysis and software

All covariance estimators and the cross-validation were computed using the Python machine learning package scikit-learn (Pedregosa et al., 2011). The empirical covariance and the regularization were computed using the MNE software (Gramfort et al., 2013a, 2014). The FA implementation was based on algorithm 21.1 from (Barber, 2012). Estimation of FA parameters is iterative with expensive SVDs, one at each iteration. To improve suitability for cross-validation and extensive rank estimation, the author of this thesis contributed a modified implementation of Factor Analysis to the scikit-learn package, based on the randomized SVD algorithm (Halko, Martinsson, & Tropp, 2011; Martinsson et al., 2011). While producing results equivalent to a full SVD, the randomized SVD uses significantly less memory and allowed to cut computation times by up to a factor of seven[3].

The MNE software (Gramfort et al., 2013a, 2014) was used to process and analyze all MEG and EEG data.

2.2.5 Simulated data

To compare the behavior of the covariance estimators across a varying numbers of samples, four different data scenarios were simulates which can be represented on a 2 (homoscedastic VS heteroscedastic noise) $\times$ 2 (low VS high rank) grid. For each scenario, covariance estimates and rank estimates were computed for PPCA, the PCA (Bayes) and FA with a

[3] cf. https://github.com/scikit-learn/scikit-learn/pull/2406

continuously increasing number of samples. In addition, model-likelihood was computed for the Ledoit-Wolf and the SC estimator as well as for PPCA and FA. To reduce data variability, results were averaged over 50 runs using different random seeds. The data were simulated as follows: to obtain low rank data, a random $N \times N$ square matrix was computed. Number of dimensions was set to $N = 50$. In a second step, the rank of the matrix was reduced by applying a truncated SVD. The K singular vectors with highest singular values were kept to form a matrix H of size $N \times K$ as in (2.8). An arbitrary orthogonal matrix of size $K \times T$ was then used to form T independent samples that were projected using H into the N dimensional space. The outcome is a $N \times T$ dataset living in a subspace of dimension K. Finally, either homoscedastic or heteroscedastic Gaussian noise was added to the data. This was achieved by adding a $N \times T$ random matrix formed by T samples drawn from Gaussian distributions with diagonal covariances. In the heteroscedastic case the entries on the diagonal are all positive but different (each feature, sensor, is corrupted with a different noise level), while in the homoscedastic case all the entries on the diagonal are positive and equal. The rank was set to either $K = 10$ (low rank) or to $K = 40$ (high rank). T was varied between 200 and 2000 in steps of 50.

To determine the optimal SC estimator with cross-validation, estimators were computed with α varying on a logarithmic grid of 30 values between 0.01 and 1. Each estimator was then evaluated with a three-fold Monte Carlo cross-validation procedure. The optimal shrinkage was then determined based on the highest likelihoods on left out data. To determine the hyperparameter k of the low rank models, PPCA and FA were computed on a grid of rank values. K varied between one to 49 in steps of three. For the sake of completeness, 50 (the number of observed dimensions) was included in this range. Each value was used to select the number of dimensions directly. At each step, the models obtained were evaluated with the same cross-validation procedure. The estimated rank was then determined by the k parameter of the model with the highest log-likelihood.

2.2.6 M/EEG datasets

The covariance and rank estimation procedures were subsequently tested using MEG data recorded by three commercial and widely used MEG systems: 1) a 4D-Neuroimaging whole-head magnetometer system with 248 channels (MAGNES-3600WH MEG), 2) a VSM MedTech Inc. whole-head axial gradiometer system with 275 channels (CTF/VSM) using second-order axial gradiometers and synthetic third gradient for denoising and 3) a Neuromag VectorView whole-head system with 306 channels, consisting of 102 magnetometers and 204 planar gradiometers (Elekta Neuromag, Finland) each comprising two orthogonal planar gradiometers and one magnetometer.

The Neuromag dataset is shipped with the MNE software (Gramfort et al., 2013a, 2014) and includes combined M/EEG recordings conducted at the Martinos Center of Massachusetts General Hospital. EEG were recorded simultaneously using an MEG-compatible cap with 60 electrodes. Data were sampled at $600\,\mathrm{Hz}$. In the experiment, auditory stimuli (delivered monaurally to the left or right ear), and visual stimuli (shown in the left or right visual hemifield) were presented in a random sequence with a stimulus onset asynchrony (SOA) of $750\ \mathrm{ms}$.

The CTF/VSM data-set includes MEG recordings conducted by the the Functional Imaging Group, London and is available at the SPM webpage[4] (Litvak et al., 2011) and can also be downloaded using the MNE software [5]. Data were sampled at $480\,\mathrm{Hz}$. In this experiment, faces and scrambled faces were presented to the participant. The paradigm is detailed in (Henson & Rugg, 2003). The 4D-Neuroimaging dataset was kindly provided by Breuer and colleagues (Breuer, Dammers, Roberts, & Shah, 2014b). Recordings were conducted at the Institute of Neuroscience and Medicine (INM-4), Forschungszentrum Jülich, Germany and sampled at $1017.25\,\mathrm{Hz}$. In the experiment, auditory stimuli (simple sinusoidal tones at $1000\,\mathrm{Hz}$ and $2000\,\mathrm{Hz}$) were presented to the participant in a random sequence with a SOA of $1000 - 2000\,\mathrm{ms}$.

All data were bandpass filtered between $1 - 45\,\mathrm{Hz}$ using a zero-phase 4th order Butterworth filter. Low pass at $45\,\mathrm{Hz}$ excluded the power line frequencies at $50\,\mathrm{Hz}$ and $60\,\mathrm{Hz}$ for data recorded in Europe and the USA. High pass at $1\,\mathrm{Hz}$ removed low-frequency drifts as well as baseline offsets from the data. To allow the comparison of the results obtained with the different datasets, all epochs were resampled at $150\,\mathrm{Hz}$. Segments contaminated by biological artifacts were detected based on peak-to-peak amplitude and ignored during estimation to avoid distorted covariance estimates due to outliers. Note that this lead to slightly different sample sizes for some datasets.

MEG data expressed in T or T/m are very small, and close to machine precision. To improve numerical stability, data were scaled by the order of magnitude corresponding to the measurement unit. For datasets combining gradiometers and magnetometers, the latter were scaled by a factor of 0.04 as recommended by maxfilter software (Elekta-Neuromag). The estimated covariances were then rescaled to the squared measurement unit. Epochs were defined from $-200\,\mathrm{ms}$ to $500\,\mathrm{ms}$ with respect to the stimulus onset. To estimate the noise covariance, baseline segments (-200 to $0\,\mathrm{ms}$) were extracted and concatenated to form a two-dimensional matrix comprising channels and time samples.

[4] http://www.fil.ion.ucl.ac.uk/spm/data/mmfaces/
[5] http://martinos.org/mne/auto_examples/datasets/plot_spm_faces_dataset.html

Table 2.1: Overview on datasets used and corresponding legend keys

key	dataset and channel type	number of channels used
bti-mag	4D Magnes 3600 WH magnetometers	248
ctf-mag	CTF-275 axial gradiometers	274
vv-eeg	VectorView EEG electrodes	59 (1 bad)
vv-grad	VectorView planar gradiometers	203 (1 bad)
vv-mag	VectorView magnetometers	102
vv-meg-grad	VectorView planar gradiometers, combined estimation	203 (1 bad)
vv-meg-mag	VectorView magnetometers, combined estimation	102

2.2.7 Sensor space validation

The same protocol was applied to the M/EEG datasets as for the simulation. For each dataset, covariances and their log-likelihoods were computed based on each estimator. The PPCA and FA parameters were evaluated using cross-validation over a range of different values for rank parameter K from five and to the multiple of five that was closest to the actual number of channels, advancing in steps of five. Subsequently, the log likelihood, the whitened evoked response and the corresponding GFP were computed for each estimator. The procedure was executed separately for each channel type as well as for magnetometers and gradiometers combined. For the combined-sensors runs, whitening effects related to either gradiometers or magnetometers are presented separately. The acronyms used to refer to the different datasets or to the views on datasets are summarized in table 2.1.

This procedure was conducted at two discrete sample sizes, one including the first 15 epochs encompassing 450 samples, and a second one including the first 50 epochs of 1550 samples. These values reflect arbitrary choices. However, both levels approximate the lower and the upper bounds for the number of samples used for the simulation. For each dataset, whitened-evoked responses were then computed based on the covariance estimator with the highest model-likelihood. A second, purely graphical monitoring techniques was implemented by computing the whitened global field-power for each estimator and super-imposing the results separate estimator. The estimators tested on M/EEG data are presented in table 2.2 with their corresponding abbreviations. The non-whitened evoked responses are displayed in figure 2.1.

2.2.8 Source estimates

To demonstrate the practical impact of estimator quality on source localization in applied contexts, the single subject SPM-faces dataset described above was analyzed at the source level using the above covariance estimation and selection procedure. This dataset was chosen because it implicates experimental contrasts relevant to cognitive and social-cognitive

Table 2.2: Overview on covariance estimators used in concert with M/EEG data

key	estimator
Raw	Empirical covariance computed from restricted number of epochs
Reg	Regularized covariance with $\alpha = 0.1$ (default regularization parameter in the MNE software)
LW	Ledoit-Wolf estimator
SC	Shrunk covariance with cross-validation
PCA	Probabilistic PCA with cross-validation to set K
FA	Factor analysis with cross-validation to set K

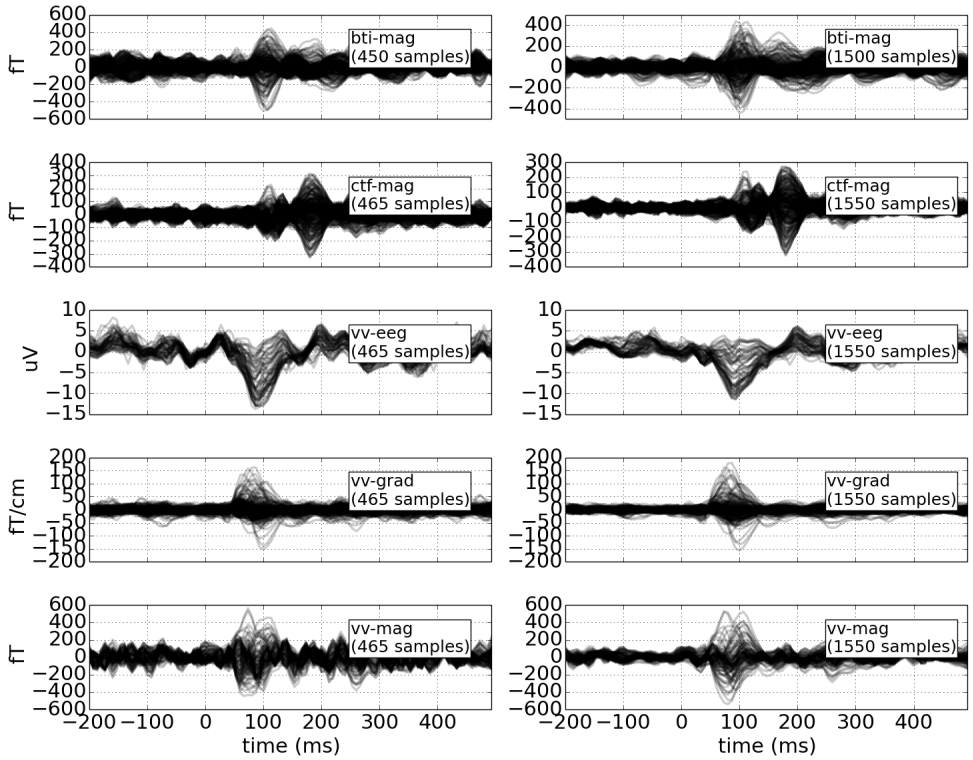

Figure 2.1: Non-whitened evoked responses of all datasets for 15 epochs (450 samples) and 50 epochs (1500 samples).

neuroscience. Data were exactly preprocessed as for the sensor-space validation. MNE source estimates were then computed separately for the faces and the scrambled faces condition. Resulting maps of cortical activity maps were then subtracted to form a paired contrast. Except for the covariance parameter, MNE estimates were computed using the default parameters proposed by the MNE-software. The regularization-parameter $\lambda 2$ was set to $1.0/SNR**2$ where, SNR refers to the signal-to-noise ratio parameter which defaults to 3. A depth-weighting of 0.8 was used in combination with a loose-constraint of 0.2 and free orientation. The parametrization of MNE will be commented in greater detail in study 2 where it is more relevant to the analysis (c.f. 3.2.2.6.4). The dSPM procedure was used for noise normalization. This resulted in unsigned dSPM source estimates reflecting normalized current magnitude. Positive values resulting from a paired contrast

of the form $dSPM_faces - dSPM_scrambled$ therefore reflect activity specific to the faces condition. To quantify differential statistical properties of the resulting dSPMs, means and standard deviations were computed across source locations, and, subsequently their temporal maxima.

To asses the differential impact of covariance estimation, this analysis was conducted over varying numbers of epochs using both best and the worst covariance estimator as parameter for the MNE computation.

2.3 Results

2.3.1 Simulated data

Figure 2.2 presents the rank estimation results based on PPCA, Minka's Bayes PCA (Minka, 2000), and, FA. All three estimators recovered the true rank of the data when noise was homoscedastic. When heteroscedastic noise was present, only FA was able to recover the true rank, irrespective of the true rank (10 or 40). When the noise was heteroscedastic, dramatic overestimations of the true rank occured for PPCA. Furthermore, it can be observed that PPCA and FA only produced stable results if the sample size exceeded a minimum of roughly 350 samples. This is further illustrated in Figure 2.3 which shows the model likelihoods of the covariance estimators. For all conditions, the model likelihood increased with the number of samples, and most steeply in the range where the rank estimates exhibited high instability. In the low rank scenario, the latent variable models were unequivocally more appropriate than the "unstructured" shrunk covariance models. For homoscedastic noise and a rank of 10, both PPCA and FA performed equal. When noise was heteroscedastic, FA had the highest model likelihood across the entire sample range, followed by the shrunk covariance models and PPCA. However, differences between the other estimator's performance disappeared with increasing number of samples. In contrast, the high rank scenario was governed by a different regime. Independent of the noise structure, a clear performance pattern emerged where SC exhibited the best results at a low number of samples while the probabilistic latent variable models only gradually improved with increasing numbers of samples, ultimately reaching comparable model probabilities.

2.3.2 Sensor space validation

2.3.2.1 Rank estimation

The results on M/EEG data are presented in figure 2.4. Probabilistic PCA and FA both indicated a low rank structure for the data, except for the EEG scenario with the larger

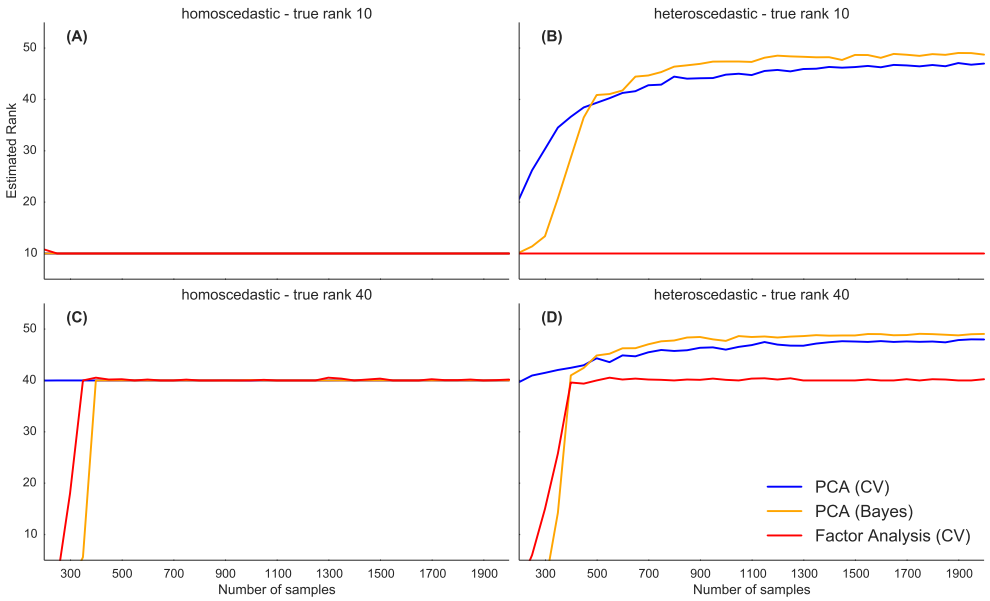

Figure 2.2: Comparison between rank estimators on simulated data. Panel (A) homoscedastic noise, ground truth rank of 10. All rank estimators converge. Panel (B) Same ground truth as in A) but heteroscedastic noise. Only FA recovers the true rank. Panel (C) homoscedastic noise, ground truth rank of 40. The low rank estimators converge, however, the sample size must be sufficiently large for FA and the PCA Bayes rank estimation procedures. Panel (D) same rank as in (C), heteroscedastic noise. Note that FA consistently recovers the true rank of the data but only if the number of samples exceeds a minimum.

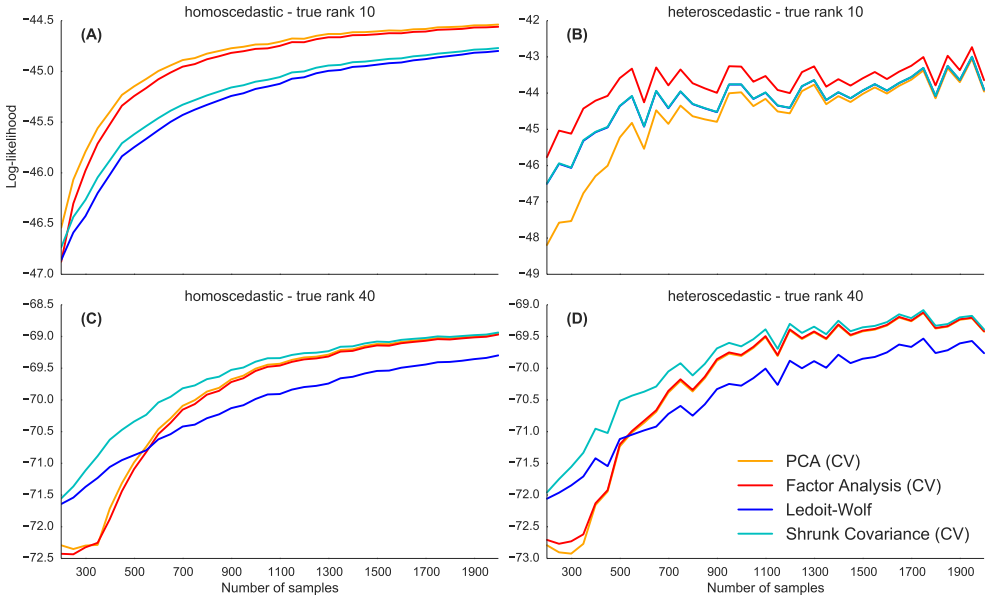

Figure 2.3: Comparison between different covariance estimators on simulated data. Panel (A) homoscedastic noise, ground truth rank of 10. Low rank models exhibit a higher model likelihood than shrunk covariance models. Panel (B). Same ground truth as in A) but heteroscedastic noise. FA exhibits the highest likelihood across different numbers of samples. Panel (C) homoscedastic noise, ground truth rank of 40. The SC covariance has the highest likelihood with few samples available. The likelihood for FA and PCA model improves with increasing numbers of samples and finally reaches the level of SC. Panel (D). Same rank as in C) with heteroscedastic noise. The same pattern emerged as in D).

sample size where PPCA suggested full rank. On average, the FA rank estimate ($M_K = 35.833, SD_K = 14.410$) was lower than the PPCA rank estimate ($M_K = 42.083, SD_K = 17.376$). Second, the estimated rank was generally higher for the high number of samples ($M_K = 26.667, SD_K = 1.952$) as compared to the low number of samples scenario ($M_K = 51.250, SD_K = 0.203$).

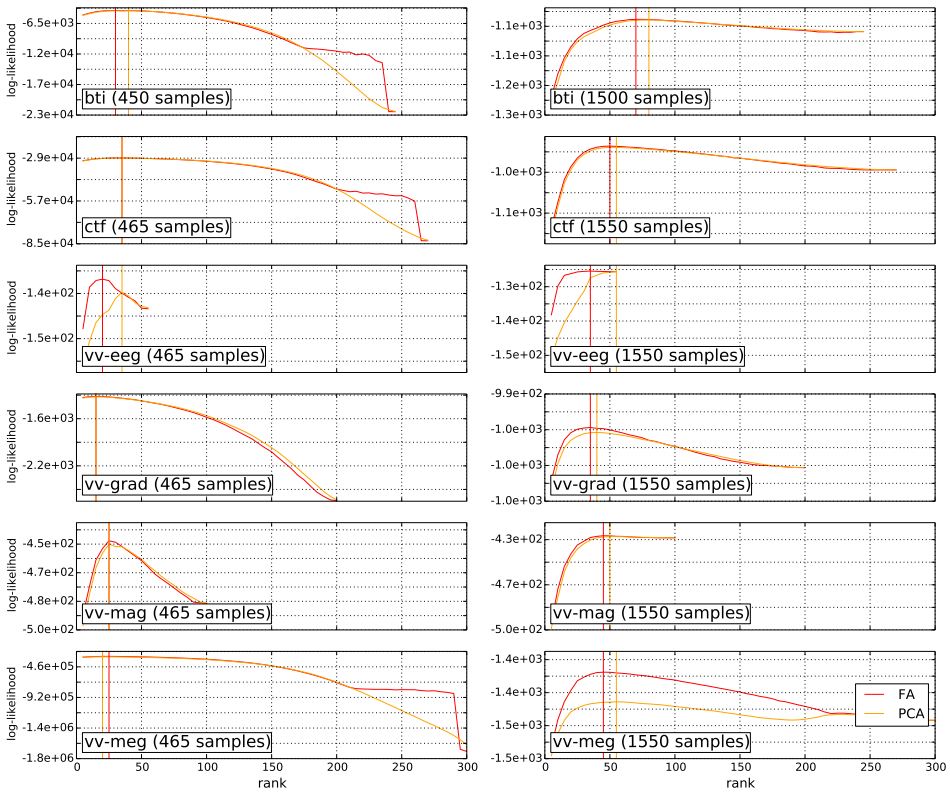

Figure 2.4: Rank estimates for low and high numbers of baseline samples computed on the different datasets. The estimated rank was higher when increasing the number of samples. FA always outperformed PCA suggesting that M/EEG noise is heteroscedastic, not homoscedastic. One also observes that PPCA rank estimates are almost always than equivalents estimated with FA.

2.3.2.2 Model likelihood

The model likelihoods of the covariance estimators are reported in figure 2.5. Three main observations can be made. First, the automatically selected covariance estimator were consistently more appropriate than the empirical covariance. Second, FA and SC consistently delivered better models than PCA and LW respectively. The SC estimator prevailed where the number of samples was lower while FA produces the most appropriate fit when applied to multi-sensor datasets or when the number of samples was high.

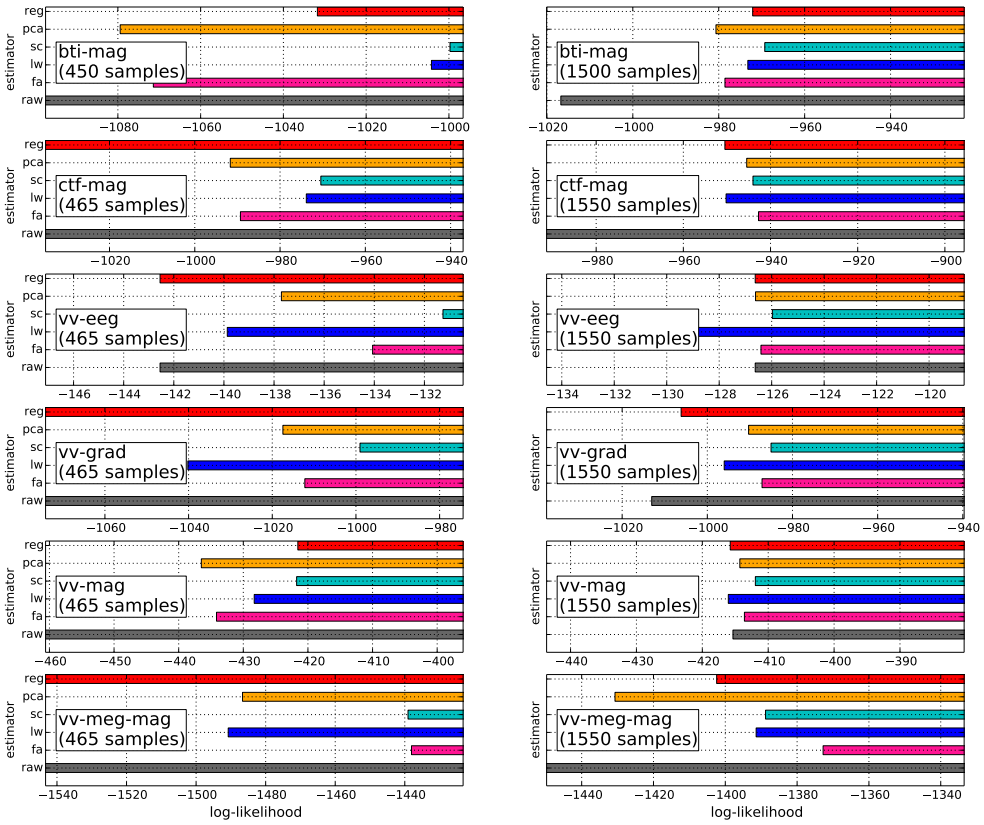

Figure 2.5: Log-likelihoods of covariance models for low and high numbers of baseline samples obtained on the different datasets. Either cross-validated SC or FA turned out to the best model. FA was always more appropriate than PCA. Except for the multi-sensor dataset, FA outperformed SC only when the number of samples was high. In most cases, standard regularization either under- or overestimated the baseline noise.

2.3.2.3 Whitened global field power

In figure 2.6 whitened GFPs are presented for each estimator. The GFP dynamics exemplify respective under- and overestimation tendencies. The black dotted horizontal line indicates the expected value for white Gaussian data. GFPs values below and above this line correspond to overestimation and underestimation of the noise level, respectively. When the noise is underestimated, that is when normalized GFPs is below one, the procedure is said to underfit. In contrast, it is said to overfit if the noise is greater than one during the baseline periods (between -200 and $0\,\mathrm{ms}$). The huge deflections in the post-baseline window represent time-locked brain responses.

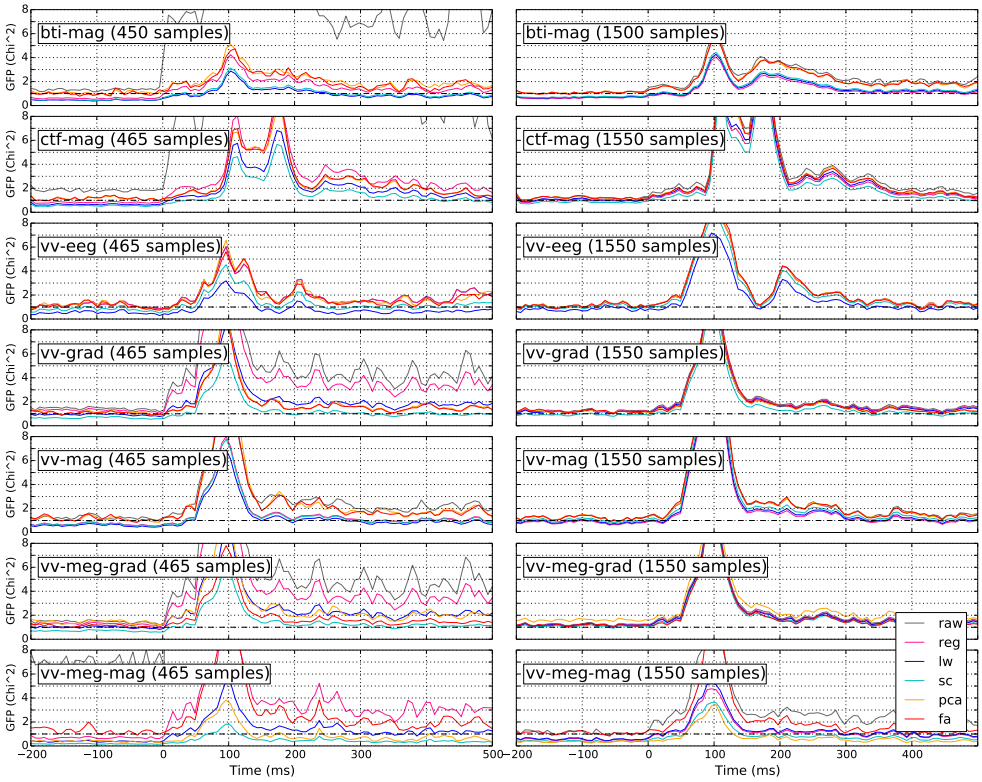

Figure 2.6: Global field power (χ^2 statistic) of whitened evoked data for low and high numbers of baseline samples and different datasets. The dotted vertical black represents the expected baseline amplitude of one, given Gaussian baseline data.

In four out of seven datasets the empirical covariance produced clearly visible overfitting while the regularized covariance tended to underfit the noise. However, in almost any other case, differences seem hard to distinguish by mere visual inspection.

2.3.2.4 Whitened evoked response

Figure 2.7 shows whitened evoked responses for each dataset where the whitener was computed from the best fitting covariance estimator determined by its log-likelihood on

unseen data. Except one case, where hand-set regularization was most-appropriate, either SC or FA performed best.

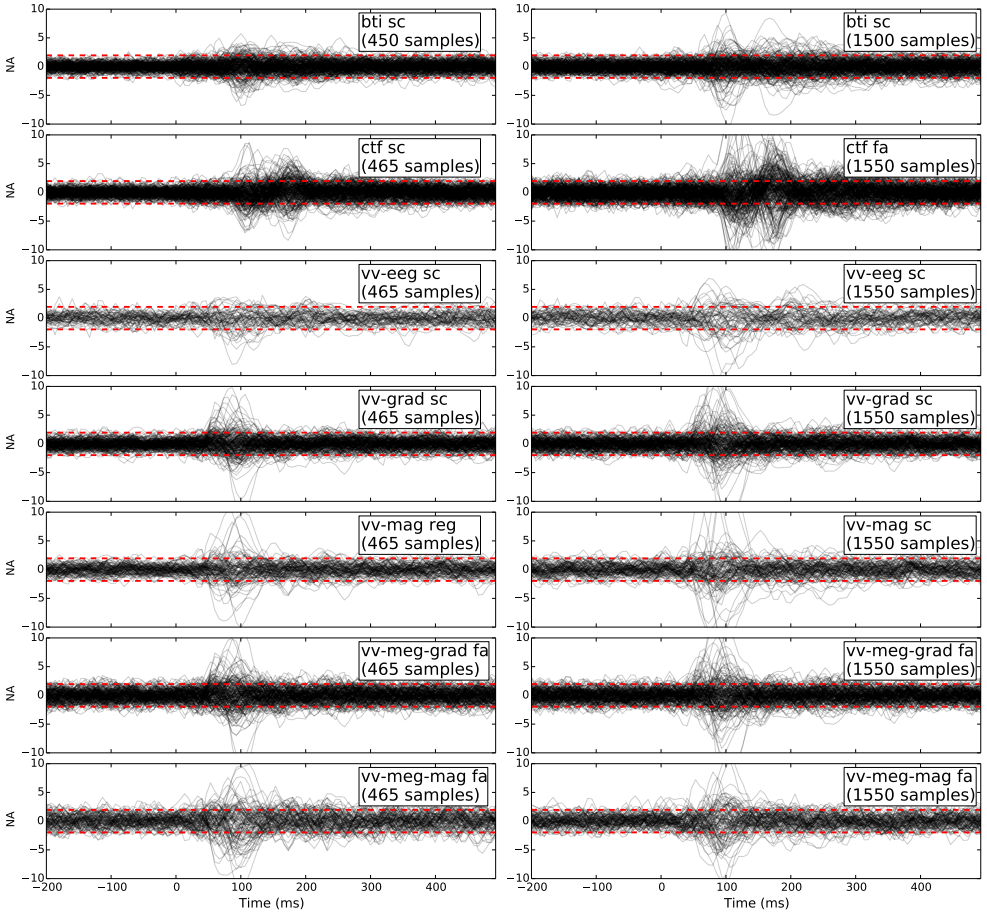

Figure 2.7: Time-locked whitened with the optimal covariance model for low and high numbers of baseline samples and different datasets. Selection based on results depicted in figure 2.5.

2.3.3 Source estimates

The impact of covariance estimation was practically examined by computing signal contrasts that reflect cortical activity related to face perception over a range of different numbers of epochs for both the worst and the best estimators. Figure 2.8 depicts contrast-results for 20, 40, and 60 input epochs, respectively. When comparing spatial signal dynamics across epochs, the best covariance estimator showed less variability while the worst estimator drastically changed depending on the number of epochs. This higher consistency for source estimates based on the best estimator were also reflected in more consistent spatial extents of the cortical activity. With 20 epochs of input data, the best estimator still showed a pronounced ventral-temporal center of activity in the mid-FG, a brain region commonly associated with processing of faces. In contrast, the worst estimator lead to source estimates which suggest strongly increased and extended activity for nearly the entire ventral part

of the temporal lobe. In general, differences between the best and the worst estimator decreased with increasing numbers of epochs.

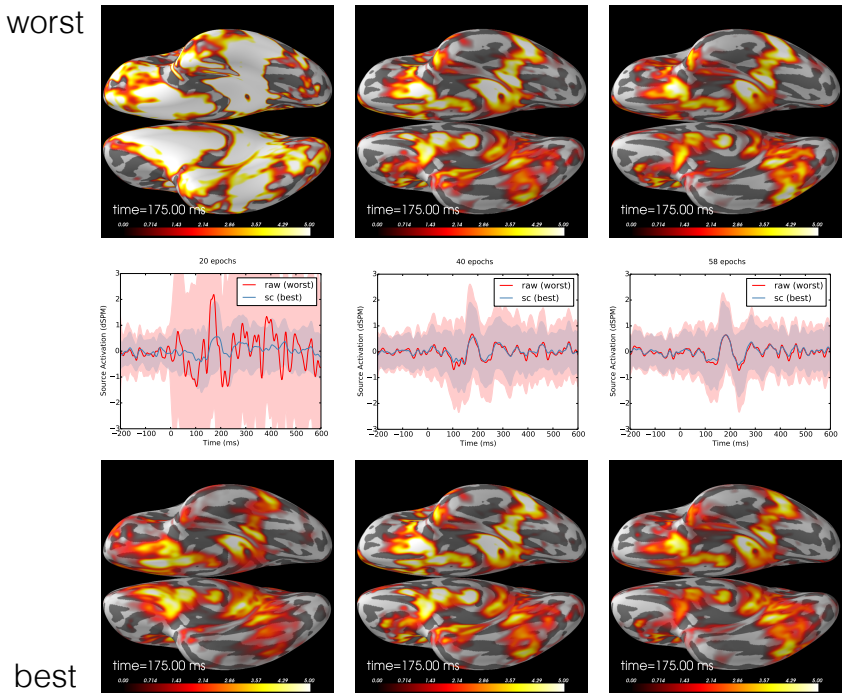

Figure 2.8: Worst and best covariance estimators for faces > scrambled contrast. The top row represents statistical parametric maps around 175 milliseconds for the worst covariance estimators. The mid-row represents average temporal dynamics for worst and best estimators superimposed. The bottom-row represents statistical parametric maps around 175 milliseconds for the best covariance estimators. The columns refer to results for 20, 40 and 60 epochs of input data, respectively. Statistical maps are constantly thresholded with a maximum at the 99th percentile. For comparability to other studies, results are shown on the FreeSurfer average brain's inflated surface in ventral view. The curvature of the cortical surface is indicated by light and and dark gray colors for gyri and sulci, respectively.

2.4 Discussion

The present study addressed the problem of data-driven regularization of spatial covariance estimates computed on M/EEG data. Such covariance estimates are a building block of most M/EEG data analysis pipelines. Their particular use case refers to spatial whitening of data which is required by most distributed source localization methods. This problem was approached by employing model-selection with cross-validation. In detail, the log-likelihood of the covariance was proposed as a metric to select the best model out of a set of alternative covariance estimators. In addition to empirical and regularized covariance estimates which reflect common standard choices, Gaussian covariance models, i.e. shrinkage estimators and latent variable models, were subjected to model-selection. Data were validated by

simulations, sensor-space metrics and, practically, by source localization of an experimental contrast from a social-cognitive science MEG experiment.

Both, simulation and sensor space results unequivocally demonstrated that there was not one single model that fitted all scenarios and datasets. Different global parameters, such as sample size, the true number of dimensions, the noise structure, and, the sensor type shaped the log-likelihood of the covariance estimators. The simulation suggested that covariance models based on latent variable models delivered a more appropriate covariance estimate if the true rank of the data was low and the number of samples was sufficient. In detail, given a sufficient sample size, FA was the best model when the structure of noise was heteroscedastic while probabilistic PCA performed best with homoscedastic noise. This stands in contrast to the M/EEG study were PPCA never achieved the highest model probability on any of the M/EEG datasets. However, the sensor-space validation suggests that on M/EEG data two solutions are likely to be selected, either favoring FA or SC models. In this context it is helpful to recapitulate differences between FA and PCA. Due to its diagonal noise term, the former tends to generate more complex noise models that can handle varying noise levels across channels. FA can therefore describe the data with fewer dimensions. This is because in such latent variable variance that is not captured by the components is captured in the noise term. However, complex models require more samples than simple models. Simulation and sensor space findings are consistent with these characteristics in suggesting that FA lead to a lower rank estimates than PPCA but was only preferred when the number of samples was sufficiently high. Second, in the multi-sensor dataset only FA produced appropriate noise estimates for combined sensor types. Also, in other cases where FA was selected the number of samples was higher, not lower. In contrast, if analysis was constrained to one sensor type, SC was selected irrespective of the sample size. Taken together, these findings indicate that the model likelihood may depended on the system type and the recordings themselves in ways which are not sufficiently understood. In this sense, M/EEG data problems are subject to the "no free lunch theorem" (Wolpert, 1996). In practice, these findings suggest to evaluate at least FA, SC in addition to the default regularization and to then chose the best model using cross-validation on unseen data.

Combining simulation and sensor-space results reveals a basic M/EEG signal-chracacteristic. Sensor noise is heteroscedastic, and not homoscedastic. This is reflected by the fact that on MEG data PPCA models never prevailed, whereas such models were preferred under certain simulated conditions. M/EEG methods should, therefore, focus on models that take into account the variable sensor noise in M/EEG. This aspect seems only partially covered by the literature. Examples are given by research on ICA in neuroimaging (Beckmann & Smith, 2004; Hyvärinen, Karhunen, & Oja, 2004; Dammers et al., 2008) and approaches which

leverage FA for source imaging and artifact rejection (Nagarajan, Attias, Hild, & Sekihara, 2007; Zumer, Attias, Sekihara, & Nagarajan, 2007, 2008).

The sensor space findings demonstrate another important implication of this study. In the context of model selection, mere visualization is insufficient to assess the quality of the whitening step. Two visual inspection methods have been demonstrated, namely GFP plots and whitened evoked plots. Both provide with basic diagnostics for spatial whitening but only provide with limited guidance on how to rank the different models. To go beyond graphical data exploration, the multivariate Gaussian log-likelihood score evaluated on left out data can be regarded an unbiased quantified measure of estimator performance. Estimating the log-likelihood of the covariance given unseen data is equivalent to estimating the amount of whitening. Assuming that the whitened noise covariance is an identity matrix, this quantity measures how close the covariance of the whitened data approximates the identity matrix. Or, put differently, to which degree the data will be whitened by a whitening operator computed from the covariance estimator under question. In other words, it is a quantified measure of the success of the spatial whitening procedure.

Importantly, the log-likelihood procedure is closely linked to commonly neglected aspect of M/EEG data analysis. Since the log-likelihood was evaluated on data that were not used for parameter estimation it measures what is called in machine learning the 'out of sample performance' (Breiman & Spector, 1992). This is relevant, since, in fact virtually all whitening operations on M/EEG data are applied to time intervals which were not used for the estimation of the noise model, i.e., post-baseline time-locked signals which reflect brain activity in addition to noise. Likewise, often the MEG noise covariance is not even computed from the dataset analyzed but from so called empty room recordings, which correspond to measurements during which no subject is present. Such empty room recordings are commonly used when running time frequency analyses and are regarded as mandatory for resting state analyses (Lin et al., 2004; Hämäläinen et al., 2010; Gramfort et al., 2013a). As a consequence, goodness of fit measures computed on unseen data generally desirable. Based on formula (2.5), the procedure that was developed and evaluated in this study can be easily generalized to any covariance estimate, even beyond the estimators that were investigated in the present context. Importantly, this new method can be used with any kind of inverse solution, whether of MNE type or beamforming type. These findings are expected to be even more relevant for beamformers, since their estimation typically relies on two covariance estimates, one that aims to describe the spatial structure of noise, and one that is concerned with the spatial structure of the data.

The practical impact assessment on a publicly available social-cognitive neuroscience dataset demonstrated at least two critical implications. Across varying amounts of learning exposure, the best estimator lead to more stable source amplitudes and spatial variability thereof.

Around 20 epochs this effect was dramatic, when compared to the worst estimator that lead to massive expansion of the cortical surface considered to represent active sources. The best estimator still estimated the same contrast-amplitudes with only 20 trials of exposure compared to three times as many trials. This new procedure is therefore expected to render datasets tractable for which a covariance estimate from baseline segments is preferred and which only consist of few epochs (see, for example (Lu, Jiang, Bi, Liu, & Yao, 2014)). But more importantly, it can be expected to reduce overall variability in source estimates across subjects. The source localization results suggest an asymptotic trend towards convergence between the worst and the best estimator. Consistent with the simulation findings, with increasing numbers of epochs their differences was becoming increasingly smaller. But, practically, stability differences are still visible when comparing results between 40 epochs and 60 epochs exposure which refers to a more common scenario than the previously mentioned analysis of events that occur at a very low rate. This implies that the worst covariance estimator which turned out to be the default empirical sample covariance, will lead to increased variance as a function of different numbers of epochs. This case is practically relevant if one assumes that, for a group of subjects different numbers of trials will be selected, based on behavioral and artifact-related exclusion criteria. It is then easily conceivable that different epochs counts can lead to a ramping-up of variance which will be prevented by a robust estimator that exerts a stabilizing impact on the amplitudes of source estimates.

To the best of the authors knowledge, this is the first time that an automated procedure based on cross-validation on unseen data has been employed for model selection in spatial whitening of M/EEG data and has been validated on source localized contrast signal relevant to the broader cognitive neuroscience community. To avoid an unbalanced view, related subjects need to mentioned though. One such approach has been recently proposed by (Woolrich et al., 2011b) who employed Bayesian PCA (Bishop, 1999) to estimate noise and data covariance matrices in the context of beamforming. Bayesian PCA is an alternative approach to infer the number of latent components in the PCA model. It solves this problem using a Bayesian inference approach, what is here achieve with PPCA (maximum-likelihood instead of Bayesian) and cross-validation (to avoid overfitting). Practically, as with the PPCA and FA estimators, the amount of regularization and the number of components is learned from the data. Also, the Bayesian PCA model is not specific to one M/EEG inverse problem. It can hence be plugged into any M/EEG imaging technique that is formulated as a constrained linear model. However, the method presented in the present study goes beyond the Bayesian PCA (Woolrich et al., 2011b), as it quantifies the benefit of each modeling assumption and can select the best estimator over a richer class of models. This is an important consideration since latent variable models can be outperformed by shrinkage

when few samples are available for estimation. Second, Bayesian PCA is a PCA model and hence assumes a homoscedastic noise which has been shown to be a suboptimal assumption for M/EEG data.

More advanced models have been proposed in which the baseline noise covariance is estimated jointly with the post baseline data covariance (Nagarajan et al., 2007; Zumer et al., 2007, 2008). However, these approaches are particularly tailored for beamformer methods and not for MNE-type inverse solvers which do not rely a post-baseline data covariance.

It is important to note that the proposed approach is subject to certain numerical constraints. The computation of the low rank estimators can result in numerical errors if the data is rank-deficient. As a consequence, at the current stage of development it is recommend to compute the PPCA and FA models before applying processing steps such as SSS, SSP or ICA (Uusitalo & Ilmoniemi, 1997; Hyvärinen et al., 2004; Taulu et al., 2005). Second, outlier samples may strongly distort model selection in certain estimators, especially FA. It is therefore recommended to remove heavily corrupted time segments before estimation.

To conclude, this study has developed an automated procedure to tune covariance estimates computed from M/EEG data. This method establishes a quality-preserving function, since it will lead to estimates that will not fall behind the default empirical covariance. Indeed the result of the automatic whitening performance was in almost all cases more accurate than whitening based on hand-set regularization. But it was always preferable to the empirical covariance. However, for the unlikely case that all other options fail, the empirical covariance would be selected as fall-back option. Automatic whitening, hence, constitutes a solution to the regularization problem and helps avoiding ad-hoc parametrization and other heuristics that are difficult to generalize across the variety of M/EEG data analysis pipelines. The impact demonstration on face-related signal contrasts suggest that this study contributes one small but important element in a set of measures which help promoting laboratory- and data-independent analysis pipelines which are so urgently needed to improve reproducibility of M/EEG research (Gramfort et al., 2013a; Gross et al., 2013; Gramfort et al., 2014).

3 Neuromagnetic decomposition of eye gaze during ongoing social interaction

Gaze processing is a fundamental primate capacity which has undergone substantial phenomenological differentiation during hominoid evolution (Call, 2009; Yovel & Freiwald, 2013). These modifications are reflected in structural expansion and differentiation of brain networks concerned with gaze-processing (Van Essen & Dierker, 2007; Mars, Sallet, Neubert, & Rushworth, 2013). Recent findings show how context shapes cognitive processing and cortical dynamics in humans (for example see Bar et al. (2005, 2006)) and numerous study detail cortical dynamics related to stimulus-driven processing of gaze (Watanabe, Kakigi, Miki, & Puce, 2006; Sato, Kochiyama, Uono, & Yoshikawa, 2008; Ulloa, Puce, Hugueville, & George, 2014). Little is known however how social interaction and intentional contexts shape visual time-locked cortical dynamics. As social interactions can be conceptualized as multi-person action-perception loops in which actions and perceptions are mutually related (Hari & Kujala, 2009), it is also less plausible to assume purely stimulus-related cortical dynamics during visual gaze-processing. This refers to commonly employed MEG study protocols which compare gaze or face related neuromagnetic recordings to baseline segments in which both visual stimulation and social context are absent (see for example Sato et al. (2008)). In such situations the exposure to social materials is known to trigger stimulus-related cortical dynamics in visual gaze processing. This can be assumed to reflect the general fact that in such situations perceptions and ensuing representations have to be constructed in the first place. As a result, related time-locked signals are referenced to a context-free baseline. In contrast, little is known about the dynamic response-characteristics of gaze-relate during ongoing interaction in which such representations are, literally, in action already. Schilbach et al. (2013) recently suggested that during ongoing interactions which contrast with passive observation, patterns of brain activity are tuned by social context, reflecting subtle predictions of others' behavior and preparation for action. It is therefore conceivable that the role of visual gaze-perception is reconfigured to subserve the needs of ongoing action and perceptual contexts. This reconfiguration could be expressed in preferential time-locking characteristics of gaze-related visual processes. If these are assumed to subserve cognitive processes which relate to ongoing social actions and interactions, one would expect preferential response-locked patterns, not stimulus- or gaze-locked patterns.

While response-locked analysis of neuromagnetic signals is not a new technique (Libet, Gleason, Wright, & Pearl, 1983), response-locked visual activity is commonly not reported in the context of face or gaze related studies. Similarly, to date, no systematic reports seem available that strictly compared expected effects with regard to preferential time-locking.

The goal of this study is to investigate preferential time-locking properties of cortical dynamics in visual gaze-related areas during ongoing social interactions. This goal is addressed by comparing cortical activity time-locked to perceived changes in eye gaze and time-locked to the subject's motor acts which closely followed perceived changes in eye gaze. To relate these events at a functional and cognitive level, a task is employed which models ongoing social interaction by establishing ongoing visual and motor processing of eye gaze. The study comprises two experiments. The first experiment optimized an existing social stimulus response compatibility (SSRC) protocol and evaluated it in terms of its capacity to establish ongoing gaze-related action perception loops. The second experiment repeated the first experiment with a second set of participants and concomitant neuromagnetic recordings.

3.1 Experiment 1

3.1.1 Objective and hypotheses

The goal of the present experiment was to establish an SSRC protocol and evaluate it with regard to the following criteria,

1. to link gaze-processing to the subject's own action-intention,
2. an enriched, quasi-naturalistic stimulation that activates 'hot' processing by entraining the subject.

To investigate how eye contact reconfigures cognition during ongoing action, researchers recently proposed to use protocols in which subjects are exposed to ongoing socially relevant visual stimulation while observing a target action they are asked to act upon. Such protocols are commonly referred to as a SSRC task and often they go along with an enriched and quasi-naturalistic context commonly implemented by continuous, blockwise visual stimulation based on video clips of a real person or animated virtual characters who perform certain target acts, such as hand, finger, or, eye movements. The social context is commonly modified by alternations between mutual and averted gaze. Importantly, in SSRC tasks, the intentional context of observing these target acts is modified by requiring persons to perform congruent or incongruent actions with respect to the observed person which helps to involve the subjects in an active manner. This modification of intention is commonly achieved by instructions previous to the stimulation. This is highly relevant for the present purposes as

it contextualizes visual perception with ongoing action plans without requiring subjects to process additional task-relevant cues as for example in a gaze-cueing or Posner task (Posner, 1980). The impact of gaze-processing on ongoing action can than be measured in terms of a modulation of reaction time differences between congruent and incongruent actions by eye gaze. To strengthen the link between action and perception and to trigger non-reflective automated processes, subjects are typically required to respond as accurately and as fast as possible. The SSRC protocol was based on a recent study by Schilbach et al. (2010) in which the social context and the target acts were implemented by eye contact and eye gaze, respectively. Following Wang, Newport, and Hamilton (2011) only human stimuli were used to modulate social context, and eye contact was varied in terms of direct and averted gaze.

The temporal structure of the paradigm was adjusted to the purposes of the MEG study. For MEG, jittering of inter-stimulus intervals does not serve the function of sampling the BOLD signal. Instead, the signals of interest referred to transient changes at the order of tens to hundreds of milliseconds. To advance the task's potential of entraining the subject to the ongoing interaction, inter-stimulus-interval (ISI), i.e., intervals between changes of eye gaze, were chosen to follow a Gaussian distribution. With a Gaussian distribution of ISIs, single events should not be consciously predictable provided the variance of the ISIs is sufficiently high. On the other hand, a Gaussian distribution should help to facilitate implicit prediction of changes in eye gaze. As inter-saccadic intervals do not follow a uniform distribution in nature but, depending on the context, can be normally or log-normally distributed (McPeek & Keller, 2002; Credidio, Teixeira, Reis, Moreira, & Andrade Jr, 2012), the chosen distribution characteristics are expected to create a more naturalistic stimulation. Interestingly, both the duration of direct gaze and the duration of laterally averted gaze exhibit optima with regard to social function and have been shown to modulate sympathy attribution (Kuzmanovic et al., 2009) and the perception of sharing attention (Pfeiffer et al., 2012), respectively. The distribution characteristics and the event timing were chosen according to these findings.

The experiment pursues the following hypotheses.

1. Gaze perception under congruent intention evokes lower reaction times.
2. The reaction time difference reflecting congruent vs incongruent intentions are modulated by eye contact.
3. The distribution of the subject's inter-button press intervals follows the distribution of ISIs and the distance between them is modulated by the task.

3.1.2 Methods

3.1.2.1 Participants

27 right handed volunteers (14 female, 13 male) between of 18 to 46 years of age (male: M = 29.99, SD = 9.426; female: M = 29.309, SD = 7.409) participated in experiment 1. All volunteers were naïve with respect to the purpose of the study. All volunteers gave informed written consent to the study protocol.

3.1.2.2 Experimental protocol

3.1.2.2.1 Design and task Participants completed an SSRC task. The experiment followed a 2 (action intention: congruent versus incongruent) $\times$ 2 (social context: direct versus averted gaze) design. The task comprised a micro structure (trial) and a macro structure (block). A block began with the action instruction, either congruent ('gleich') or incongruent ('gegen') followed by a continued visual presentation of a human face (either male or female) that lasted for about 50 seconds. Within one such block, 12 trials were presented. Each trial was composed of an contact phase and a lateral changes of eye gaze (to the left or to the right) that served as target events. Subjects were required to respond to target events with an ipsilateral or a contralateral key-press during congruent ('gleich') and incongruent ('gegen) blocks, respectively.

For the entire duration of one block, the faces displayed direct gaze or averted gaze during the eye contact phase. The conditions were presented in random order and were counter-balanced. Participants where instructed to respond as quickly and accurately as possible.

The time between two gaze shifts was artificially subdivided into two time windows for procedural reasons, one before the gaze shift and one after the gaze shift. Three uniform jitters were drawn from an identical uniform distribution to produce structured ISIs following a Gaussian distribution. The time-window before the gaze shift was jittered between 1000 and 1750 milliseconds. The duration of the virtual character's lateral eye gaze was jittered between 400 and 800 milliseconds. The time after the lateral gaze shift was jittered between 350 and 1675 milliseconds. According to the central limit theorem Feller, 1945 the inter-stimulus-intervals should therefore approximately converge on a Gaussian distribution with a mean around 3 seconds. To help subjects sustain their attention, the avatar performed an eye blink on 50 % of the trials that lasted about 70 ms. A constant delay of 800ms was added to each trial to allocate time-windows of non-interest in case more samples are needed for covariance estimation or spectral analyses. Figure 3.2 depicts the expected distribution for these timing parameters.

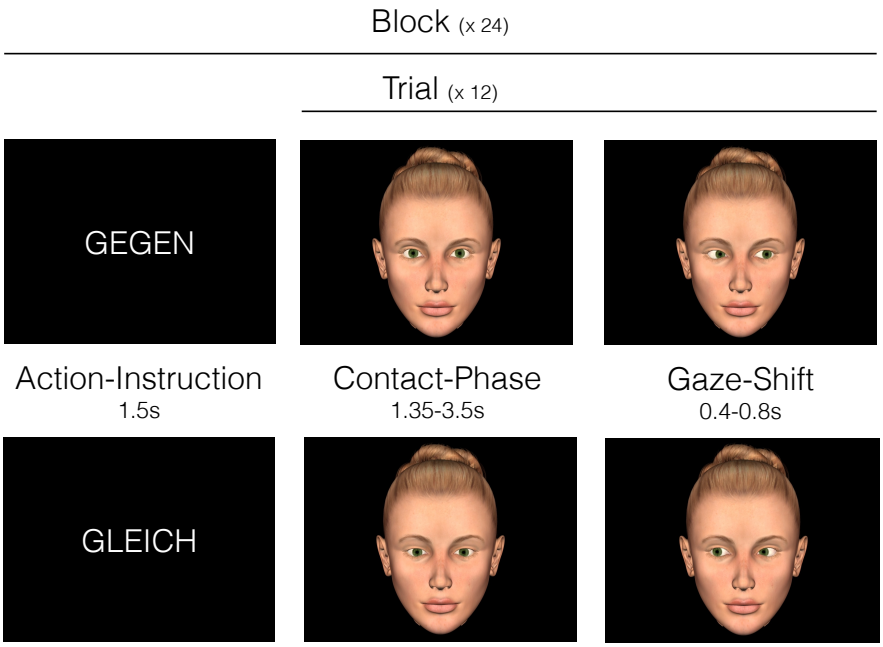

Figure 3.1: Stimulus materials and procedure.

3.1.2.2.2 Stimulus materials The faces were created using the commercially available Poser 8 application (Smith Micro Software, Inc., Columbia, USA) for Max OS X 10.6.8. The face stimuli comprised a male face and a female face and were used as shipped with the software. For each face a set of 4 images was created that encompassed straight direct gaze, straight but downward-gaze as well as gaze, laterally deviated to the left and right. Intermediate images were used for creating the impression of smooth movement. Additional images showing the faces with eye lids closed were produced to create short blinks that served to refresh the subject's attention and promote a more natural visual experience. The facial expression and the vertical position of straight gaze were chosen based on the author's subjective perception of mutual eye contact. An internet-based pre-study based on 370 participants established that the stimuli consistently varied the impression of eye contact over a wider range of persons.

The stimuli were animated using the Python language (2.7) and the PsychoPy toolbox (Peirce, 2007, 2008).

3.1.2.2.3 Procedure The experiment was conducted at the Institute of Neuroscience and Medicine (INM-3), Forschungszentrum Jüelich. The protocol was administered in a dedicated psychophysical examination booth. The experimental stimuli were presented on a monitor with a resolution of 1280 $\times$ 720 pixels with a refresh-rate of 60Hz at a visual angle of $4°$. The difference between straight-direct gaze and straight-averted gaze

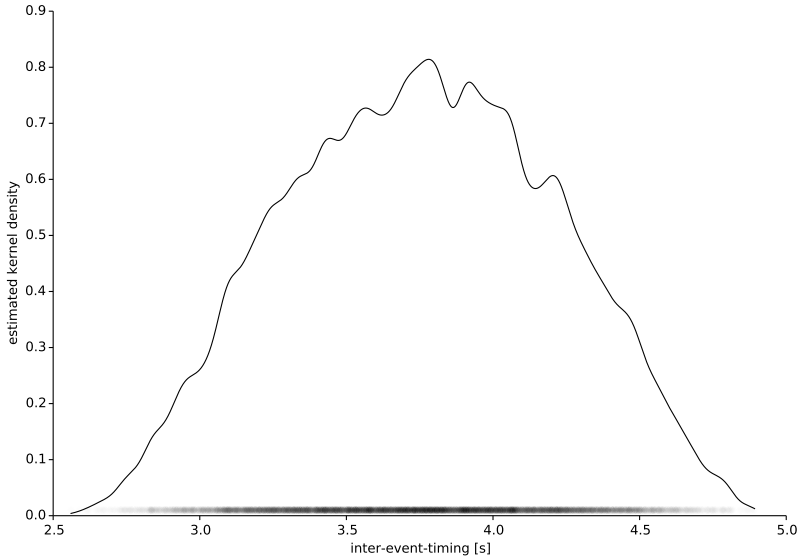

Figure 3.2: Estimated kernel density (c.f. section) of the theoretical distribution of inter-gaze shift intervals. The data were simulated based on the jitters employed for the experiment and the sample size of the present experiment.

amounted to approximately 0.1° visual angle. The experimenter welcomed the participants and announced that they would now be going to take part in a study on social perception. After that, they sat down in a chair in front of the psychophysical booth to give informed written consent. Subsequently, the subjects were guided inside the testing booth and sat down on a chair, approximately 114 cm away from the computer monitor. They put their head on a chin-rest so that could easily view the center of the screen. The experimenter closed the door and turned off the light. A black screen was displayed with instructions printed in white letters. Participants read the instructions at their own pace and subsequently performed to the task. Participants responded by pressing a button on a Lumitouch optical response keypad, either with their right middle or with their right index finger. The task took about 20 minutes to complete. After the experiment the BDI (Beck, Ward, Mendelson, et al., 1961; Beck, Steer, & Hautzinger, 1994), the AQ (Baron-Cohen, Hoekstra, Knickmeyer, & Wheelwright, 2006), and the IRI (Davis, 1996) were administered.

3.1.2.3 General data analysis and software

All data processing and visualization steps were carried out using the Python language (2.7). For analyses of central tendency, mean variability and mean measures of distribution, the R-language was used (R Core Team, 2014). To explore differential distribution characteristics, kernel density estimates were computed using the scikit-learn library for machine learning (Pedregosa et al., 2011). Such kernel density estimates are nonparametric

estimators of the distribution of a random variable and are closely related to histograms. In a plot they can be superimposed for the purpose of comparing different distributions. All error bars represent the standard error of the mean (SEM). Outliers were defined based on the inter-quartile range (IQR),

$$IQR = Q_1 - Q_3, \qquad T_1 = Q_1 - 1.5 \times IQR, \qquad T_2 = Q_3 + 1.5 \times IQR \tag{3.1}$$

Where Q_1 is the first quartile, Q_3 the third quartile, T_1 is the lower threshold and T_2 is the upper threshold.

3.1.3 Results

Subjects performed an SSRC task, which required to look at a face that either was looking at the subject (direct gaze) or was looking downwards (averted gaze). Whenever the face's eye gaze laterally changed, the subject was required to press a key that was contra-lateral (incongruent action intention) or ipsilateral (congruent action intention) to the faces gaze shift.

3.1.3.1 Distribution

To characterize the distribution of reaction times within each condition, kernel densities were estimated for each condition over all subjects. The estimates shown in figure 3.3 indicate a lower mean and a lower variance for reaction times resulting from congruent as compared to incongruent action intentions. The distributions suggest that reaction times under congruent intentions and direct gaze had a higher density between 200 and 300 milliseconds. Moreover, cases above 800 ms appear to be outliers. An outlier classification based on the IQR rule suggests inclusion boundaries of 102.563 and 859.462 milliseconds, respectively. Subsequent analysis focussed on this reaction time range.

3.1.3.2 Central tendency and mean variability

To statistically analyze the central tendencies under each condition displayed in figure 3.4, a 2 (intention: congruent VS incongruent) $\times$ 2 (gaze: direct VS averted) repeated measures ANOVA was conducted on median reaction times. The test revealed a significant main effect of action intention ($F(1, 26) = 226.500, p = 4.24e-11$) and a significant interaction between action intention and gaze ($F(1, 26) = 4.590, p = 0.042$). No effect of gaze was found significant. Participants showed higher reaction time differences between congruent and incongruent action intentions when they had experienced eye contact. This point is further

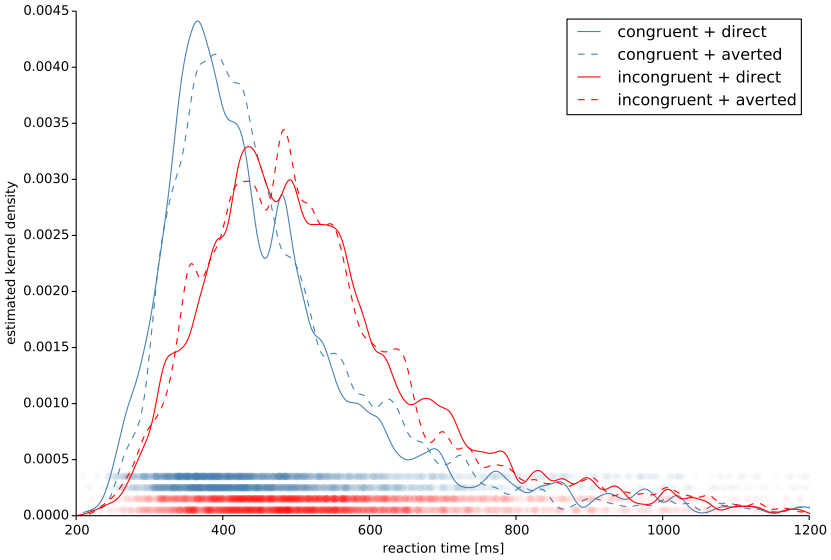

Figure 3.3: Kernel density estimation of reaction times for each condition (bandwidth of 10 ms). Button presses plotted in bottom rows, order follows the legend.

illustrated by reaction differences between responses following congruent and incongruent action intentions shown in figure 3.5. While eye contact did not directly modulate reaction times, it modulated the influence of action intention on motor execution.

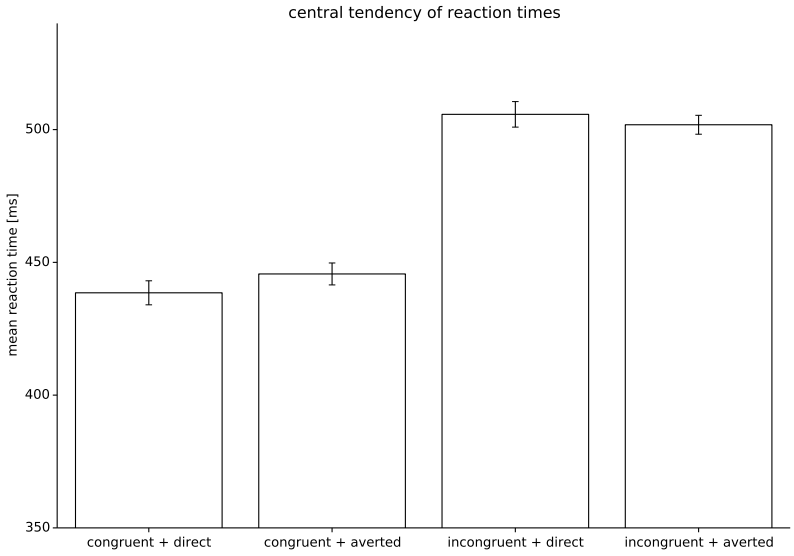

Figure 3.4: Mean reaction time for each condition. Error bars show the SEM.

Figure 3.6 depicts the average median absolute deviation (MAD) across conditions. The mean variability seems to follow the pattern visible for the kernel density estimates. However, the error-bars indicated huge variability of dispersion across subjects. A subsequent 2

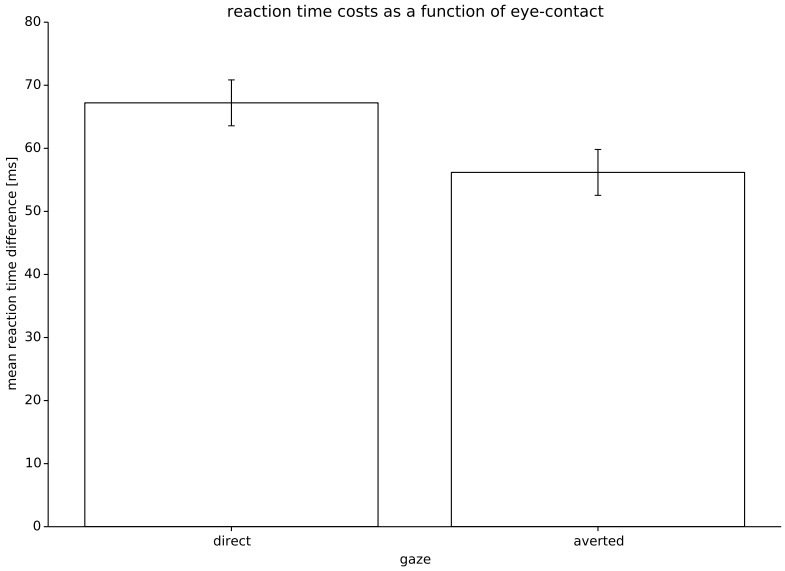

Figure 3.5: Mean reaction time difference between actions given congruent and actions given incongruent intentions. Error bars show the SEM.

(intention: congruent VS incongruent) $\times$ 2 (gaze: direct VS averted) repeated measures ANOVA on mean MAD scores did not yield any significant effect.

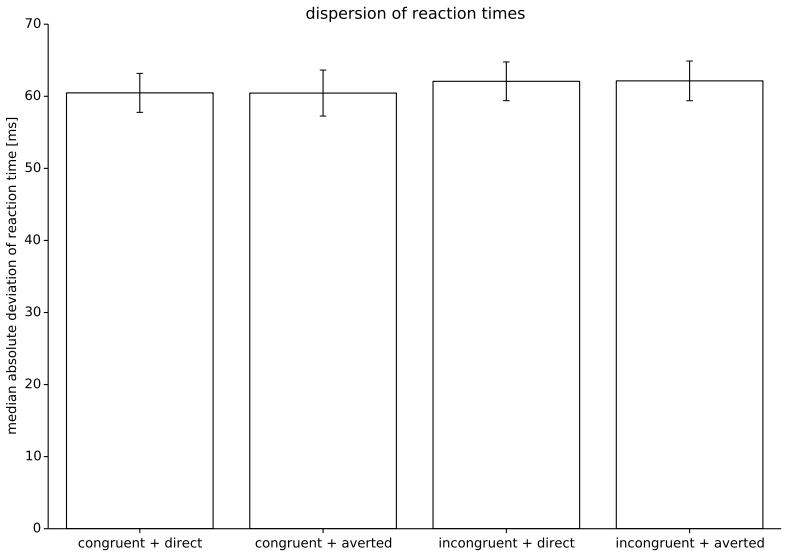

Figure 3.6: Median absolute deviation across conditions. Error bars show SEM.

3.1.3.3 Entrainment

The distributions of the avatar's inter-gaze shift intervals and the subject's inter-button press intervals depicted in figure 3.7 suggest a highly similar statistical structure for

both types of events. A subsequent Kolmogorov-Smirnoff test for two samples yields a tendency towards significance $D = 0.024, p = 0.06$, suggesting that both, inter-saccadic intervals and button presses, originate from the same distribution. To further investigate the distribution dynamics in a task-related fashion, mean distribution distances as measured by the Kolmogorov-Smirnoff statistic were computed for each condition. The pattern depicted in figure 3.7 follows the pattern of mean reaction times in figure 3.4. To statistically analyze the distribution similarity as function of the task, a 2 (intention: congruent VS incongruent) $\times$ 2 (gaze: direct VS averted) repeated measures ANOVA was conducted on Kolmogorov-Smirnoff distances. The test reveals a significant main effect of intention $F(26, 1) = 10.600, p = 0.003$. This suggests that the rhythm of subject's responses more closely followed the rhythm of the avatar's gaze when subjects acted upon congruent action intentions. No other contrast of interest reached statistical significance.

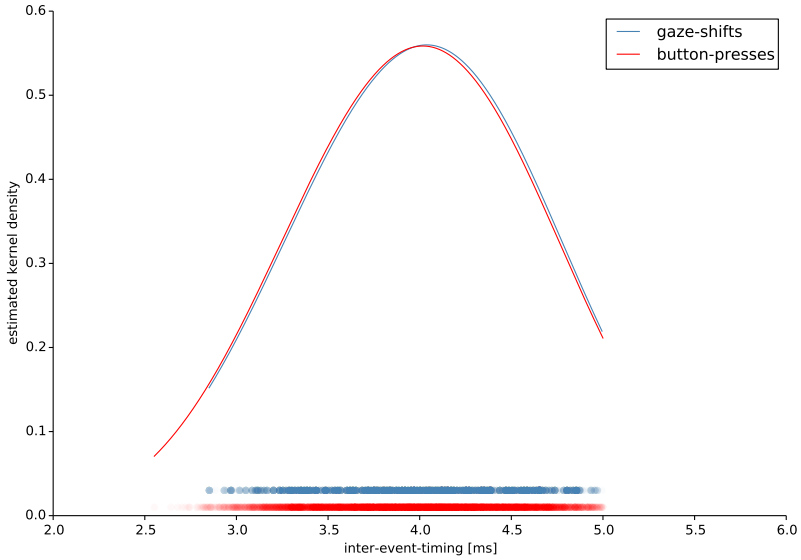

Figure 3.7: Kernel density estimation of inter-gaze shift intervals and button presses (bandwidth of 300 ms).

3.1.3.4 Speed-accuracy trade-off

Figure 3.9 shows the task performance in terms of accuracy for each condition. The overall pattern suggests higher accuracy for conditions involving congruent action intentions. A 2 (intention: congruent VS incongruent) $\times$ 2 (gaze: direct VS averted) repeated measures ANOVA on accuracy revealed a significant main effect of action intention ($F(26, 1) = 9.4, p = 0.005$). Subjects committed more errors when acting upon incongruent intentions. No other contrast of interest reached statistical significance.

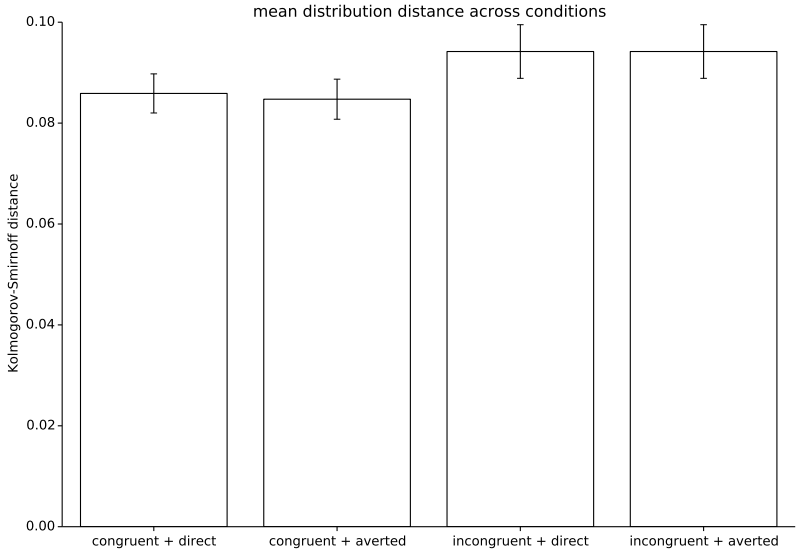

Figure 3.8: Mean distance between the distribution of inter-gaze shift and button presses intervals for each condition. Error bars show the SEM.

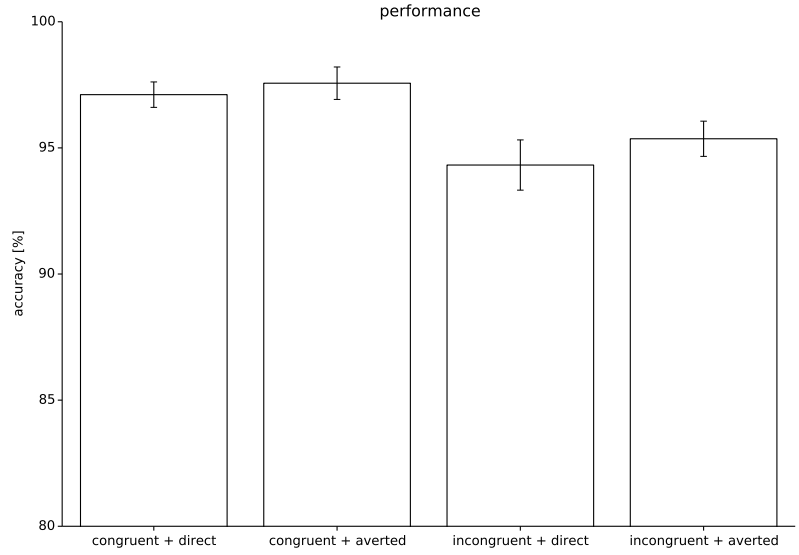

Figure 3.9: Mean accuracy for each condition. Error bars show the standard error of the mean.

3.1.4 Discussion

Subjects have been found to respond about 50 milliseconds faster in the congruent intention condition compared to the incongruent intention condition. Likewise, the accuracy was higher for the congruent intention condition. These results suggests that planning and performing movements defined as contra-lateral to the observed person's target act posed significant cognitive load. This observation is in line with findings on attention, motor

execution and cognitive control (see Hommel (2011) for a broad review of that subject matter). The high accuracy unequivocally indicates that the subject's action intention was successfully manipulated while the reaction time differences between conditions clearly show that the action intention influenced the processing of the task. Importantly, the correspondence between high accuracy and low reaction times suggest that participants did not strategically optimize their response speed at the expense of accuracy.

Importantly, reaction time differences between the congruent intention and the incongruent intention condition were modulated by eye contact. This dependency rules out an explanation of the task performance in terms of pure cognitive control or spatial attention. Since the task did not involve any cueing it can be ruled out that the effect is the result of enhanced visual saliency. Moreover, the stimulus materials were designed in a way that the size of the avatar's sclera and pupil were constant across conditions. In other words, if eye contact exerted any saliency effect it cannot be purely visual but must be explained by a taking into account higher visual processing steps related to mutual gaze, conforming to the 'eye contact-effect' hypothesis (Senju & Johnson, 2009). Interestingly, the ranking of mean reaction times flipped as function of gaze across the intention conditions. For the congruent conditions, direct gaze went along with the faster reaction times, for the incongruent conditions, it resulted in greater reaction times. This suggests, that eye contact might exert its modulatory impact by subtly modifying performance in both conditions instead of boosting or interfering processing in one of the conditions. In other words, eye contact is suggested to enhance following another person's gaze and interfere with the plan for a spatially opposed action. This view would also be compatible with the distribution densities observed (c.f. 3.3). Acting congruently upon direct gaze, an increase in response-density relative to the averted gaze condition can be observed in the congruent intention between 200 and 300 millisecond. In contrast, a similar increase is present for the incongruent condition between 700 and 800 milliseconds. It is important to note that no interaction effect was found in the analysis of accuracy, which rules out a trivial explanation in terms of strategic task-sets.

As a third important finding, the statistical structure of button presses closely matched the distribution of ISIs. This finding suggests that the task was easy to understand and to follow and, hence, the distribution of inter-gaze intervals directly shaped the frequency of button presses. Importantly, the fact that the distance between stimulus and response distribution was modulated by action intention indicates that subjects were indeed entrained to the task. In other words, in the congruent intention condition subjects synchronized their action to the virtual character's gaze more strongly than in incongruent intention condition. This finding suggests that the distribution pattern expresses a cognitive mechanism rather than arbitrary correlation.

Taken together, the overall response profile closely matched the results reported by Wang et al. (2011) who used a similar SSRC protocol which measured automated gaze-dependent adjustments of mimicry. The findings, therefore indicate that the task captured an intrinsic and automated cognitive mechanism. it can be argued that the present experiment established a quasi-naturalistic paradigm that captured cognitive processes, which relate action intentions and action execution to the perception of other person's eye gaze. The quasi-naturalistic characteristic of the paradigm was achieved by a sustained visual stimulation typical for social encounters and by structuring the avatar's gaze behavior, which allowed subjects to become entrained. The task successfully setup different action intentions as a context for gaze processing and impacted on several statistical properties of reaction times. These results indicate task-related neuromagnetic dynamics.

3.2 Experiment 2

3.2.1 Objective and hypotheses

The objective of the present experiment is the exploration of cortical dynamics that underly processing the eye gaze of another person during social interaction. Experiment 1 had revealed modulatory effects of previous eye contact on action control as indicated by latency differences for responses resulting from congruent versus incongruent intentions. The results of experiment 1 conformed to other findings based on SSRC protocols which were used to measure automated modulatory mechanisms related to processing eye gaze (Wang et al., 2011). Such behavioral interaction effects indicate that processing eye gaze is relevant to action-related cognitive processes such as preparation for action, or the implementation of motor commands or a series thereof. This raises the question, whether gaze-processing is preferentially recruited during cognitive processes related to action or whether early and perception-locked processes also equally contribute to this behavioral effect.

This question can be addressed by an MEG experiment based on the protocol of experiment 1. This protocol has been shown to establish a statistical link between the ISIs and the subject's responding rhythm. The subject's repsonses can, hence, be regarded as as a shifted version of the stimulus-related event, just with higher uncertainty due to variance in reaction times. As a consequence, activity time-locked to the eye gaze should also be visible when averaging signals on the subject's response and observing the temporal window before the response event. The presence of differential activity when averaging on the stimulus event paired with the absence of differential activity when averaging on the subjects' response would indicate a dominantly stimulus-locked role of gaze-related cortical activity during ongoing interactions. Effects that follow this pattern will be referred as response-locked. The

temporal structure of differential components and their localization would then be expected to conform the findings from studies which investigated dynamics time-locked to changes in eye gaze (for example Sato et al. (2008), Dumas et al. (2013)). The absence of differential activity when averaging on the stimulus event paired with the presence of differential activity when averaging on the subjects response would indicate a dominantly response-locked role of gaze-related cortical activity during ongoing interactions. Such effects will be referred to as response-locked. As, to the best of my knowledge, to date, this phenomenon has not been systematically investigated, predictions are difficult to formulate. However, neuro-behavioral correlations should give additional hints and should be most pronounced in regions which are known to possess anatomical connections to the motor-system.

3.2.2 Methods

3.2.2.1 Participants

Sixteen right handed, healthy university students and employees of the Jülich Research Centre (7 female, 9 male) ranging in age between 20 and 31 years (male: M = 23.000, SD = 1.291; female: M = 25.800, SD = 3.780) volunteered to participate in this experiment. All volunteers were naïve with respect to the purpose of the study. All volunteers gave informed written consent to the study protocol that had been approved by the local ethics committee of the Medical Faculty of the University of Cologne, Germany.

3.2.2.2 Experimental protocol

3.2.2.2.1 Design, task and stimulus materials Participants completed a SSRC task as described in experiment 1. To take into account the loss of trials due to artifact rejection and to acquire sufficient data for covariance computation, 336 trials were acquired instead of 288. Trials were grouped in blocks of 14 instead of 12 directional cues. The experiment followed a 2 (action intention: congruent versus incongruent) $\times$ 2 (eye contact-phase: direct versus averted gaze) design. Stimulus materials and instructions were identical to experiment 1. One detail regarding the instruction-phase was modified. In the present experiment, subjects were required to confirm that they had read the instruction by pressing a key in a self paced manner. The next block begun once the subject had confirmed.

3.2.2.2.2 Procedure The experiment was conducted at the Institute of Neuroscience and Medicine (INM-4), Forschungszentrum Jüelich. Stimuli were generated by a stimulus generator board (ViSaGe MKII, Cambridge Research System Ltd.) and projected using a DLP Projector (Luxion LM-X 25) onto a mirror system inside the MSR on a nonmagnetic

back-projection screen. The screen was affixed about 1m above of the participants. Stimuli were presented at about $2.5° \times 4°$ visual angle. The difference between straight-direct gaze and straight-averted gaze amounted to approximately 0.1 ° visual angle. The stimuli were presented jitter free with a refresh rate of 60 Hz. A system specific constant time delay of 2 ms respective to the stimulus onset was taken into account and subtracted for subsequent event-related analysis.

The experimenter welcomed the participants and announced that they would now be going to take part in a study on social perception. After that, they sat down in a chair in front of the MSR to give informed written consent. Subsequently, the subjects were guided inside the magnetically shielded room by the experimenter and a medical research assistant and sat down on the MEG system's bed. The assistant subsequently affixed electrocardigram (ECG), electrooculogram (EOG), and, fiducial electrodes. The subject was then guided into the supine position and the experimenter made final adjustments to the subjects position to ensure that the head and eye region of the avatar were clearly visible to the subject. For this purpose a gray shape was used as landmark to avoid uncontrolled familiarization with the stimuli. The experimenter then closed the door and dimmed the light. Then the subject's head position was digitized. A black screen was displayed with instructions printed in white letters. Participants read the instructions at their own pace and subsequently performed the task. Participants responded by pressing a button on an MEG-compatible Lumitouch optical response keypad in a bimanual fashion using their left and right index fingers. The task took about 15 minutes to complete. After the experiment the BDI (Beck et al., 1961; Beck et al., 1994), the AQ (Baron-Cohen et al., 2006), and the IRI (Davis, 1996) were administered.

3.2.2.3 Data acquisition

Neuromagnetic signals were recorded using a whole-head 248-channel magnetometer system in a supine position (Magnes 3600-WH, 4D-Neuroimaging, San Diego, CA, USA). The signals were continuously sampled at 601.25 Hz with a bandwidth ranging from 0.1 to 400 Hz. Reference gradiometers and magnetometers were concomitantly applied to the ongoing recordings to compensate for environmental noise. Ocular movements and cardiac signals were monitored using EOG and ECG. The participant's position was tracked by three head location coils attached to the forehead, the left and the right postauricular points. The head shape was measured at the beginning and at the end of each recording using the Polhemus FASTRAK head digitization system. For each subject, T1-weighted structural MR scans were acquired using a 3-T Siemens Trio system (voxel size of $1 \times 1 \times 1 mm^3$). Recordings were

converted to the Neuromag format using the a designated conversion tool that the author implemented in Python and contributed to the MNE-Python project[1].

3.2.2.4 Cortical reconstruction and volumetric segmentation

The anatomical processing was performed using the Freesurfer image analysis suite. The implementation details of the Freesurfer segmentation procedures have been described in prior publications (Dale, Fischl, & Sereno, 1999; Fischl, Sereno, & Dale, 1999a; Fischl, Sereno, Tootell, & Dale, 1999; Fischl & Dale, 2000; Fischl, Liu, & Dale, 2001; Fischl et al., 2002; Fischl et al., 2004a, 2004b; Segonne et al., 2004; Han et al., 2006; Jovicich et al., 2006; Reuter, Rosas, & Fischl, 2010; Reuter, Schmansky, Rosas, & Fischl, 2012). These processing steps included motion correction and averaging (Reuter et al., 2010) of multiple volumetric T1 weighted images, removal of non-brain tissue based on a hybrid watershed/-surface deformation procedure (Segonne et al., 2004), automated Talairach transformation, segmentation of the subcortical white matter and deep gray matter volumetric structures, including hippocampus, amygdala, caudate, putamen, ventricles (Fischl et al., 2002; Fischl et al., 2004a), intensity normalization (Sled, Zijdenbos, & Evans, 1998), tessellation of the gray matter white matter boundary, as well as automated topology correction (Fischl et al., 2001; Segonne, Pacheco, & Fischl, 2007). In addition, surface deformation were performed following intensity gradients to optimally place the gray/white and gray/cerebrospinal fluid borders at the location where the greatest shift in intensity defines the transition to the other tissue class (Dale et al., 1999; Fischl & Dale, 2000). The outputs of the segmentation procedure were than refactored for the computation of the source space, based on surface inflation (Fischl, Sereno, & Dale, 1999b) and, the group analysis, based on registration to a spherical atlas. The latter takes into account individual cortical folding patterns and has been shown to improve the match of cortical geometry across subjects (Fischl et al., 1999a). Finally, the Freesurfer software was used to obtain a parcellation of the cerebral cortex into units with respect to gyral and sulcal structure Desikan et al., 2006, later used for narrowing the source analysis.

3.2.2.5 Signal extraction

All MEG data have been been processed using custom scripts built on-top of functionality provided the MNE software suite (Gramfort et al., 2013a, 2014), a publicly available open source software which implements solutions at all common stages of M/EEG data processing. All programming has been carried out with the Python language (2.7). For particular

[1] c.f. https://github.com/mne-tools/mne-python/pull/385. Critical parts of this conversion routine were previously only available under the Solaris platform.

statistical analyses of behavioral data the R-language was used (R Core Team, 2014). Parts of the methods that have been implemented by the author and contributed to the MNE suite are additionally highlighted.

3.2.2.5.1 Denoising and bad channel handling Data were bandpass filtered between 1 and 20 Hz using a zero-phase 4th order Butterworth filter based on infinite impulse response (IIR) time domain implementation. This filter type has been chosen since it avoids ringing artifacts around the cutoff frequency, as compared to frequency domain implementations. It's weak attenuation curve justifies the relatively low lowpass frequency. The highpass cutoff frequency of 1 Hz was chosen to remove low frequency drifts from the data and achieve baselining by removing inter-trial offsets. Bad channels were detected based on visual inspection after training by the MEG system's operators.

3.2.2.5.2 Removal of biological artifacts using independent component analysis (ICA) ICA is a matrix decomposition technique similar to FA and is commonly used in neuroimaging to explore latent data features (Beckmann & Smith, 2004; Salustri & Kronberg, 2004; Lu, Wang, Luo, Li, & Yao, 2013) and to remove artifacts from the data (Dammers et al., 2008; Breuer, Dammers, Roberts, & Shah, 2014a). The FastICA model proposed by Hyvärinen, Karhunen, and Oja (2004) explains the observed data as a product of the true latent sources and a weigh- or mixing matrix:

$$X = A * S \ . \tag{3.2}$$

In contrast to methods based on PCA(c.f. section 2.2.1.5.1) that achieve decomposition into a subspace of linearly independent components, ICA estimates statistically independent sources, based on non-linear distribution moments such as kurtosis or skewness. This characteristic is of advantage when tackling biological artifacts such as ECG or EOG signals which do not follow a Gaussian distribution. In such cases, ICA provides a more exact approach to separating such dynamics from the signal of interest (Dammers et al., 2008; Gramfort et al., 2014). When ICA is successfully applied to M/EEG data, typically a few components emerge that describe these common artifacts. These can be identified by signal comparisons with actual ECG and EOG recordings. A clean MEG signal can then be produced by transforming the raw data into ICA space, zeroing out the latent sources corresponding to the previously identified artifacts and then inverse transforming the modified latent sources using the inverse of the unmixing matrix.

Here, ICA was performed to remove ECG and EOG artifacts using the FastICA algorithm (Hyvärinen et al., 2004). To decorrelate the ICA input signals, PCA was used. This step is mandatory, since the FastICA algorithm does not possess noise term (see (3.2)). The number of estimated

ICA components was determined as the number of PCA components that explain 99% of the signal variance. To exclude contaminated, non-stationary segments during model estimation, a peak-to-peak rejection was performed with a threshold of $5e-12$ Tesla. ECG artifacts were identified using the cross-trial-phase-statistic proposed by Dammers et al., 2008. ECG related trials were accordingly defined as time windows ranging from -500 to 500 ms around the ECG r-peak. The latent sources ICA sources were obtained from applying the estimated unmixing matrix to each ECG related epoch. The resulting source epochs (in ICA space) were then bandpass filtered between 8 and 16 Hz. Subsequently, a Hilbert transform was applied to obtain the phase information. To assess the cross-trial phase coupling, Kuiper's test was computed across all ICA source epochs. This significance test quantifies the uncertainty of inferring uniform distribution characteristics from a sample distribution. In the present context, it was used to asses whether the phase angles across epochs are widely dispersed across the time points of an epoch or concentrated around certain samples. The latter constitutes typical behavior for components related to the respective artifact. Components with a significance value exceeding a value of 0.25 were considered as phase-coupled to the r-peak and hence marked for exclusion. To balance the trade-off between denoising and preservation of signal, the maximum number of components to exclude was set to four. To identify EOG related components, Pearson correlations were computed between the reconstructed latent sources and the EOG recoding after bandpass filtering signals between 1 and 10 Hz. EOG-related components were then identified using repeated z-scoring and rejection at an absolute threshold of three and two iterations. A maximum of three EOG components was excluded. The ICA computation relied on the scikit-learn (Pedregosa et al., 2011) implementation of FastICA. This ICA procedure was implemented by the author and was contributed to the MNE-Python project (Gramfort et al., 2013a). The source code is publicly available at the project website[2]. Previous versions of the procedure have also been detailed in Gramfort et al. (2013a, 2014). Figure 3.10 displays a typical solution for one representative subject.

3.2.2.5.3 Epoching, rejection of contaminated trials, and averaging For stimulus-related time-locked analysis, data were segmented at the onset of the gaze shift, encompassing a temporal window between -200ms and 1500ms. For response-related time-locked analyses data were segmented at the onset of the button press, encompassing a temporal window between -800ms and 700ms. After cleaning the epochs using ICA, remaining bad epochs were rejected based peak-to-peak amplitude and using a threshold of 4000 fT, or, were declared as bad if the subject failed to respond correctly. To avoid biasing the statistical analysis to any of the conditions, the resulting epoch counts were equalized across conditions.

[2]https://github.com/mne-tools/mne-python

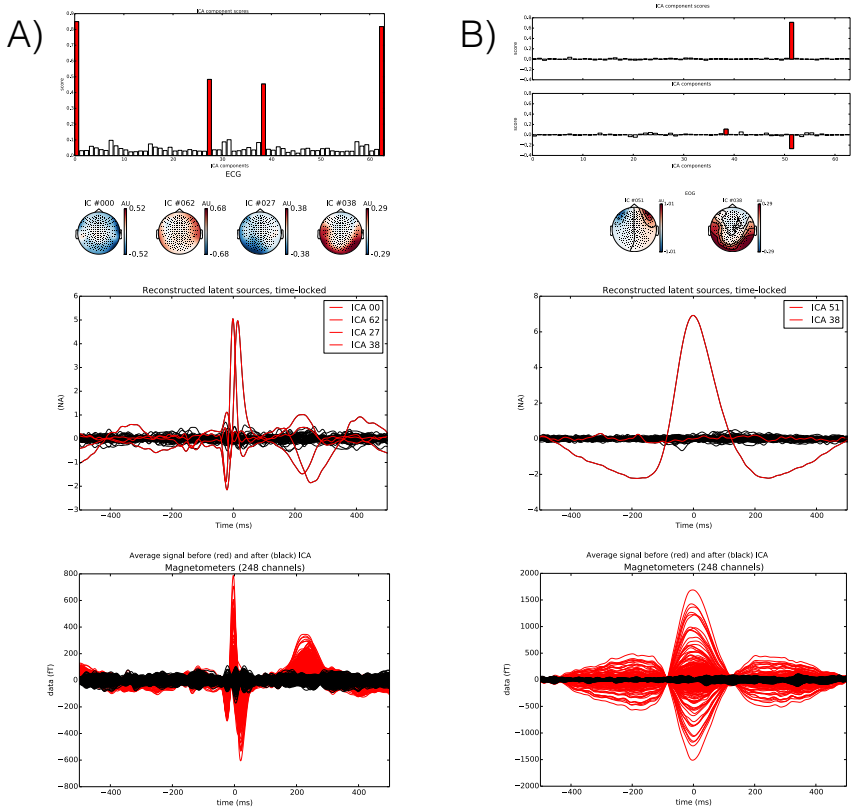

Figure 3.10: Diagnostic visualizations of the ICA solution for a representative subject. Panel A) displays detection and removal results for ECG artifacts. Panel B) displays detection and removal results for EOG-artifacts. From top to bottom: Scores for the detection-metric across ICA components, detected components marked in red. Topographic patterns of the detected ICA components. Time-courses of ICA components averaged across trials defined by artifact-events. Overlay diplays of averaged artifacts in sensor space, before and after applying ICA.

The baseline mean was not subtracted from the window of interest as offsets were already removed by highpass-filtering the data at 1 Hz. Data were then averaged across trials.

3.2.2.6 Source localization

To determine the origins of the neuromagnetic recordings an MNE inverse solution (c.f. section 2.2.1.1 for a detailed description) was computed for each condition and subject. The following paragraphs will detail parameter choices at each step of computing the MNE solution. In this section, all mathematical descriptions are adopted from the MNE-manual[3]. The corresponding parameter descriptions are based on Gramfort et al. (2014).

3.2.2.6.1 Forward modeling For any distributed inverse solution, the dipole locations need to be determined in advance to compute the forward model. This step is achieved by constructing a source space that places the dipole sources on a chosen surface model and specifies a subsampling factor. The latter helps to reduce computation times and is justified by the fact of field spread. The spread of electromagnetic fields leads to spatial correlation of the MEG signal and, hence, sets boundaries to the maximum spatial resolution.

To construct the source space, the FreeSurfer inflated surfaces was used, which defines the boundary between gray and white matter. It was subsampled using a 6-fold subdivision of an octahedron (oct-6), yielding 4098 sources per hemisphere. This subsampling realizes an average distance of approximately 4.9mm between the sources and spans a surface of $24\,mm^2$ per source.

To compute the actual forward solution, a boundary element model (BEM) was used(Mosher, Leahy, & Lewis, 1999), which assumes a constant conductivity per shell; skin, skull, brain (c.f. 1.2.3.2). As no EEG data were recorded, a single layer BEM, consisting of 5120 triangles, was computed based on the linear collocation method (Mosher et al., 1999) and an isolated skull approach (Hämäläinen & Sarvas, 1989) which are implemented in the MNE software (Gramfort et al., 2014).

3.2.2.6.2 Coordinate alignment To compute an inverse solution, the BEM surfaces, the source space, and the sensor positions need to be aligned in a shared coordinate system. Computing the transformation matrix that satisfies this requirement is achieved by co-registration, as the fiducial electrodes used during recording deviated from standard positions and the nose was included in digitization. Initial alignments were then manually performed using the graphical co-registration-tool provided by the MNE software. The strategy was to approximate the nose-related digitization points to the nose clearly visible on the skull

[3] http://martinos.org/mne/stable/manual.html#manual

surface obtained from the BEM computation. Final alignments were performed using the iterative closest point procedure (Besl & McKay, 1992) implemented by the MNE software.

3.2.2.6.3 Covariance estimation The modern MNE inverse solution requires a noise covariance estimate to whiten the input data (Dale et al., 2000; Gramfort et al., 2013a, 2014). As a result, the spatial configuration captured by the noise covariance will be suppressed in the resulting source estimates (Gramfort et al., 2013a, 2014). Segments of 200 milliseconds preceding the gaze shift were used to compute the noise covariance based on trials from all conditions. The automated estimation technique described in chapter 2 was used to compute the covariance. To match the rank and contents of the data as closely as possible, the noise covariance was computed after cleaning the data using ICA. Since the computation of FA on rank-reduced data has been shown to lead to numerical errors it was not included in the list of potential estimators. The choice of these time segments is justified by the role of the noise covariance in computing spatial filters: in the current experiment, the segments preceding the events of interest did not reflect steady-state activity but background activity characterized by visual processing of the idle face stimulus and waiting for the next event for interest. The choice of noise covariance is hence expected to produce more focal post-baseline source estimates.

3.2.2.6.4 Computation of source estimates Modern MNE inverse solutions implement a set of additional parameters that allow to adjust the behavior of the source estimates to the requirements of analyses.

Orientation constraints To improve the accuracy of the inverse solution, anatomical priors are typically incorporated in the inverse solution. Postsynaptic currents in the cortical pyramidal neurons are believed to be the primary sources of M/EEG signals (Hämäläinen, Hari, Ilmoniemi, & Knuutila, 1993; Murakami & Okada, 2006). The net primary current associated with these currents is oriented normal to the cortical mantle. Therefore, a cortical normal orientation constraint is commonly employed in source estimation.

One such approach strictly fixes the source orientation to the surface normal direction resulting in signed amplitudes related to the dipole's direction relative to the cortical surface. As a consequence, the source amplitudes will be directly influenced by the quality of the anatomical surface reconstruction used to determine the normal direction. Second, this approach poses challenges to comparisons across subjects, since anatomical variability will necessary lead to different amplitudes and different signs, even if a putative neuromagnetic component behaves identically for all subjects with regard to its dynamics. In contrast, for an MNE solution with free orientation the norm is computed over the three spatial components of the current estimates. In that case, the resulting estimate reflects a summary

of each spatial component's current strength. However, such a solution is supposed to be less susceptible to anatomical between-subject variability and sign differences. While a fixed orientation is mandatory for certain types of analyses, for example time-frequency analyses, in time locked analyses it is not mandatory. One additional option that is compatible with a free orientation is a so called loose constraint. The columns of the gain matrix represent the corresponding x, y and z directions of the unit dipoles' fields at a given source location. The loose constraint approach will put the source's first two components on a plane that is normal to the remaining third component which is normal to the surface. The variance of the first two components is then scaled by a specified factor. This constraint, hence, considers anatomical information, but instead of ignoring the non-normal components, they are summarized and re-scaled.

To improve comparability between amplitudes, a free orientation was chosen in combination with a loose constraint of 0.2. This value is preset as default parameter by the MNE software.

Noise normalization To further improve comparability between subjects, Dale et al. (2000) proposed a procedure called dynamical dSPM. This approach normalizes each source estimate by its variance and yields a dimensionless neural activation index. Given the present choice of unsigned free-orientation source estimates, the normalization of the kth dipole at the tth time can be denoted as

$$F_{kt}^{dSPM} = \frac{\sum_{q=1}^{3}(X_{3(k-1)+q,t}^{MNE})^2}{\sum_{q=1}^{3} w_{3(k-1)+q}^2}, \tag{3.3}$$

where w is the variance of a given source and X is the source estimate (Lin et al., 2006). Under the null-hypothesis, the dSPM score follows an F-distribution with three degrees of freedom for the numerator. The degrees of freedom of the denominator depend on the source space and the number of time samples analyzed. This normalization technique has been shown to produce source estimates that are less dependent on the location of the source on the cerebral cortex and that dSPM amplitudes are not subject to the surface bias of MNE (Lin et al., 2006).

All analyses presented are based on dSPM scores.

Depth weighting MNE inverse solutions are known to be biased towards superficial locations. To mitigate this problem, depth weighting of cortical sources is commonly employed. One common approach to depth weighting directly modifies the entries of the source covariance matrix R (cf. (2.3)), which is a diagonal matrix in which the diagonal

contains the variance of each source. The weighting of the variances is then proportional the function f_k at the kth dipole (Liu & Ioannides, 2006).

$$f_p = (g_{1p}^T g_{1p} + g_{2p}^T g_{2p} + g_{3p}^T g_{3p})^{-\gamma} , \tag{3.4}$$

where gi is the ith column of the gain matrix and γ is the variable depth weighting parameter that determines the steepness of (3.4). Given the regularization in (2.3), this weighting can be interpreted as penalty that is inversely proportional to the depth of the source. Given a fixed amount of activation, superficial sources would then be assumed to have less influence on the final estimate compared with deeper ones.

Since it has been shown that the depth-weighting does not significantly affect noise normalized estimates (Lin, Belliveau, Dale, & Hamalainen, 2006) the default parameter of 0.8 was kept.

3.2.2.7 Group analysis

3.2.2.7.1 Common source space To make the individual source estimates comparable, the spherical morphing procedure has been employed (Dale et al., 2000; Fischl & Dale, 2000). The procedure makes use of the spherical coordinate system which is computed for each hemisphere using the the FreeSurfer anatomy pipeline. The source estimates are defined on a subsampled cortical surface model. Therefore, aligning a subject with an average brain model that uses the full cortical surface tessalation includes three steps (Gramfort et al., 2013a). First, the source estimates have to be extrapolated to all vertices of the high-resolution cortical tessalation, which are not already included in the source space. This spreading of source estimates to neighboring vertices is achieved using an iterative diffusion process. Subsequently, the FreeSurfer spherical registration is used to linearly interpolate data defined on the subject's cortical model to the average cortical surface. The final data are then obtained by re-subsampling to the number of source locations defined by the source space of interest.

For producing the final source estimates subject to statistical analysis, 20 smoothing steps have been used. The default ico-5 source space (obtained from a fivefold subdivision of an icosahedron) has been chosen for the final subsampling. It comprises 10242 cortical sources per hemisphere.

3.2.2.7.2 Statistical contrasts and nonparametric testing For the present experiment, a nonparametric clustering permutation test was used (Maris & Oostenveld, 2007). The permutation test was computed based on a repeated measures f-statistic. In the case of a

2×2 design with multiple measurements per sample unit, i.e., the subjects, a 1-sample t-test on the paired contrast of the main effect is mathematically equivalent to a t-test for related samples where each factor level serves as related sample. By squaring, the resulting t-statistic can be directly converted into the corresponding f-test with 1 numerator and n-1 denominator degrees of freedom. Compared to a designated repeated measures ANOVA, this implementation involves less computational steps and can be implemented in an efficient vectorized fashion while producing equivalent results. In combination with the subsequently described clustering permutation test this procedure cuts down computation times by one to several hours.

To compute main effects, the conditions belonging to one factor level were averaged. The resulting aggregated signals were then subtracted to form a paired contrast. The interaction effect was implemented based on the higher-order difference between contrasts. This resulted in the following three contrasts:

A $(A1 + A2) - (B1 + B2)$

B $(A1 + B1) - (A2 + B2)$

A:B $(A1 - A2) - (B1 - B2)$

Letters denote the main effect of action intention and numbers denote the main effect of eye contact. The third contrast tested for the interaction between action intention and eye contact, specifically, the statistical hypothesis that the difference between direct and averted gaze was different across action the factor levels of action intention.

Definitions of spatial adjacency were used as anatomical prior for the clustering and were based on the triangle configuration of the cortical surface tessalation that was computed with FreeSurfer. For temporal adjacency a regular lattice adjacency was assumed (a variable at t_i is connected to variables at t_{i-1} and t_{i+1}). To obtain the F-statistic for a given paired contrast, a 1-sample t-test was computed and its output squared. A liberal clustering-threshold was chosen, which was equivalent to an F-value at a 5% significance level. This means, having computed the initial test statistic, features that exceeded this threshold were included in the clustering-procedure. To mitigate problems related to low-variance variables, a constant of $1 \times 10^{-}3$ has been added to the variance term of the t-test as recommended by the "hat" method (Ridgway, Litvak, Flandin, Friston, & Penny, 2012). This technique can be considered as smoothing or regularization of the test statistic and has been shown to remove edge artifacts in a given test's spatial distribution. Since the biggest clusters can overshadow activity in smaller clusters, a step-down test was additionally employed (Holm, 1979; Holmes, Blair, Watson, & Ford, 1996). Applied to the clustering permutation test,

clusters below the critical value are rejected and the procedure is repeated on the remaining clusters until no further significant cluster is found. This technique can increase the chance of detecting additional active variables. To facilitate the interpretation of results, parametrical statistical maps resulting from this permutation clustering test were thresholded at a value that corresponded to an F-value from a repeated measures ANOVA at a 1% significance level.

3.2.2.7.3 Anatomical masking and sources of interest In addition, prior knowledge about the potential source locations has been incorporated by constraining the analysis to a subset of the cortical surface. This search space comprised an anterior part and a posterior part which were composed of adjacent definitions of Brodmann areas (BA), based on the PALS B12 Brodmann annotation (Van Essen, 2005; Van Essen & Dierker, 2007) and were selected based on the literature review presented in chapter 1.1.2. The posterior search surface included BA 18-19 (extra-striate visual cortex including MT/V5), BA 37 (including the face-sensitive parts of the fusiform gyrus), BA22, BA39 BA40 (including parts of the superior temporal sulcus and the temporoparietal junction), BA7 (including regions attributed to the dorsal attention network). The anterior surface included BA32, BA9-12, BA40-46. The resulting anatomical mask is displayed in figure 3.11.

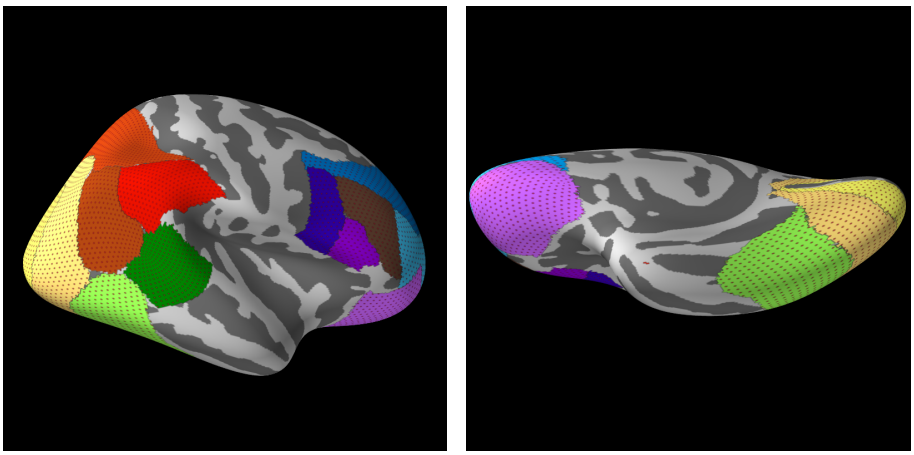

Figure 3.11: Cortical mask used to constrain source analysis. The different colors correspond to Brodmann areas included. The small dots on the surface indicate dipole locations defined by the ICO-5 source spaces used for group analyses.

3.2.2.7.4 Neurobehavioral correlation To compute correlations between cortical activity and reaction times, data were normalized for each subject based on a normalization technique adopted from Larson and Lee (2012). Here, $x_i a$ and $x_i b$ denote the measurements

corresponding to the first and the second factor level of a contrast for a given subject, respectively.

$$x_i' = \frac{(|x_i a| - |x_i b|)}{(|x_i a|/2 + |x_i b|/2)}, \tag{3.5}$$

In the case of cortical activity, $x_i a$ and $x_i b$ refer to the sum over the activity in a significant cluster for a given subject. This normalization assumes a two-sided paired contrast. That is why the data terms in the denominator are divided by 2, which is the number of conditions (in contrast Larson and Lee (2012) investigated a paired contrasts where 1 condition was a baseline condition). The resulting score, hence, expresses percentages of signal change and the sign indicates the relative direction of the effect. A score of 15% would read as relative signal increase in the condition referred to by $x_i a$. Such a normalization is required to eliminate a subjects's bias regarding the overall activity level and its bias regarding preferential activity relative to one condition.

3.2.3 Results

The task required to look at a face that either was looking at the subject (direct gaze) or was looking downwards (averted gaze). Whenever the face's eye gaze laterally changed, the subject was required to press a key that was contra-lateral (incongruent action intention) or ipsilateral (congruent action intention) to the faces gaze shift.

3.2.3.1 Behavioral data

3.2.3.1.1 Distribution To characterize the distribution of reaction times within each condition, a kernel density estimation was conducted. The results depicted in figure 3.12 indicate a lower mean and a lower variance of reaction times for action backed by congruent as compared to incongruent intentions. The distributions suggest that reaction times under congruent intentions and direct gaze seemed to have a higher density between 200 and 300 milliseconds. An outlier classification based on the IQR rule suggested inclusion boundaries of 150.405 and 622.263 milliseconds, respectively. Subsequent analysis focused on responses within this time range.

3.2.3.1.2 Central tendency and mean variability To statistically analyze the central tendencies under each condition (figure 3.13), a 2 (intention: congruent VS incongruent) $\times$ 2 (gaze: direct VS averted) repeated measures ANOVA was conducted on mean reaction times. The test revealed a significant main effect of action intention ($F(15, 1) = 90.870, p = 9.35e - 08$) and a significant interaction between action intention and gaze ($F(1, 15) =$

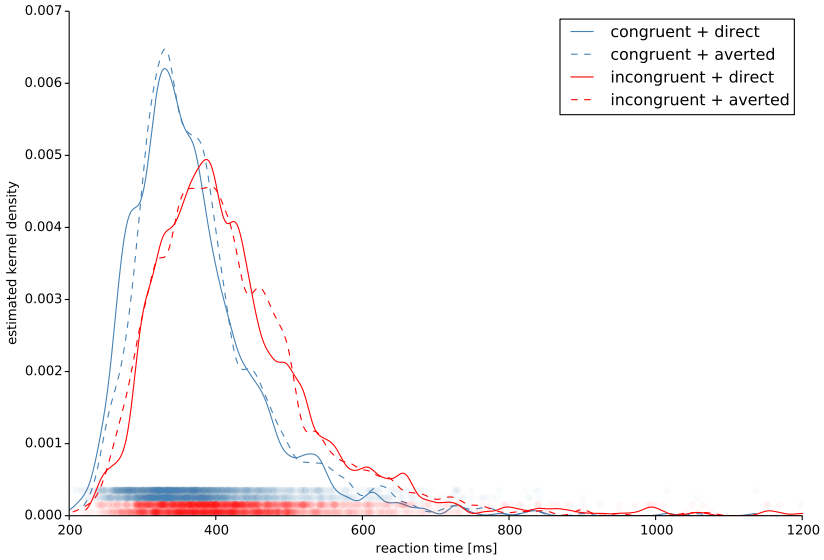

Figure 3.12: Kernel density estimation of reaction times for each condition (bandwidth of 10 ms). Button presses plotted in bottom rows, order follows the legend.

$4.806, p = 0.045$). No effect of gaze has been detected. Participants showed faster reaction times under congruent intentions than under incongruent intentions. While gaze did not directly modulate reaction times, reaction times were fastest when lateral gaze shifts were processed under congruent action intentions and preceding eye contact, which is clearly reflected in the related nonoverlapping error bars depicted in figure 3.13.

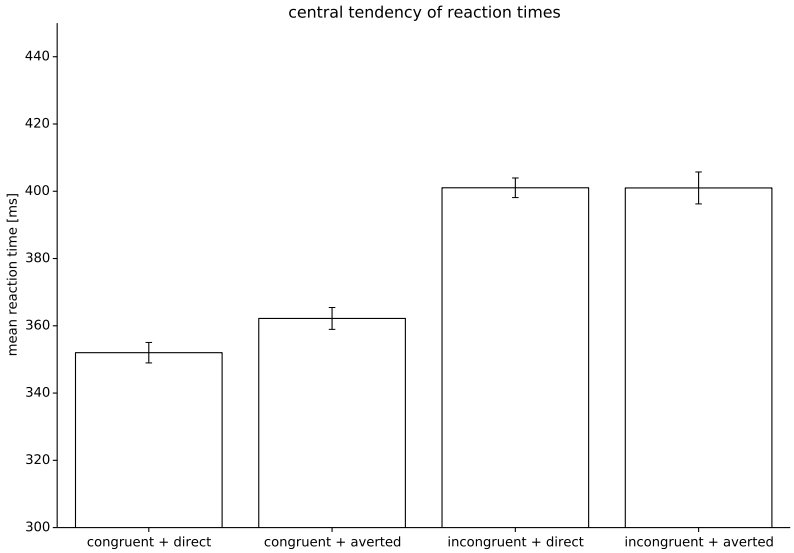

Figure 3.13: Mean reaction time for each conditions. Error bars show the standard error of the mean.

Figure 3.14 depicts the average median absolute deviation (MAD) across conditions. The mean variability seems to follow the pattern visible for the kernel density estimates. A subsequent 2 (intention: congruent VS incongruent) $\times$ 2 (gaze: direct VS averted) repeated measures ANOVA on mean MAD score yielded a significant effect of intention (F(15, 1)=11.920, p=0.004). This suggests that the overall variability in responses was lower for the congruent intention condition.

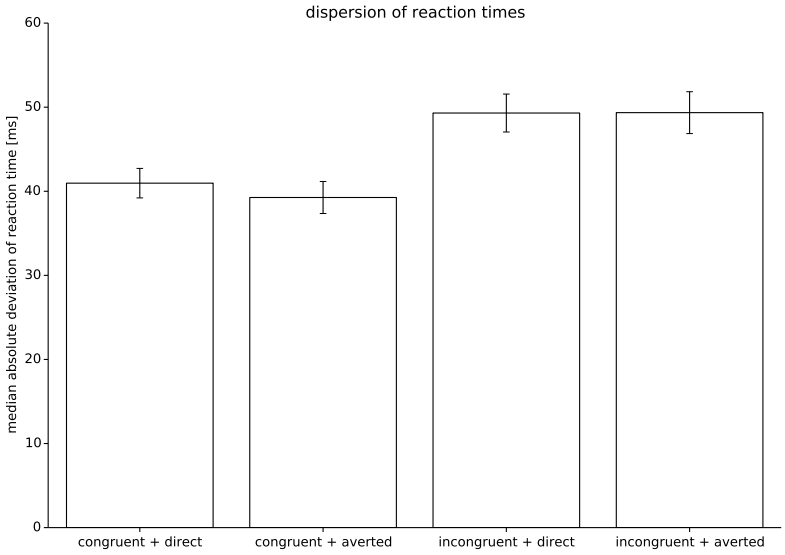

Figure 3.14: Mean standard-deviation for each conditions. Error bars show the standard error of the mean.

3.2.3.1.3 Entrainment The distributions of the avatar's inter-gaze shift intervals and the subject's inter-button press intervals depicted in figure 3.7 suggest a highly similar statistical structure for both types of events. A subsequent Kolmogorov-Smirnoff test for two samples yielded a significant test statistic $D = 0.034, p = 0.009$, suggesting that both, inter-saccadic intervals and button presses, originate from the same distribution. To demonstrate that this match is task-related rather than a spurious correlation, mean distributions distances as measured by the Kolmogorov-Smirnoff statistic were computed for each condition. The pattern depicted in 3.15 follows the pattern of mean reaction times in figure 3.13. To statistically analyze the distribution similarity as function of the task, a 2 (intention: congruent VS incongruent) $\times$ 2 (gaze: direct VS averted) repeated measures ANOVA was conducted on Kolmogorov-Smirnoff distances. The test reveals a significant main effect of intention $F(26, 1) = 10.600, p = 0.003$. This suggests that the rhythm of subject's responses more closely followed the rhythm of the avatar's gaze when subjects acted upon congruent action intentions. No other contrast of interest reached statistical significance.

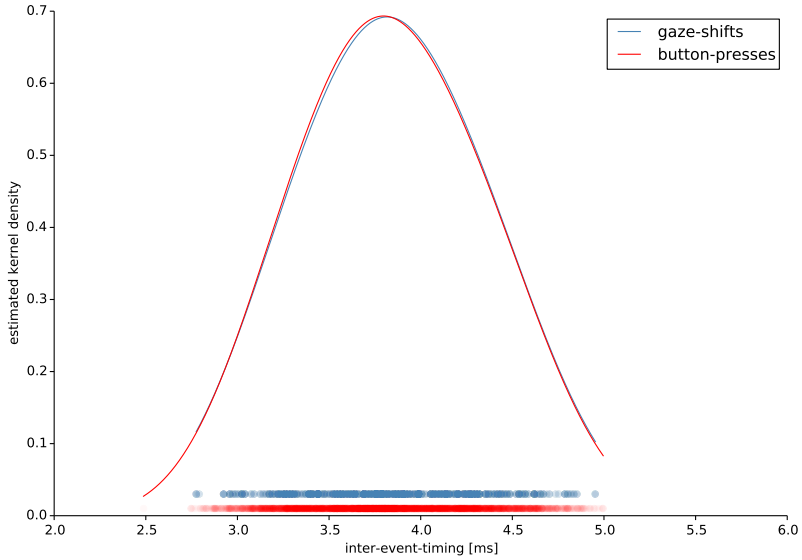

Figure 3.15: Kernel density estimation of inter-gaze shift intervals and button presses (bandwidth of 300 ms).

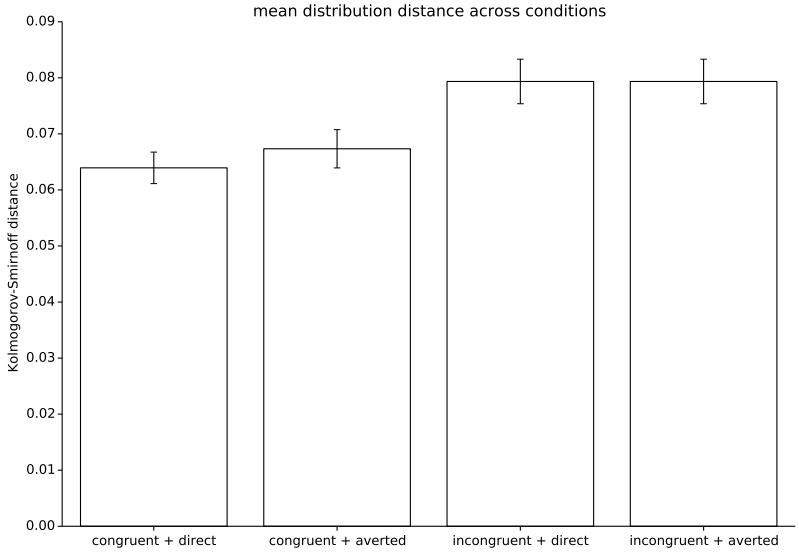

Figure 3.16: Mean distance between the distribution of inter-gaze shift and button presses intervals for each condition. Error bars show the standard error of the mean.

3.2.3.1.4 Speed-accuracy trade-off Figure 3.17 shows the task performance in terms of accuracy for each condition. The overall pattern suggests higher accuracy for conditions involving congruent action intentions. A 2 (intention: congruent VS incongruent) $\times$ 2 (gaze: direct VS averted) repeated measures ANOVA on accuracy did not reveal any significant effect. It is noteworthy, however, that the contrast related to the main effect of action

intention was the only comparison that implicated variation. The F-values for all other contrasts amounted to zero.

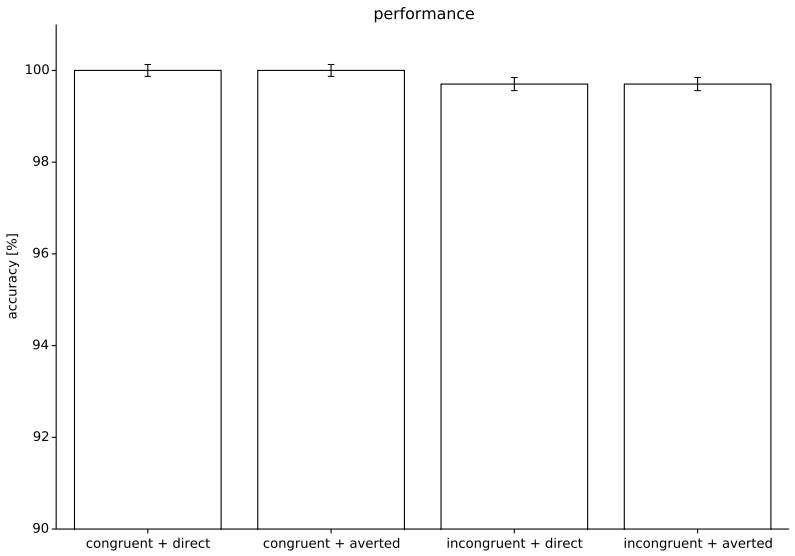

Figure 3.17: Mean accuracy for each condition. Error bars show the standard error of the mean.

3.2.3.2 Neuromagnetic data

Table 3.1: Significant spatiotemporal clusters found for the main effect of action intention (A) and of eye contact (B), time-locked to the subject's response (R) or the stimulus (S), p-values corrected for multiple comparisons, temporal window with temporal center of mass, approximate anatomical region, MNI coordinates for peak activation, normalized correlation with changes in reaction time, family-wise error corrected using the Bonferroni procedure ($p < 0.05/4 = 0.0125.$). ***Note.*** Time ranges related to response onsets are negative.

id	effect	onset	p-value	time range (ms)	region	MNI-RAS	correlation (r, p)
1	B	S	.046	30–174 (121)	visual ventral R	-23 -85 -13	.153, 0.5
2	A	R	.002	226–52 (138)	visual dorsolateral R	26 -79 15	**-.758, 1e-4**
3	A	R	.001	189–52 (107)	visual ventral L	-20 -85 17	-.346, .069
4	B	R	.001	167–77 (120)	visual ventromedial L	-20 -96 -15	-.250, .351

MEG data were concomitantly recorded to investigate the implication of cortical dynamics in gaze-processing during continuous action-perception loops. The neuromagnetic recordings were co-registered with the subject's anatomical model based on structural MRI. Averaged sensor space time series were then used to reconstructed time-locked cortical activation using an anatomically constrained minimum norm estimate (MNE) (Hämäläinen & Ilmoniemi, 1994). Spatiotemporal clustering (Maris & Oostenveld, 2007) was employed to detect task-specific gaze-locked and response-locked activation inside a predefined cortical search

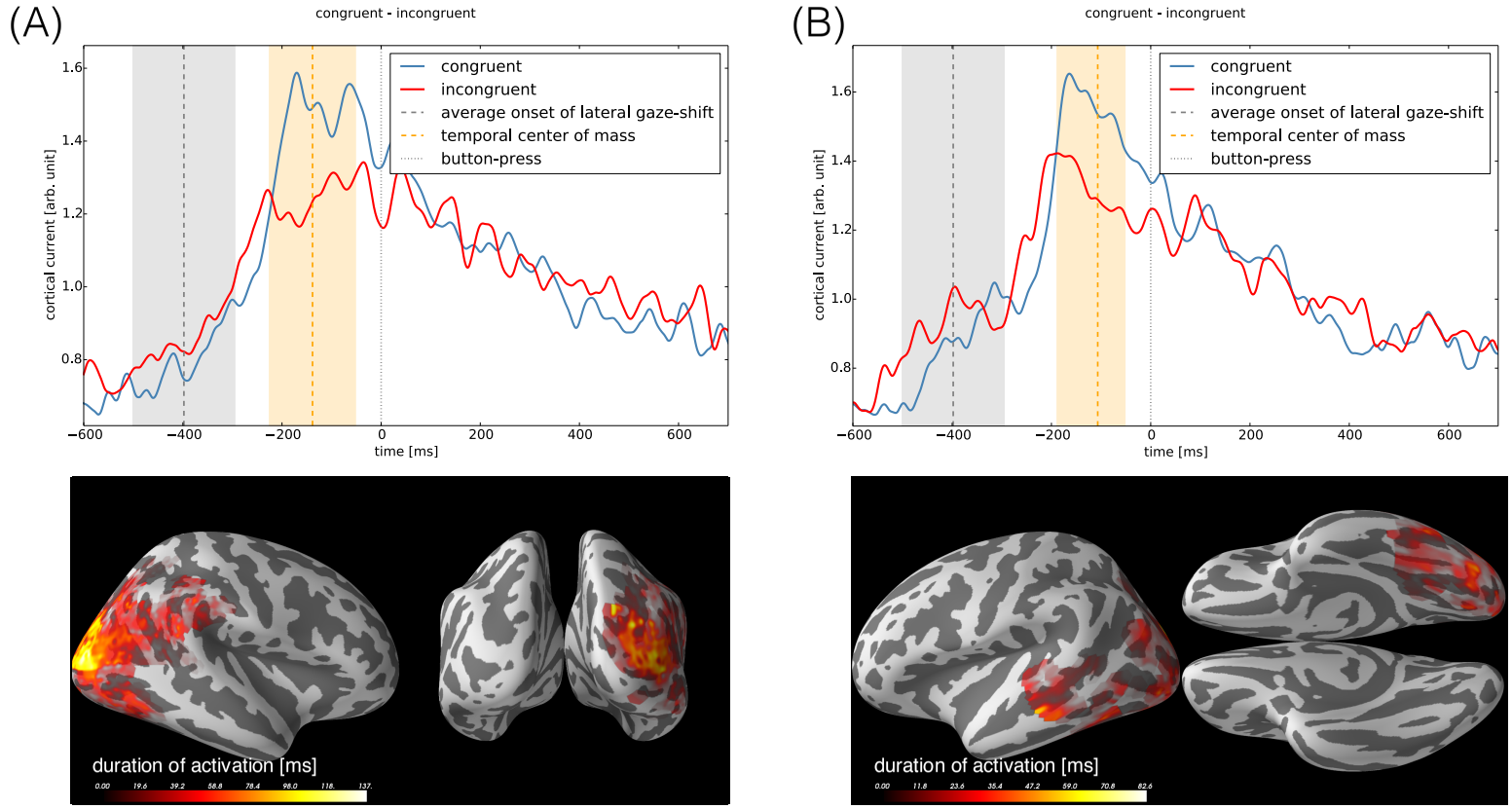

Figure 3.18: Spatiotemporal clustering in source space related to the effect of action intention. Panel (A) and (B) depict two independent clusters in which cortical and temporal locations have shown a significant effect response-locked of action intention. Panel (A) depicts cluster 2 and Panel (B) depicts cluster 3 (see table 3.1). The cortical surface displays map the test statistics weighted by the duration of significance, thresholded at a p-value of 0.01. The time courses represent averages of normalized brain activity at the location displayed in the lower panel. To take into account different levels of signal-to-noise ratio, time courses were previously normalized for each subject by dividing the time series by the mean time course across time. The time window of significance is highlighted in orange. The curvature of the cortical surface is indicated by light and and dark gray colors for gyri and sulci, respectively.

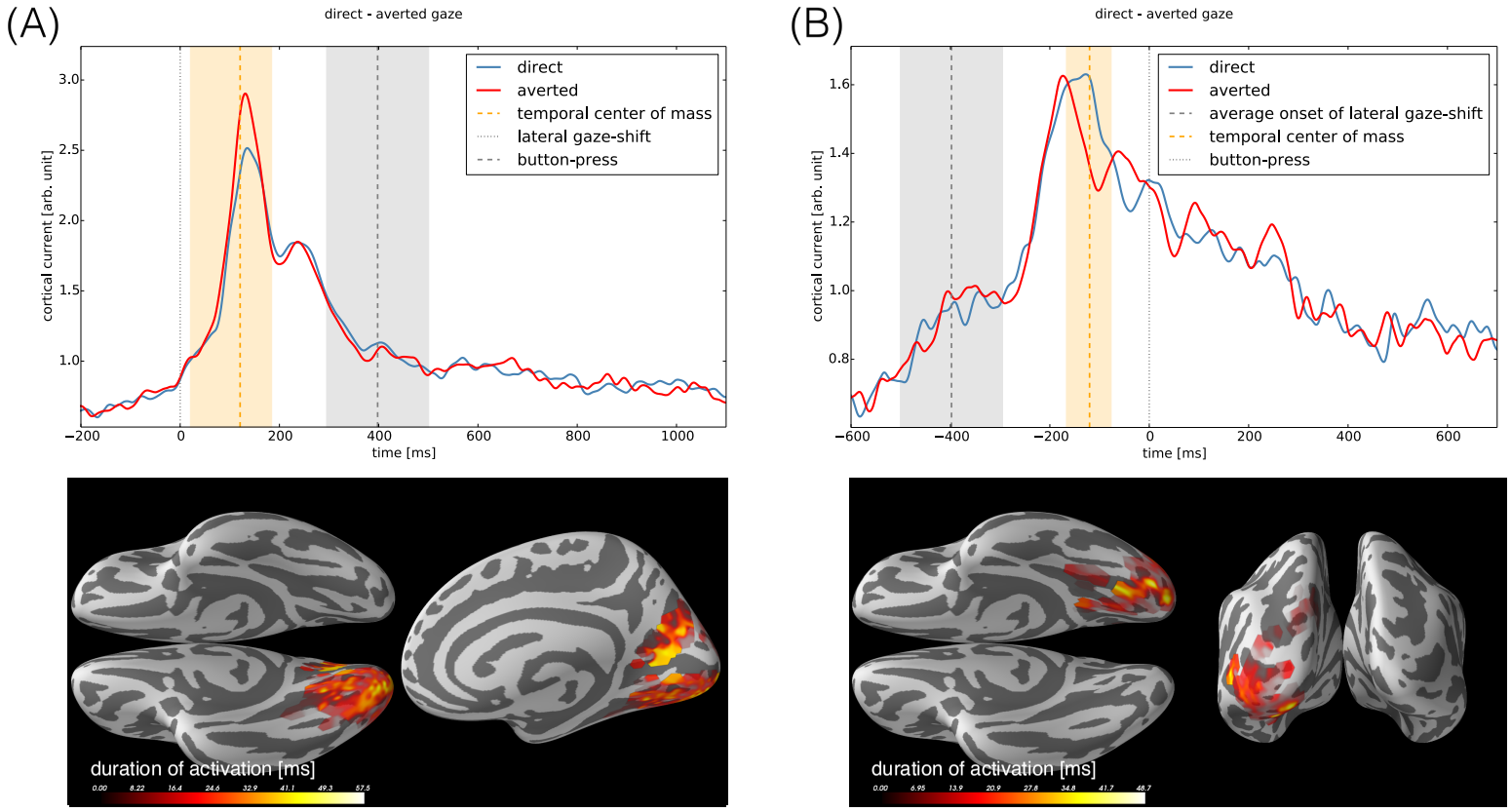

Figure 3.19: Spatiotemporal clustering in source space related to the effect of action eye contact. Panels (A) and (B) depict independent clusters in which cortical and temporal locations have shown a significant effect of action intention. Panel (A) shows activity time-locked to the gaze shift. Panel (B) shows activity time-locked to the button press. For visualization-related details see figure 3.18.

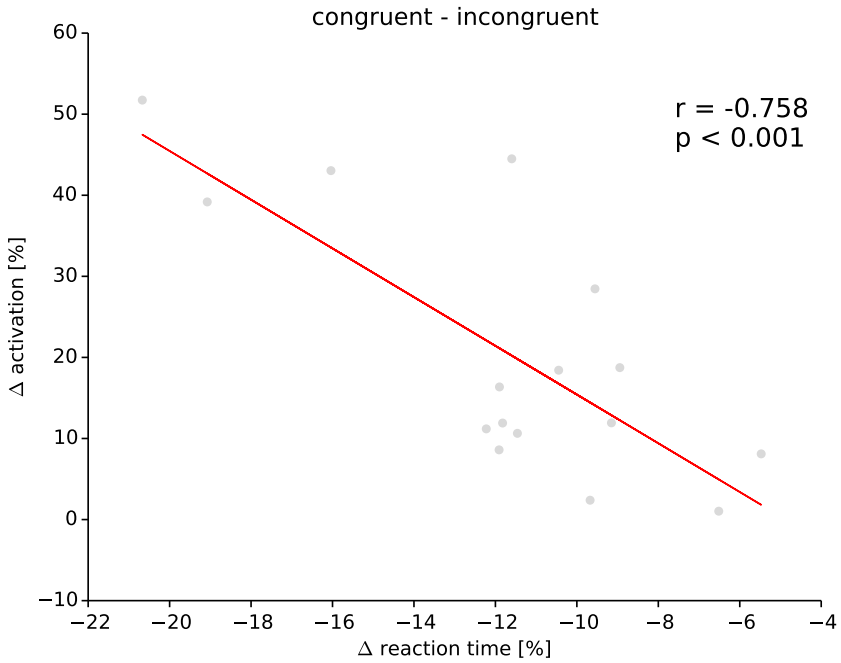

Figure 3.20: Neurobehavioral correlation between normalized changes in cortical current relative to the condition and relative changes in reaction time.

area (c.f. section 3.2.2.7.3) for all contrasts of interest (see section 3.2.2.7.3). Subsequently, the relationship between activation in significant spatiotemporal clusters and the subjects' reaction times was examined. For that purpose, source estimates were averaged within the cluster for each of the conditions contrasted. Normalized differences between conditions were computed for source estimates and reaction times, reflecting contrast-relative changes in cortical activation and reaction time. A conservative Bonferroni correction was employed to correct for multiple comparisons. The analysis revealed four significant clusters which are summarized in table 3.1. The following passage will present these four spatiotemporal segments in the order of their appearance, detail the contrast, its direction and time-locking properties, and, highlight specific regional and behavioral correlates.

The first significant dissociation of neuromagnetic signals occurred gaze-locked, 30 milliseconds post-stimulus, and terminated on average 230 milliseconds prior to the subjects' response (cluster 1). During this time interval, increased cortical activation for averted-gaze was observed in visual cortices, extending to the face-sensitive fusiform gyrus and the parieto-occipital sulcus (panel (A) in 3.19). All subsequent dissociations were response-locked.

The next dissociation occurred on average 174 milliseconds posterior to the lateral gaze shift and 226 milliseconds prior to the subject's response (cluster 2). It lasted throughout the remaining part of the observation window, terminating 52 milliseconds prior to the subject's response. During this time window, increased cortical activation was observed in

the congruent intention condition (panel (A) in figure 3.18). Specific regional activation was found in the MT/V5 region and the right TPJ, extending into the right pSTS. A significant neurobehavioral correlation was established between activity changes in this cluster and changes in reaction time ($r = -.758, p < 1.0 \times 10^{-4}$), depicted in figure 3.20.

The third dissociation was observed, on average, 211 milliseconds posterior to the gaze shift, lasting for about 107 milliseconds and terminating 52 milliseconds prior to the response (cluster 3, panel (B) in figure 3.18). During this interval, the left mid-STS, the left face-sensitive fusiform gyrus, and the left intraparietal sulcus showed increased activation for the congruent intention condition as compared to the incongruent intention condition. A correlation tendency was observed which, however, did not survive the correction for multiple comparisons.

On average, the last window of dissociation began 233 milliseconds after the gaze shift and terminated 77 milliseconds before the subject's response (cluster 4, panel B) in figure 3.19). During this time segment, increased cortical activity was found in the MT/V5 area, the left lingual gyrus, extending into the face-sensitive fusiform gyrus. While the first cluster did not show any substantial temporal overlap with the other clusters, the last three clusters shared common time windows between 167 and 77 milliseconds prior to the subject's response.

For the purpose of unambiguous discussion, these four clusters will be referred to by their corresponding entry in the id-column of table 3.1.

3.2.4 Discussion

3.2.4.1 Behavioral data

The present experiment replicated nearly all behavioral findings from experiment 1. The following passage will therefore only discuss findings which differed from experiment 1.

Subjects were found to respond about 50 milliseconds faster in the congruent intention condition as compared to the incongruent intention condition. These results conform to the findings in experiment 1, arguing for the presence of an automated cognitive mechanism related to action execution. Identical to experiment 1, reaction time differences between the congruent intention and the incongruent intention condition were modulated by eye contact, suggesting that as in experiment 1, the statistical structure of button presses closely matched the distribution of ISIs and was modulated by action intention in exactly the same direction as in experiment 1. These findings support the interpretation that the subjects were entrained to the task.

In contrast to experiment 1, the structure of the interaction between eye contact and action intention for average reaction times was different. In experiment 1, the difference between reaction times under congruent compared to incongruent intentions was modulated by eye contact. In the present experiment, reaction times under congruent intention were different for direct compared to averted gaze. These findings suggest that eye contact might have boosted responses following from congruent intentions reactions, but did not significantly interfere with incongruent action intentions. Such an interpretation would be consistent with previous findings based on SSRC protocols (Wang et al., 2011; Wang, Ramsey, & De C Hamilton, 2011). This finding might be explained by at least two factors. In the present experiment, the sample size was more than one third smaller than in experiment 2. Given the subtleties of the two alternative mechanisms at stake, this finding might therefore reflect inherent instability, or, sample bias. Both alternatives might relate to individual or group differences. The present sample might have represented a group of persons for whom direct gaze exerts facilitating effects during congruent actions. The larger sample in experiment 1 might have represented a wider range of individuals, also including persons for whom direct gaze might be irritating during incongruent action. Such a difference might be moreover related to age, which considerably differed between both samples. Future research on individual differences regarding the responsiveness to SSRC may therefore be fruitful. While the differences between the two experiments indicate that different mechanisms may be at stake, both experiments captured interaction effects between eye contact and action intention, which indicate action-related contextualization of gaze-processing.

Another notable difference between the findings from both experiments refers to the average variability of reaction times across conditions. The distributions displayed for each condition in experiment 1 (cf. figure 3.3) had already suggested differences in variability between congruent and incongruent responses. This suggested tendency turned statistically significant in the present experiment and conforms to the modulation of similarity between the distribution of ISIs and the between-button press intervals. Lower variance in reaction times, necessarily, implicates stricter coupling between these two inter-event intervals. The fact that experiment 1 showed a modulation of distribution similarity by intention without yielding significantly differences in reaction time variability might simply reflect the characteristics of the Kolmogorov-Smirnoff statistic, which is known to be more sensitive around the mode of the distribution and less so at its tails. The definitive result might be explained by the use of a more fine-grained stimulation and recording technique in the present experiment. A designated external graphics computation unit allowed jitter-free stimulation, and responses were recorded virtually analog, using the designated input channels of MEG acquisition system. In contrast, a regular office workstation is less exact with regard to timing and might therefore lack the temporal precision required to differentiate such subtleties. Differences

between both experiments regarding overall reaction times point into a similar direction. Given the differences between the acquisition system that were used in both experiments, it is conceivable that data in experiment 1 are subject to a constant offset due to the comparably less specialized hardware employed. This point, further, highlights the importance of specialized acquisition devices for the study of behavioral temporal dynamics.

Finally, the low overall error rate is remarkable. While descriptive results are in line with experiment 1, variability of errors was not sufficient to compute meaningful inferential statistics. This result might indicate cognitively more favorable conditions provided by the MEG-acquisition setup, but the details, which might help concretizing this line of thought, are not obvious. One explanation might refer to the breaks between the blocks that were provided to the subjects. Before advancing with the experiment, subjects were required to confirm that they had read the instruction by pressing a key in a self paced manner.

3.2.4.2 Neuromagnetic data

The analysis of source estimates revealed four spatiotemporal clusters of differential cortical signals. These clusters were characterized by activation of common cortical regions, notably, visual areas V1-3, and to a more variable extent, the face-sensitive areas in the FG and the lateral occipital cortices, and the MT/V5 area. Second, they were characterized by different time-locking properties and different temporal on- and offsets. Importantly, three out of four effects where response-locked, not gaze-locked, suggesting preferentially response-dominant gaze-processing during ongoing social interactions. The following paragraphs will integrate these temporal and regional facets in discussing findings by contrasts of interest. To provide with additional context, the following paragraphs will comment in greater detail on regional findings. Contrasts will be referred to according to section 3.2.2.7.3 and table 3.1.

The main effect analysis of action intention (contrast **A**) revealed two congruency-positive clusters (2 & 3) with identical time-locking properties (response-locked) and similar temporal onsets (around 200 milliseconds prior to the subject's response). It is therefore conceivable that cluster 2 and cluster 3 represent a bihemispheric congruency-positive network. Cluster 2 implicated differential activity in the MT/V5 and the rTPJ.

The **MT/V5** is located at the temporo-occipital border inside the visual extra-striate cortex (Brodmann area 19). The region possesses anatomical connections to visual cortical areas, from which it receives modulatory input, and, provides inputs to other areas participating in the dorsal visual processing stream (Born & Bradley, 2005). The tuning properties of the cells inside the MT area refer to speed and direction of motion and it has been implicated with the analysis of optical flow and motion in both monkeys and humans (Shipp, Blanton, & Zeki, 1998; Born & Bradley, 2005). The area has further been implicated in processing

biological motion (Bonda, Petrides, Ostry, & Evans, 1996). Recent connectivity analyses have linked this region to the pSTS, suggesting its implication in a network concerned with processing motion of eye gaze (Nummenmaa, Passamonti, Rowe, Engell, & Calder, 2010).

The **TPJ** is commonly defined as a region that encompasses the SMG, posterior parts of the STG, and dorsal-rostral parts of the occipital gyri. As suggested by Bzdok et al. (2013b), anatomical labeling of the TPJ is highly inconsistent and the TPJ is often also referred to as Brodmann area 39 or 40, angular gyrus or posterior part of the pSTS. The TPJ is a hetero-modal cortex and does not possess any obvious structural-functional equivalents in monkeys. Recent research, however, has linked the rTPJ to the monkeys mSTS based on its overall connectivity pattern (Mars et al., 2013), which is characterized by common coactivation with the anterior cingulate, the posterior cingulate, the anterior insula and the cingulate motor area, which all possess unequivocal equivalents in monkeys. The middle temporal cortex and the adjacent parts of the parietal cortex that harbor the human TPJ are believed to have progressively expanded during human evolution (32 times the size of the macaque's corresponding area), purportedly resulting in regional and functional differentiation of the macaque's temporal face- and action processing battery into several distinct subunits in humans (Van Essen & Dierker, 2007; Mars et al., 2013). Seemingly contradictory interpretations of this region's cognitive profile have been proposed (Corbetta, Patel, & Shulman, 2008), mainly referring to colocalization of attentional reorienting to relevant stimuli (Arrington, Carr, Mayer, & Rao, 2000; Corbetta, Kincade, Ollinger, McAvoy, & Shulman, 2000; Macaluso & Patria, 2007) with social attribution processes (Saxe & Kanwisher, 2003; Aichhorn et al., 2009). A recent meta-analysis by Decety and Lamm (2007) summarizes this debate in showing that the rTPJ was implicated in four distinct cognitive domains across a large set of studies: spatial-attentional processing, sense of agency, empathy, and Theory of Mind. Beyond targeting explanations that refer to the tasks and materials, researchers have sought to identify conceptual abstractions that are general enough to harmonize these different cognitive interpretations. A nonexhaustive list of candidates includes switching between frames of reference (Corbetta et al., 2008), updating predictions about external events (Decety & Lamm, 2007), and most recently, the production self-awareness and its social attribution (Graziano & Kastner, 2011; Graziano, 2014; Kelly, Webb, Meier, Arcaro, & Graziano, 2014). A recent meta-analytic and connectivity-based approach helped further differentiating the TPJ's role in cognitive processes and lead to the proposal of a twofold functional subdivision into a posterior part and an anterior part related to spatial-attentional and social-cognitive processing, respectively (Bzdok et al., 2013b). In the present experiment, increased activity in this region was found for the congruent intention condition with local peaks inside to both clusters reported in Bzdok et al. (2013b). Figure 3.21 shows the source activation for this effect with the cluster centroids superimposed.

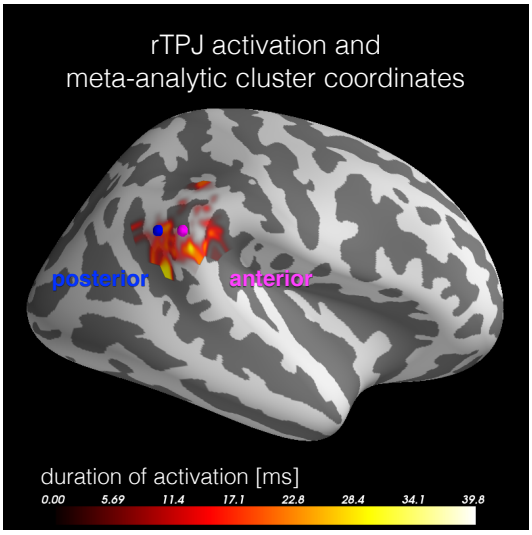

Figure 3.21: Right TPJ activation and clusters based on metaanalytic connectivity. Colored markers represent cluster centroids reported in Bzdok et al. (2013b). Activity has been masked to Brodmann area 40, based on the PALS B12 annotation (Van Essen, 2005).

Cluster 3 implicated differential activity the FG, the STS, and the IPS.

The ventrally located **FG** is part of the temporal lobe and extends into Brodmann area 37 in the occipital lobe. Together with the STS and the OFA its mid and posterior parts belong to a core-network subserving visual perception of faces and is believed to constitute a uniquely human functional specialization (Tsao, Moeller, & Freiwald, 2008; Yovel & Freiwald, 2013). Typically, this area has been associated with processing of static aspects of faces, such as identity. This aspect is illustrated by neurological case studies which demonstrate that patients suffering from lesions of this area were unable to identify a person based on her face. Similarly, for prosopagnosia patients, reduced activation has been reported in this area (Dobel, Junghofer, & Gruber, 2011). MEG studies have localized components between 110 and 170 milliseconds into this region which were sensitive to the onset or the offset of face stimuli (Halgren, Raij, Marinkovic, Jousmaki, & Hari, 2000; Sato et al., 2008; Hadjikhani, Kveraga, Naik, & Ahlfors, 2009; Tanaka, Inui, Kida, & Kakigi, 2009; Susac, Ilmoniemi, Ranken, & Supek, 2011; Taylor, Bayless, Mills, & Pang, 2011; Perry & Singh, 2014). Interestingly, based on a seed in the face-sensitive FG, Khan et al. (2013) found reduced long-range MEG connectivity patterns in persons suffering from autism spectrum disorders, suggesting a wider implication of this area in networks concerned with attribution of mental states and nonverbal communication. This conforms to a series of recent findings suggesting face-sensitive FG functionality beyond static face processing. According to this line of literature the face-sensitive FG is also involved in processing valence (Pizzagalli et al., 2002; Lewis et al., 2003; Japee, Crocker, Carver, Pessoa, & Ungerleider, 2009; Monroe et al., 2013) and specifically, social and affective judgments of persons (Bzdok et al., 2012). In contrast to the canonical view of the FG's function, recent findings have suggest that the FG

area is related to processing gaze direction (George, Driver, & Dolan, 2001; Dumas et al., 2013). Evidence based on intracranial recordings from the intact FG highlights a possible dissociation of these functional contexts based on signal latency and waveform (Pourtois, Spinelli, Seeck, & Vuilleumier, 2010; Kawasaki et al., 2012). These findings detail early components around 200 ms post-stimulus which were related to purely perceptual face processing and low-level categorization. In contrast, late components were reported, which were related to processing affect and gaze-direction.

The **STS** constitutes a major anatomical landmark on the temporal cortex and belongs to Brodmann areas 39 and 22. Monkeys do not seem to possess a ventral brain region, analogously to the human FG, concerned with processing faces and gaze (Yovel & Freiwald, 2013). Instead, their STS has been shown to harbor numerous patches concerned with high-level visual processing of social stimuli, such as gaze, faces, body parts and their characteristics such as spatial appearance, motion and goal-directedness (Bruce, Desimone, & Gross, 1981; Hasselmo, Rolls, Baylis, & Nalwa, 1989; Brothers & Ring, 1993; Umilta et al., 2001; Tsao & Freiwald, 2003; Keysers et al., 2004; Tsao, Freiwald, Tootell, & Livingstone, 2006). This link is drastically illustrated by post-operative debilitation of gaze-differentiation capacities in monkeys after removal of the banks and the floor of the STS region (Campbell, Heywood, Cowey, Regard, & Landis, 1990) and single gaze-selective patches (Heywood, Cowey, & Rolls, 1992), respectively. Recent comparative findings have implicated a functional expansion of the STS region in humans compared to monkeys (Mars et al., 2013). Indeed, in humans the STS region that includes the adjacent gyral structures, has been associated with a wide array of cognitive functions including multimodal perceptual integration, perception of motion, perception of faces and gaze, speech processing, and Theory of Mind and is commonly subdivided into a posterior and an anterior part (Allison, Puce, & McCarthy, 2000). A recent meta-analytic study reported clustering solutions supporting this subdivision (Hein & Knight, 2008) and suggested a bilateral posterior cluster concerned with processing of eye gaze while, in contrast, anterior clusters have been predominantly associated with speech processing. Interestingly, peak maxima from experiments which were concerned with Theory of Mind were found bilaterally dispersed across the entire STS region, conforming to the functional link between ToM and both speech processing and eye gaze (Mundy, Sigman, & Kasari, 1990; Tomasello, Carpenter, Call, Behne, & Moll, 2005). The same pattern applied to motion-processing in the left STS. Importantly, the pSTS receives modulatory input from the MT/V5 region, highlighting its role in movement-related and directional processing (Nummenmaa et al., 2010). Consistent with this classification, neuromagnetic studies on eye gaze and face-processing have mainly reported activation in the posterior part of the pSTS detailing time-locked dynamics related to averted gaze that peak around 250 milliseconds (Sato et al., 2008), transient BOLD-correlated beta-band modulations related to emotion recognition (Jabbi et al., 2014) and experience based processing of facial

expressions (Furl, van Rijsbergen, Treves, Friston, & Dolan, 2007). Recent neuroanatomical work based on individual differences in gyration proposes a refined subdivision of the STS into an anterior part, a middle part and a posterior part with two distinct terminal endings (Ochiai et al., 2004). Based on this subdivision, the mSTS region has been associated with a wide array of social-perceptual tuning-characteristics including human voices, faces, and, biological motion related to hand- and mouth and eye movement (Grafton, Arbib, Fadiga, & Rizzolatti, 1996; Rizzolatti et al., 1996; Grezes, 1998; Haxby, Hoffman, & Gobbini, 2000), suggesting a generalized functional selectivity to people (Watson, Latinus, Charest, Crabbe, & Belin, 2014). This link is further reminiscent of the evolutionary link between the monkey's mSTS and the human pSTS and rTPJ (Mars et al., 2013). Applying these proposed subdivisions, activity in cluster 3 showed local maxima that were located in the mid-STS and extended into the pSTS.

The **IPS** is located inside the parietal lobe, Brodmann area 7, and is attributed to the dorsal attention network (Corbetta et al., 2008). In monkeys, this region has been related to visuomotor-processing, such as the preparation of saccadic and reach-to-grasp movements in monkeys (Snyder, Batista, & Andersen, 1997). In humans, this region has also been linked to action preparation, but additionally, stands in close relationship to covert selective attention, goal representation (Astafiev et al., 2003; Hamilton & Grafton, 2006), and exerts putative top-down tuning of feature processing in sensory areas (Corbetta et al., 2008). The IPS is further believed to link incoming sensory information to action intentions (Snyder et al., 1997) and has been associated with processing gaze direction (Haxby et al., 1994; George et al., 2001) as expressed by frequent co-activation with the pSTS when processing eye gaze.

Based on the regional implications of cluster 2 and 3 it can therefore be argued that performing congruent actions with regard to another persons's eye gaze recruited a wide array of areas related to visual processing of motion, spatial attention, face and gaze perception, and, object-related attention. The identical timing properties of cluster 2 and 3 argue in favor of their interpretation as bihemispheric network that facilitates socially defined target actions. This is consistent with the finding that contrast-relative increases of activity were significantly related to contrast-relative decreases in reaction time, indicating a direct involvement of this network in action preparation.

The current time-locked analysis does not allow to assess the flow of information or changes in connectivity. However, at least two scenarios are conceivable. The visual gaze and attention related areas are triggered by an unknown, common cortical or subcortical driver. Following the phase-resetting view of time-locked responses (e.g. see Hanslmayr et al. (2007)), activity would therefore reflect modulatory top-down input, potentially reflecting visual and objected-related feature-tuning. Second, the evoked activity might reflect network-intrinsic, endogenous phase resets. Ensuing potentials might then propagate

to motor cortices along anatomical connections, reflecting a ramping-up process which might be observed as 'readyness-potential' at later stages. The high correlation between changes of cortical activity and relative decrease of reaction time in cluster 3 indeed support the second scenario. In this context, it is tempting to regard the rTPJ as a hub concerned with high-level parsing of visual-spatial and social perceptions and its forwarding to motor networks based on its functional connectivity with the cingulate motor area (Mars et al., 2013). This, however, would not explain the role of activity in the left hemispheric cluster that was not significantly related to reaction time changes. It is therefore most likely that both scenarios apply to different degrees. One more additional cue is given by the correlation differences between the left and the right cluster. In regional and related functional terms, one striking difference between the left and the right clusters refers to the implication of the dorsal and the ventral attention network, respectively. The left hemispheric cluster 3 differentially involved the mSTS, the mid FG and the IPS. Given the previous discussion, these findings might argue in favor of a subnetwork concerned with processing gaze direction. In contrast, the right hemispheric cluster 2 implicated the rTPJ, which belongs to the ventral attention network. Following the previous discussion, this suggests a right hemispheric subnetwork concerned with object-related, in this case: social and attentional processing. The fact that differential activity in the left hemispheric cluster started later than in the right hemispheric cluster, but only the latter exhibited significant correlation with reaction times might even indicate a hierarchical relationship between cluster 2 and cluster 3, hence, between spatial and object-related attentional processes during action-oriented processing of eye gaze. In other words, the dominant frame of reference was object-based, social, whereas spatial computations were possibly subordinated and terminated before final execution. In this sense, it might be speculated that activity in cluster 2 rather followed the second interpretation of evoked activity as endogenous processes while activity in cluster 3 might be more accurately understood in terms of exogenous modulation.

The main effect analysis of eye contact (contrast **B**) revealed one direct-gaze-negative gaze-locked cluster in the right hemisphere (cluster 1) and one direct-gaze-positive response-locked cluster in the left-hemisphere (cluster 4).

The overall time course of activity in cluster 1 is reminiscent of a M170 waveform and exhibits differential increases of activity for averted gaze. In regional terms, primary and higher visual areas including the parieto-occipital sulcus have been differentially implicated. Activity extended into the posterior FG.

The **parieto-occipital sulcus** serves as a macroanatomical landmark which separates occipital from parietal lobes. In both monkeys and humans the V6 has been located in this area, which belongs to the dorsal visual pathway and exhibits anatomical connections to the motor cortices. This region has been linked to visual attention (Vanni, Revonsuo, & Hari,

1997), representation of one's own eye gaze (Galletti, Battaglini, & Fattori, 1995; Nakamura, Chung, Graziano, & Gross, 1999), and planning of reach-to-grasp movements (Galletti, Kutz, Gamberini, Breveglieri, & Fattori, 2003). Based on its time-locking properties, this effect might refer to stimulus-driven bottom-up modulations of visual face-related attention that is triggered by changes of eye gaze in the absence of preceding eye contact.

One remarkable detail refers to the early onset of activation after 30 milliseconds only. Such early cortical activations have only rarely been reported in the gaze-literature, but are not unexpected in situations in which subjects have been entrained to a task (Stefanics et al., 2010; Besle et al., 2011). This finding might therefore indicate enhanced cortical sensitivity to directional eye gaze cues following prolonged exposure to averted gaze. Signals were subtracted from each other and differences between averted and direct gaze stimuli where minima. Importantly, they manifested prior to the time-locking event which was identical in all conditions (lateral gaze shift). These facts pose a severe problem to purely visual interpretation of this effect. One putative explanation might refer to social factors. A lack of eye contact might impair the subject's tendency to predict changes in eye gaze, which then might appear as more surprising as reflected in stronger update-signals reflecting prediction-error. Alternatively, a lack of eye contact might enhance fixation of the eye region, leading to enhanced visual processing. Such construals will be examined later in greater detail (c.f. 3.3).

Cluster 4 was characterized by increased activity time-locked to changes of eye gaze following previous eye contact and differentially implicated the MT/V5 region, the lingual gyrus, extending into the middle FG and the lateral occipital cortex.

The **lingual gyrus** is located medially in the occipital and temporal cortices, and traverses Brodmann areas 18 and 19. This region has been associated with various cognitive processes that relate visual processing to language (Damasio & Damasio, 1983), object memory (Allison et al., 1994; Perani et al., 1995), cross-modal attentional (Macaluso, Frith, & Driver, 2000), and social cognition (Rilling, Sanfey, Aronson, Nystrom, & Cohen, 2004; Völlm et al., 2006).

Against the background of the previous discussion, this regional pattern argues in favor of a network related to the perception of eye movements. Based on its time-locking characteristics and the absence of meaningful correlation with reaction time changes, this activation might reflect top-down-modulations from other networks during action preparation. Interestingly, the temporal window of activity is endorsed by the temporal windows defining clusters 2 and 3, which also implicated activity in the MT/V5 region and the functionally connected STS. This provides with another additional cue for the interpretation of its cognitive role. Significant activity in the congruent-intention network lasted until the end of the temporal observation window, and, most likely, extended into the time around the motor act. Activity in this spatiotemporal segment terminated within the temporal observation-window,

which argues for a sub-process, that is action-related but not necessarily execution-related. At a cognitive level, intensified processing of gaze-related motion during planning of socially defined actions might refer to the ostensive role of eye contact (Tomasello, Hare, Lehmann, & Call, 2007). Eye contact serves as a major communicative cue, or marker of relevance (Sperber, Wilson, & Ziran, 1986), and commonly modulates the interpretation of subsequent behaviors as deictic or of communicative intent. Such modulations might include social-visual feature tuning with regard to processing deictic gestures, such as changes of eye gaze. The fact that such a modulation is found to be response-locked indicates that preceding ostensive-cues, that lie in the past are effectively evaluated, during action planing. In other words, the recognition of ostensive cues as such might refer to post-hoc contextualization of present events at a time at which they become relevant for the implementation of the intended action.

3.3 General discussion

The overall goal of this study was to investigate the time-locking properties of visual gaze-related cortical dynamics during ongoing social interaction. In detail, the hypothesis pursued in this study referred to changes of related time-locking properties from stimulus-dominance to action-dominance. The study comprised two experiments, of which the first evaluated a novel SSRC protocol which was used in the second experiment to evoked gaze-related cortical dynamics tuned to interaction. The plausibility of this novel protocol was evaluated with regard to rapid reaction time dynamics related to varied intentional context and, second, with regard to entrainment to the task as expressed by context-dependent distance-reduction of ISI distributions and response-interval distributions. These characteristics turned out to be robust as indicated by replication of the main findings in the second experiment. Behavioral findings in both experiments conformed to the patterns reported by Wang et al. (2011), Wang et al. (2011), which comprised a main effect of action intention (congruent actions were faster than incongruent actions) and its modulation by eye contact. The mean reaction time patterns across conditions in both experiments argued in favor of a rapid, automatic, or implicit modulation of action control by social context, i.e., eye gaze, resulting in facilitated performance of socially congruent action. The task-induced entrainment constitutes a novel finding for which the literature regarding SSRC protocols did not report any equivalent. This aspect therefore required internal validation in terms of cortical dynamics. In total, behavioral findings unequivocally indicated cross-talk between action intentions and eye contact during visual processing of changes in eye gaze.

Experiment 2 manifested response-dominant time-locking characteristics manifested for differential signals with regard to action intention and with regard to eye contact. For

action intention the case was unequivocal, no differential gaze-locked activity occurred. Instead, response-locked and congruency-positive differential activity was observed in a wide array of visual areas and regions related to higher visual attention, social perception and face processing. Given the significant correlation with reaction times observed inside this network, it can be argued that this congruency-positive activity explains the behavioral main effect of gaze observed over both experiments. One fundamental ambiguity of the behavioral findings related to the direction of modulation, i.e., as to whether actions following congruent intentions receive a boost or whether, alternatively, actions following incongruent intentions were inhibited. The intrinsic low error rate for congruent intentions and the higher distribution-similarities with regard to ISIs and response rhythms, had made the existence of a congruency-positive mechanism plausible. The present neuromagnetic findings unambiguously argue in favor of such a mechanism, which might be concerned with enhancing action-perception integration during ongoing social interaction by allocating visual attention to the eye region of another person and by establishing 'fast', direct mappings between perceived gaze direction and ipsilateral motor commands. Given the wide array of cortical sites along the visual ventral and dorsal pathways, which included both attention-, gaze- and self-other-related networks, it is likely that this phenomenon is related to the social properties of the task. Additional clues were given by the putative hierarchical subordination of spatial-processing under object-related social processing, which was indicated by the different correlation patterns in both congruency-positive clusters. At a cognitive level, these findings would implicate a proactive adjustment and sensitivity-boosting towards others when acting in mutually compatible or congruent ways. This finding would be compatible with the joint action literature that has described vast forms of intuitive mutual, often automated synchronization. On the other hand, some caution is indicated, since the correlation roughy explains 17 percent of the behavioral variance, and therefore the current analysis might have been blind to a congruency-negative network that relates to impaired reaction times during incongruent processing. In fact, the fMRI data by Schilbach et al. (2010) found such a network, prominently highlighting the role of the dorsal attention network during incongruent processing. However, no congruency-positive network was found in their study. This might be due to the neuroimaging modality, implicating transient activity that might not have been captured by fMRI, or due to the present protocol that had a tighter and more intuitive temporal structure. The fact that activity dissociations were rather enduring than transient would argue in favor of the second interpretation. In this context, it is noteworthy to highlight the fact that the congruent intention contrast in the present study implicated regions which Schilbach et al. (2010) exclusively reported in either the congruent intention contrast or in the social versus object contrast.

For eye contact, both gaze-locked and response-locked differential signals were observed. But based on the location, the contrast and the timing of these effects, it can be ruled out that both clusters in any sense refer to the same activity. The gaze-locked cluster implicated early visual activity, which was increased for change of eye gaze in the averted gaze condition and terminated before activity in the other cluster started. In the second cluster, activity was increased with regard to changes of eye gaze in the direct gaze condition. Activity for the effect of eye contact hence clearly dissociated as a function of time-locking properties. It has been suggested that the first finding does not reflect stimulus-properties, as in both conditions, the stimuli to which activity was time-locked to have been identical. One interpretation suggested intensified update-signals as a consequence of the presumably aversive experience of sustained averted gaze. However, averted-gaze might also have lead subjects to enter a spectatorial mode which might have facilitated to focus on the eye region. This idea refers to interpersonal distance norms with regard to the socially tolerable duration of mutual gaze. Experiments based on one-way mirrors have shown that humans tend to fixate other humans' eye region significantly longer as long the other could not see them (Argyle, Ingham, Alkema, & McCallin, 1973). However, the lack of eye tracking data and also the lack of obvious behavioral correlates makes it hard to decide between those two cognitive interpretations. In contrast, the second activation cluster was linked to referential-ostensive processing based on its regional and its time-locking properties.

At first glance, the absence of any significant interaction contrast seems astonishing given the interaction between eye contact and action intention at the behavioral level, which was observed in experiment 1 and experiment 2. This phenomenon may be explained in at least four ways. The interaction effect might not be reflected in time-locked but in induced oscillatory activity. The interaction effect, at the behavioral level, might not be reflected in a corresponding interaction effect at the level of cortical dynamics. The subtle boosts of reaction time observed for congruent intentions with preceding eye contact (c.f. figure 3.13) might by implemented in a 'sparse-coded' manner, for example as simultaneous time-locked activity inside regions clusters 2 and 3. Such a scenario might implicate an unknown aggregation mechanism which nonadditively translates into reaction time benefits. In a third scenario the driver for this interaction effect is not captured by cortical MEG signals. Finally, the effect might have been too weak to be detected by the clustering permutation test. Recent studies have highlighted the relevance of the dMPFC and the IFG for interaction effects in SSRC protocols. Assuming that related effects can be found in neuromagnetic signals from frontal and prefrontal cortical locations, this approach would also explain the absence of any significant cluster in the frontal cortical search surface. These potential mechanisms warrant further investigations in future studies.

One common, but remarkable characteristic of the neuromagnetic findings refers to the regional structure of maximum duration of significance. All clusters show peaks of sustained activation in occipital visual cortices. These activations, depending on the related time-locking characteristics, as suggested by the discussion of contrasts, most likely reflect bottom-up or top-down feature tuning of face and gaze-related perception. Importantly, for none of the contrasts, stimuli that defined the time-locking events systematically differed. For the eye contact contrast, the previous visual context slightly differed between the conditions, but for the congruent intention contrast, strictly speaking, no difference existed with regard to visual stimulation. These facts rule out purely stimulus-based explanations of this phenomenon. Instead, the extended duration of visual activity argues in favor of this experiment's online character implicating continuous action-perception loops. These observations clearly warrant further investigations of temporal succession and causality at the single trial level and call for an investigation of oscillatory behavior. Given the present evidence, no unequivocal conclusions are permitted with regard to the direction and the structure of modulation.

4 Conclusion

The overarching goal of this thesis was to promote the magnetoencephalographic study of social cognition. This agenda was addressed by choosing two forefront research questions in MEG and social cognitive neuroscience, the regularization of covariance and the cortical dynamics underlying gaze processing during ongoing social interactions, respectively.

Study 1 investigated the problem of between-sensors noise covariance and its implications for spatial whitening of MEG data. A new method was developed, based on recent machine learning techniques and evaluated on simulate data and several MEG datasets and one EEG dataset. The method permits to determine the most appropriate M/EEG covariance estimator out of a set of different candidates by using a maximum-likelihood metric. A list of conceivable candidate models was identified based on applicability to the signal characteristics of M/EEG data and subsequently examined. Simulation results and results based on M/EEG data showed that different models can describe the MEG between-sensors noise covariance most appropriately, depending on various circumstances. The study demonstrated that the proposed method is both automatic and quality preserving, since the ultimate metric chosen was always superior to the default choice, i.e., the sample covariance. Importantly, the impact of the method was practically assessed by analyzing signal contrasts related to face-processing from a publicly available MEG dataset. Results demonstrated that the new estimation method helps stabilizing the source amplitudes of inverse solutions and identified one candidate mechanism which explains between-subject variability in group analysis. Because of the far-reaching implication of covariance estimation in M/EEG analysis the results of study 1 help to solve multiple problems at once over a general range of particular methods MEG from which researchers can choose.

Study 2 investigated the time-locking properties of cortical dynamics during ongoing social interactions. The results showed that the majority of significant spatiotemporal signal dissociations were found time-locked to the subject's actions, not to the onset of eye gaze. Importantly, these response-locked signals implicated visual processing, areas commonly related to spatial- and object-oriented attention, and areas commonly associated with social perception and Theory of Mind. The study found differential correlation between cortical activity and reaction times which additional served the validation of the results. The findings from this study suggest that response-locked cortical responses become increasingly dominant during social interaction. This might indicate that during ongoing interaction, gaze processing is tuned to social coordination.

Study 1 did not investigate the impact of covariance estimators on preprocessing techniques such as SSP and ICA. Such investigations are relevant given the mathematics implied and are warranted given the challenges associated with MEG signal processing. Second, single subject datasets where used for validation. While this does not relativize the results of study 1, group level benchmarks are highly desirable for cognitive researchers. Future studies, therefore, should investigate spatial whitening in the context of preprocessing ICA, where the current procedure could be used to optimally decorrelate input signals before actually computing ICA and, second, yield automated rank estimates that would help addressing another unsolved problem, i.e., the informed choice of numbers of components. Such a project should be based on a large group of subjects, for example EEG patient data, to further limit potential overfitting during the development of methods.

Study 2 suffered from exposing a phenomenon which has been rarely reported and that is insufficiently investigated. The study therefore generated a series of questions which need to be addressed in future studies. The study has based its observations on an approximation to social interaction by using a protocol which facilitated entrainment. To maximize the expected effects, different means where combined at the same time ('sledge hammer approach'). As a consequence, the exact mechanisms by which the protocol achieved its goals are not yet well understood. Additional, purely visual-directional experimental contexts investigating different jitter distributions for ISIs might help to better understand the exact implications of the present protocol. A future study should closely investigate oscillatory characteristics of gaze-related cortical dynamics during social interaction. Especially single trial analyses might help track-down routes of entrainment with the ultimate aim of showing under which circumstance cortical time-locking properties may swap between two macroscopic systemic attractor events, such as stimulus changes and intended action. Most importantly, the physiological meaning of nonmotor response-locked activity is poorly understood. The related literature seems to be sparse if not non-existing. In this context, future studies should dedicate a reasonable amount of time into modeling and simulation of time-locking properties. In a minimum scenario, distinct time-locked sources would be placed around alternative trigger-events to exactly quantify the conditions of dissociation and overlap at the observational level of source analysis. A further limitation refers to the approximative nature of the interaction task which is markedly different from investigating ongoing multi-person dynamics. While this does not weaken the present findings, more fine-grained conclusions might be reached based on multi-person protocols. One first modification of the protocol in this direction would point to the use of eye-tracking. This would allow to replace the manual response channel by subjects' eye gaze and would allow to track subjects' behavior during the task in a more fine-grained fashion which can facilitate interpretation of results. A future variant of the protocol could involve a second subject and

interactions could be based on mutual congruent versus incongruent looking. Comparing such two-person interactions to the statistical entrainment that was used in this study might further help to differentiate cortical effects of entrainment.

The two problems investigated by this thesis are related in several ways. MEG instrumentation and choice of analysis parameters can impact neuromagnetic findings in complex ways which are not yet fully understood. Often, local ad-hoc solutions are propagated which, globally, complicate analyses as they reduce the reproducibility of findings and impact creativity by multiplying uncertainty. This is even more true where the signals of interests and contrasts between them lend themselves towards low signal-to-noise ratios, as it is the case for social cognition data. Arguably, methods research and engineering are inextricably linked with domain specific progress, especially when working on forefront challenges. At the same time, the MEG methods research can test its relevance and generality by including domain specific perspectives during development and evaluation. From a data scientific point of view, signal contrasts which are relative to subtly varied social interactive contexts pose challenges to instrumentation and development. These can easily be missed when only testing novel methods against less demanding data that neither involves contrast signals nor demanding experimental protocols. In this sense, the results from this thesis motivate a close exchange and collaboration between researchers who focus on engineering problems and researchers whose work poses engineering problems.

References

Abraham, A., Pedregosa, F., Eickenberg, M., Gervais, P., Mueller, A., Kossaifi, J., ... Varoquaux, G. (2014). Machine learning for neuroimaging with scikit-learn. *Frontiers in Neuroinformatics*, *8*(14). doi:10.3389/fninf.2014.00014

Ahlfors, S. P., Han, J., Belliveau, J. W., & Hämäläinen, M. S. (2010). Sensitivity of meg and eeg to source orientation. *Brain topography*, *23*(3), 227–232.

Ahlfors, S. P., Han, J., Lin, F.-H., Witzel, T., Belliveau, J. W., Hämäläinen, M. S., & Halgren, E. (2010). Cancellation of eeg and meg signals generated by extended and distributed sources. *Human brain mapping*, *31*(1), 140–149.

Aichhorn, M., Perner, J., Weiss, B., Kronbichler, M., Staffen, W., & Ladurner, G. (2009). Temporo-parietal junction activity in theory-of-mind tasks: falseness, beliefs, or attention. *Journal of Cognitive Neuroscience*, *21*(6), 1179–1192.

Akiyama, T., Kato, M., Muramatsu, T., Umeda, S., Saito, F., & Kashima, H. (2007). Unilateral amygdala lesions hamper attentional orienting triggered by gaze direction. *Cerebral Cortex*, *17*(11), 2593–2600.

Allison, T., Ginter, H., McCarthy, G., Nobre, A. C., Puce, A., Luby, M., & Spencer, D. D. (1994). Face recognition in human extrastriate cortex. *Journal of neurophysiology*, *71*, 821–821.

Allison, T., Puce, A., & McCarthy, G. (2000). Social perception from visual cues: role of the STS region. *Trends in Cognitive Sciences*, 267–278.

Argyle, M. & Dean, J. (1965). Eye-contact, distance and affiliation. *Sociometry*, *28*(3), 289–304.

Argyle, M. & Ingham, R. (1972). Gaze, mutual gaze, and proximity. *Semiotica*, *6*(1), 32–49.

Argyle, M., Ingham, R., Alkema, F., & McCallin, M. (1973). The different functions of gaze. *Semiotica*, *7*(1), 19–32.

Arrington, C., Carr, T., Mayer, A., & Rao, S. (2000). Neural mechanisms of visual attention: object-based selection of a region in space. *Cognitive Neuroscience, Journal of*, *12*(Supplement 2), 106–117.

Aschersleben, G., Hofer, T., & Jovanovic, B. (2008). The link between infant attention to goal-directed action and later theory of mind abilities. *Developmental Science*, *11*(6), 862–868.

Astafiev, S. V., Shulman, G. L., Stanley, C. M., Snyder, A. Z., Van Essen, D. C., & Corbetta, M. (2003). Functional organization of human intraparietal and frontal cortex for attending, looking, and pointing. *The Journal of Neuroscience*, *23*(11), 4689–4699.

Bar, M., Kassam K.S., Ghuman, A. S., Boyshan J. Schmid, A. M., Dale, A. M., Hämäläinen, M. S., ... Halgren, E. (2005). Top-down facilitation of visual recognition. *Proceedings of the National Academy of Sciences*, *103*(2), 449–454.

Bar, M., Kassam, K. S., Ghuman, a. S., Boshyan, J., Schmid, a. M., Schmidt, a. M., ... Halgren, E. (2006, January). Top-down facilitation of visual recognition. *Proceedings of the National Academy of Sciences of the United States of America*, *103*(2), 449–54. doi:10.1073/pnas.0507062103

Barber, D. (2012). *Bayesian reasoning and machine learning*. Cambridge University Press.

Bard, K. & Vauclair, J. (1984). The communicative context of object manipulation in ape and human adult-infant pairs. *Journal of Human Evolution*, *13*(2), 181–190.

Baron-Cohen, S., Hoekstra, R. A., Knickmeyer, R., & Wheelwright, S. (2006). The autism-spectrum quotient (aq)—adolescent version. *Journal of autism and developmental disorders*, *36*(3), 343–350.

Beck, A. T., Steer, R. A., & Hautzinger, M. (1994). *Beck-depressions-inventar:(bdi); testhandbuch*. Huber.

Beck, A. T., Ward, C., Mendelson, M., et al. (1961). Beck depression inventory (bdi). *Arch Gen Psychiatry*, *4*(6), 561–571.

Beckmann, C. F. & Smith, S. M. (2004). Probabilistic independent component analysis for functional magnetic resonance imaging. *Medical Imaging, IEEE Transactions on*, *23*(2), 137–152.

Behrens, T. E., Hunt, L. T., & Rushworth, M. F. (2009). The computation of social behavior. *Science*, *324*(5931), 1160–1164.

Beier, J. S. & Spelke, E. S. (2012). Infants' developing understanding of social gaze. *Child development*, *83*(2), 486–496.

Berger, H. (1929). Hans berger on the electroencephalogram of man (in german). *In: Arch F Psychiatr. 87*, 527–70.

Besl, P. & McKay, N. D. (1992). A method for registration of 3-d shapes. *Pattern Analysis and Machine Intelligence, IEEE Transactions on*, *14*(2), 239–256. doi:10.1109/34.121791

Besle, J., Schevon, C. A., Mehta, A. D., Lakatos, P., Goodman, R. R., McKhann, G. M., ... Schroeder, C. E. (2011). Tuning of the human neocortex to the temporal dynamics of attended events. *The Journal of Neuroscience*, *31*(9), 3176–3185.

Bishop, C. M. (1999). Bayesian PCA. *Advances in neural information processing systems*, 382–388.

Blais, C., Jack, R. E., Scheepers, C., Fiset, D., & Caldara, R. (2008). Culture shapes how we look at faces. *PLoS One*, *3*(8), e3022.

Bohil, C. J., Alicea, B., & Biocca, F. A. (2011). Virtual reality in neuroscience research and therapy. *Nature reviews neuroscience*, *12*(12), 752–762.

Bonda, E., Petrides, M., Ostry, D., & Evans, A. (1996). Specific involvement of human parietal systems and the amygdala in the perception of biological motion. *The Journal of Neuroscience*, *16*(11), 3737–3744.

Born, R. T. & Bradley, D. C. (2005). Structure and function of visual area mt. *Annu. Rev. Neurosci. 28*, 157–189.

Breiman, L. & Spector, P. (1992). Submodel selection and evaluation in regression. the x-random case. *International statistical review/revue internationale de Statistique*, 291–319.

Breuer, L., Dammers, J., Roberts, T., & Shah, N. (2014a). Ocular and cardiac artifact rejection for real-time analysis in meg. *Journal of neuroscience methods*, *233*, 105–114. doi:10.1016/j.jneumeth.2014.06.016

Breuer, L., Dammers, J., Roberts, T. P., & Shah, N. J. (2014b). A constrained ica approach for real-time cardiac artifact rejection in magnetoencephalography. *Biomedical Engineering, IEEE Transactions on*, *61*(2), 405–414.

Brothers, L. & Ring, B. (1993). Mesial temporal neurons in the macaque monkey with responses selective for aspects of social stimuli. *Behavioural brain research*, *57*(1), 53–61.

Bruce, C., Desimone, R., & Gross, C. G. (1981). Visual properties of neurons in a polysensory area in superior temporal sulcus of the macaque. *J Neurophysiol*, *46*(2), 369–384.

Brunet, N. M., Bosman, C. A., Vinck, M., Roberts, M., Oostenveld, R., Desimone, R., ... Fries, P. (2014). Stimulus repetition modulates gamma-band synchronization in primate visual cortex. *Proceedings of the National Academy of Sciences*, *111*(9), 3626–3631. doi:10.1073/pnas.1309714111. eprint: http://www.pnas.org/content/111/9/3626.full.pdf+html

Bzdok, D., Langner, R., Hoffstaedter, F., Turetsky, B. I., Zilles, K., & Eickhoff, S. B. (2012). The modular neuroarchitecture of social judgments on faces. *Cerebral Cortex*, *22*(4), 951–961.

Bzdok, D., Langner, R., Schilbach, L., Engemann, D. A., Laird, A. R., Fox, P. T., & Eickhoff, S. B. (2013a). Segregation of the human medial prefrontal cortex in social cognition. *Frontiers in human neuroscience*, *7*.

Bzdok, D., Langner, R., Schilbach, L., Jakobs, O., Roski, C., Caspers, S., ... Eickhoff, S. B. (2013b). Characterization of the temporo-parietal junction by combining data-driven parcellation, complementary connectivity analyses, and functional decoding. *Neuroimage*, *81*, 381–392.

Call, J. & Tomasello, M. (1999). A nonverbal false belief task: the performance of children and great apes. *Child development*, *70*(2), 381–95.

Call, J. (2009). Contrasting the social cognition of humans and nonhuman apes: the shared intentionality hypothesis. *Topics in Cognitive Science*, *1*(2), 368–379.

Callaghan, T., Moll, H., Rakoczy, H., Warneken, F., Liskowski, U., Behne, T., & Tomasello, M. (2011, August). Early social cognition in three cultural contexts. IV. General discussion. *Monographs of the Society for Research in Child Development*, *76*(2), 105–15. doi:10.1111/j.1540-5834.2011.00607.x

Campbell, R., Heywood, C. A., Cowey, A., Regard, M., & Landis, T. (1990). Sensitivity to eye gaze in prosopagnosic patients and monkeys with superior temporal sulcus ablation. *Neuropsychologia*, *28*(11), 1123–1142.

Carpenter, M., Nagell, K., Tomasello, M., Butterworth, G., & Moore, C. (1998). Social Cognition, Joint Attention, and Communicative Competence from 9 to 15 Months of Age. *Monographs of the Society for Research in Child Development*.

Cauchoix, M., Barragan-Jason, G., Serre, T., & Barbeau, E. (2014). The neural dynamics of face detection in the wild revealed by mvpa. *The Journal of neuroscience : the official journal of the Society for Neuroscience*, *34*(3), 846–54. doi:10.1523/JNEUROSCI.3030-13.2014

Charman, T., Baron-Cohen, S., Swettenham, J., Baird, G., Cox, A., & Drew, A. (2000). Testing joint attention, imitation, and play as infancy precursors to language and theory of mind. *Cognitive Development*, *15*(4), 481–498.

Chen, Y.-H., Edgar, J. C., Holroyd, T., Dammers, J., Thönnessen, H., Roberts, T. P. L., & Mathiak, K. (2010, May). Neuromagnetic oscillations to emotional faces and prosody. *Eur J Neurosci*, *31*(10), 1818–27. doi:10.1111/j.1460-9568.2010.07203.x

Chen, Y., Wiesel, A., Eldar, Y. C., & Hero, A. O. (2010). Shrinkage algorithms for MMSE covariance estimation. *Signal Processing, IEEE Transactions on*, *58*(10), 5016–5029.

Ciulla, C., Takeda, T., & Endo, H. (1999). Meg characterization of spontaneous alpha rhythm in the human brain. *Brain topography*, *11*(3), 211–222.

Corbetta, M., Kincade, J. M., Ollinger, J. M., McAvoy, M. P., & Shulman, G. L. (2000). Voluntary orienting is dissociated from target detection in human posterior parietal cortex. *Nature neuroscience*, *3*(3), 292–297.

Corbetta, M., Patel, G., & Shulman, G. L. (2008, May). The reorienting system of the human brain: from environment to theory of mind. *Neuron*, *58*(3), 306–24. doi:10.1016/j.neuron.2008.04.017

Corrigan, N. M., Richards, T., Webb, S. J., Murias, M., Merkle, K., Kleinhans, N. M., ... Dawson, G. (2009). An investigation of the relationship between fmri and erp source localized measurements of brain activity during face processing. *Brain topography*, *22*(2), 83–96.

Credidio, H. F., Teixeira, E. N., Reis, S. D., Moreira, A. A., & Andrade Jr, J. S. (2012). Statistical patterns of visual search for hidden objects. *Scientific reports*, *2*.

Dale, A. M., Liu, A. K., Fischl, B. R., Buckner, R. L., Belliveau, J. W., Lewine, J. D., & Halgren, E. (2000, April). Dynamic statistical parametric mapping: combining

fMRI and MEG for high-resolution imaging of cortical activity. *Neuron*, *26*(1), 55–67.

Dale, A., Fischl, B., & Sereno, M. I. (1999). Cortical surface-based analysis: i. segmentation and surface reconstruction. *NeuroImage*, *9*(2), 179–194.

Damasio, A. R. & Damasio, H. (1983). The anatomic basis of pure alexia. *Neurology*, *33*(12), 1573–1573.

Dammers, J., Schiek, M., Boers, F., Silex, C., Zvyagintsev, M., Pietrzyk, U., & Mathiak, K. (2008). Integration of amplitude and phase statistics for complete artifact removal in independent components of neuromagnetic recordings. *Transactions on Biomedical Engineering*, *55*(10), 2353–2362. doi:10.1109/TBME.2008.926677

Davis, M. (1996). Interpersonal reactivity index. *Empathy: A Social Psychological Approach*, 55–6.

De Munck, J., Goncalves, S., Huijboom, L., Kuijer, J., Pouwels, P., Heethaar, R., & Lopes da Silva, F. (2007). The hemodynamic response of the alpha rhythm: an eeg/fmri study. *Neuroimage*, *35*(3), 1142–1151.

Decety, J. & Lamm, C. (2007). The role of the right temporoparietal junction in social interaction: how low-level computational processes contribute to meta-cognition. *The Neuroscientist: a review journal bringing neurobiology, neurology and psychiatry*, *13*(6), 580.

Deffke, I., Sander, T., Heidenreich, J., Sommer, W., Curio, G., Trahms, L., & Lueschow, A. (2007). Meg/eeg sources of the 170-ms response to faces are co-localized in the fusiform gyrus. *NeuroImage*, *35*(4), 1495–501. doi:10.1016/j.neuroimage.2007.01.034

Desikan, R. S., Ségonne, F., Fischl, B., Quinn, B. T., Dickerson, B. C., Blacker, D., ... Killiany, R. J. (2006). An automated labeling system for subdividing the human cerebral cortex on mri scans into gyral based regions of interest. *NeuroImage*, *31*(3), 968–980. doi:DOI:10.1016/j.neuroimage.2006.01.021

Dobel, C., Junghofer, M., & Gruber, T. (2011). The role of gamma-band activity in the representation of faces: reduced activity in the fusiform face area in congenital prosopagnosia. *PloS one*, *NA*(5), e19550. doi:10.1371/journal.pone.0019550

Dumas, G., Chavez, M., Nadel, J., & Martinerie, J. (2012). Anatomical connectivity influences both intra-and inter-brain synchronizations. *PloS one*, *7*(5), e36414.

Dumas, G., de Guzman, G. C., Tognoli, E., & Kelso, J. S. (2014). The human dynamic clamp as a paradigm for social interaction. *Proceedings of the National Academy of Sciences*, *111*(35), E3726–E3734.

Dumas, T., Dubal, S., Attal, Y., Chupin, M., Jouvent, R., Morel, S., & George, N. (2013). Meg evidence for dynamic amygdala modulations by gaze and facial emotions. *PloS one*, *8*(9), e74145. doi:10.1371/journal.pone.0074145

Dunbar, R. (1993). Coevolution of neocortex size, group size and language in humans. *Behavioral and Brain Sciences*, *16*(4), 681–735.

Emery, N. J. (2000). The eyes have it: the neuroethology, function and evolution of social gaze. *Neuroscience {&} Biobehavioral Reviews*, *24*, 581–604.

Emery, N. & Lorincz, E. (1997). Gaze following and joint attention in rhesus monkeys (Macaca mulatta). *Journal of comparative psychology*, *111*(3), 286.

Engemann, D. A., Bzdok, D., Eickhoff, S. B., Vogeley, K., & Schilbach, L. (2012). Games people play—toward an enactive view of cooperation in social neuroscience. *Frontiers in Human Neuroscience*, *6*.

Farroni, T., Csibra, G., & Simion, F. (2002). Eye contact detection in humans from birth. *Proceedings of the National Academy of Sciences*, *99*(14), 9602–9605.

Feller, W. (1945). The fundamental limit theorems in probability. *Bulletin of the American Mathematical Society*, *51*(11), 800–832.

Field, T. M. (1981). Infant gaze aversion and heart rate during face-to-face interactions. *Infant behavior and development*, *4*, 307–315.

Fischl, B., Liu, A., & Dale, A. M. (2001, January). Automated manifold surgery: constructing geometrically accurate and topologically correct models of the human cerebral cortex. *IEEE Medical Imaging*, *20*(1), 70–80.

Fischl, B., Salat, D. H., Busa, E., Albert, M., Dieterich, M., Haselgrove, C., ... Dale, A. M. (2002). Whole brain segmentation: automated labeling of neuroanatomical structures in the human brain. *Neuron*, *33*, 341–355.

Fischl, B., Sereno, M., & Dale, A. (1999a). Cortical surface-based analysis ii: inflation, flattening, and a surface-based coordinate system. *NeuroImage*, *9*, 195–207.

Fischl, B. & Dale, A. M. (2000). Measuring the thickness of the human cerebral cortex from magnetic resonance images. *Proceedings of the National Academy of Sciences of the United States of America*, *97*(20), 11050–11055. eprint: http://www.pnas.org/content/97/20/11050.full.pdf+html

Fischl, B., Sereno, M. I., & Dale, A. (1999b). Cortical surface-based analysis: ii: inflation, flattening, and a surface-based coordinate system. *NeuroImage*, *9*(2), 195–207.

Fischl, B., Sereno, M. I., Tootell, R. B., & Dale, A. M. (1999). High-resolution intersubject averaging and a coordinate system for the cortical surface. *Human Brain Mapping*, *8*(4), 272–284. doi:10.1002/(SICI)1097-0193(1999)8:4<272::AID-HBM10>3.0.CO;2-4

Fischl, B., Van Der Kouwe, A., Destrieux, C., Halgren, E., Ségonne, F., Salat, D. H., ... Dale, A. (2004a). Automatically parcellating the human cerebral cortex. *Cerebral Cortex*, *14*(1), 11–22.

Fischl, B., van der Kouwe, A., Destrieux, C., Halgren, E., Ségonne, F., Salat, D. H., ... Dale, A. M. (2004b). Automatically Parcellating the Human Cerebral Cortex. *Cerebral Cortex*, *14*(1), 11–22. doi:10.1093/cercor/bhg087. eprint: http://cercor.oxfordjournals.org/content/14/1/11.full.pdf+html

Fiske, S. T. & Taylor, S. E. (2013). *Social cognition: from brains to culture*. Sage.

Freiwald, W. A., Tsao, D. Y., & Livingstone, M. S. (2009). A face feature space in the macaque temporal lobe. *Nature neuroscience*, *12*(9), 1187–1196.

Frith, C. D. & Frith, U. (2008). Implicit and explicit processes in social cognition. *Neuron*, *60*(3), 503–510.

Furl, N., van Rijsbergen, N., Treves, A., Friston, K., & Dolan, R. (2007). Experience-dependent coding of facial expression in superior temporal sulcus. *Proceedings of the National Academy of Sciences of the United States of America*, *NA*(33), 13485–9. doi:10.1073/pnas.0702548104

Galletti, C., Battaglini, P., & Fattori, P. (1995). Eye position influence on the parieto-occipital area po (v6) of the macaque monkey. *European Journal of Neuroscience*, *7*(12), 2486–2501.

Galletti, C., Kutz, D. F., Gamberini, M., Breveglieri, R., & Fattori, P. (2003). Role of the medial parieto-occipital cortex in the control of reaching and grasping movements. *Experimental Brain Research*, *153*(2), 158–170.

George, N., Driver, J., & Dolan, R. J. (2001). Seen gaze-direction modulates fusiform activity and its coupling with other brain areas during face processing. *Neuroimage*, *13*(6), 1102–1112.

Gräfenhain, M., Behne, T., Carpenter, M., & Tomasello, M. (2009). Young children's understanding of joint commitments. *Developmental Psychology*, *45*(5), 1430.

Grafton, S. T., Arbib, M. A., Fadiga, L., & Rizzolatti, G. (1996). Localization of grasp representations in humans by positron emission tomography. *Experimental Brain Research*, *112*(1), 103–111.

Gramfort, A., Luessi, M., Larson, E., Engemann, D., Strohmeier, D., Brodbeck, C., ... Hämäläinen, M. (2013a). MEG and EEG data analysis with MNE-Python. *Frontiers in Neuroscience*, *7*(267). doi:10.3389/fnins.2013.00267

Gramfort, A., Luessi, M., Larson, E., Engemann, D., Strohmeier, D., Brodbeck, C., ... Hämäläinen, M. (2014). MNE software for processing MEG and EEG data. *Neuroimage*, *86*, 446–460. doi:http://dx.doi.org/10.1016/j.neuroimage.2013.10.027

Gramfort, A., Strohmeier, D., Haueisen, J., Hämäläinen, M., & Kowalski, M. (2013b). Time-frequency mixed-norm estimates: sparse M/EEG imaging with non-stationary source activations. *Neuroimage*, *70*, 410–422.

Gramfort, A., Kowalski, M., & Hämäläinen, M. (2012, March). Mixed-norm estimates for the M/EEG inverse problem using accelerated gradient methods. *Physics in Medicine and Biology*, *57*(7), 1937–1961.

Graziano, M. (2014). Speculations on the evolution of awareness. *Cognitive Neuroscience, Journal of*, *26*(6), 1300–1304.

Graziano, M. S. & Kastner, S. (2011). Awareness as a perceptual model of attention. *Cognitive neuroscience*, *2*(2), 125–127.

Grezes, J. (1998). Top down effect of strategy on the perception of human biological motion: a pet investigation. *Cognitive Neuropsychology*, *15*(6-8), 553–582.

Gross, J., Baillet, S., Barnes, G., Henson, R., Hillebrand, A., Jensen, O., ... Schoffelen, J. (2013, January). Good practice for conducting and reporting meg research. *NeuroImage*, *65*(15), 349–363.

Gross, J., Kujala, J., Hämäläinen, M., & Timmermann, L. (2001, January). Dynamic imaging of coherent sources: studying neural interactions in the human brain. *Proceedings of the National Academy of Sciences*, *98*(2), 694–699.

Hadjikhani, N., Kveraga, K., Naik, P., & Ahlfors, S. (2009). Early (m170) activation of face-specific cortex by face-like objects. *Neuroreport*, *20*(4), 403–7. doi:10.1097/WNR.0b013e328325a8e1

Haith, M. M., Bergman, T., & Moore, M. J. (1977). Eye contact and face scanning in early infancy. *Science*, *198*(4319), 853–855.

Halgren, E., Raij, T., Marinkovic, K., Jousmaki, V., & Hari, R. (2000). Cognitive response profile of the human fusiform face area as determined by meg. *Cerebral cortex (New York, N.Y. : 1991)*, *10*(1), 69–81. doi:None

Halko, N., Martinsson, P.-G., & Tropp, J. A. (2011). Finding structure with randomness: probabilistic algorithms for constructing approximate matrix decompositions. *SIAM review*, *53*(2), 217–288.

Hämäläinen, M. S. & Sarvas, J. (1989, February). Realistic conductivity geometry model of the human head for interpretation of neuromagnetic data. *IEEE Transactions on Biomedical Engineering*, *36*(2), 165–171.

Hämäläinen, M., Hari, R., Ilmoniemi, R. J., & Knuutila, J. (1993). Magnetoencephalography — theory, instrumentation, and applications to noninvasive studies of the working human brain. *Reviews of Modern Physics*, *65*(2), 413–506.

Hämäläinen, M. & Ilmoniemi, R. (1994, January). Interpreting magnetic fields of the brain: minimum norm estimates. *Med Biol Eng Comput*, *32*(1), 35–42.

Hämäläinen, M., Lin, F.-H., & Mosher, J. C. (2010). Anatomically and Functionally Constrained Minimum-Norm-Estimates. In P. C. Hansen, M. L. Klingelbach, & R. Salmelin (Eds.), (Chap. 8, pp. 186–215). Oxford University Press.

Hamilton, A. F. d. C. & Grafton, S. T. (2006). Goal representation in human anterior intraparietal sulcus. *The Journal of Neuroscience*, *26*(4), 1133–1137.

Han, X., Jovicich, J., Salat, D., van der Kouwe, A., Quinn, B., Czanner, S., ... Fischl, B. (2006). Reliability of MRI-derived measurements of human cerebral cortical thickness: The effects of field strength, scanner upgrade and manufacturer. *NeuroImage*, *32*(1), 180–194.

Hansen, P., Kringelbach, M., & Salmelin, R. (2010). *Meg: an introduction to methods*. Oxford university press.

Hanslmayr, S., Klimesch, W., Sauseng, P., Gruber, W., Doppelmayr, M., Freunberger, R., ... Birbaumer, N. (2007). Alpha phase reset contributes to the generation of erps. *Cerebral Cortex*, *17*(1), 1–8.

Hari, R. & Kujala, M. V. (2009). Brain basis of human social interaction: from concepts to brain imaging. *Physiological reviews*, *89*(2), 453–479.

Hasselmo, M., Rolls, E., Baylis, G., & Nalwa, V. (1989). Object-centered encoding by face-selective neurons in the cortex in the superior temporal sulcus of the monkey. *Experimental Brain Research*, *75*(2), 417–429.

Haxby, J. V., Hoffman, E. A., & Gobbini, M. I. (2000). The distributed human neural system for face perception. *Trends in Cognitive Sciences*, *4*(6), 223–233.

Haxby, J., A., H. E., & Gobbini, M. I. (2002). Human neural systems for face recognition and social communication. *Biological Psychiatry*, *51*(59-67).

Haxby, J. V., Horwitz, B., Ungerleider, L. G., Maisog, J. M., Pietrini, P., & Grady, C. L. (1994). The functional organization of human extrastriate cortex: a pet-rcbf study of selective attention to faces and locations. *Journal of Neuroscience*, *14*(11), 6336–6353.

Hein, G. & Knight, R. T. (2008). Superior Temporal Sulcus—It's My Area: Or Is It? *Journal of Cognitive Neuroscience*, *20*(12), 2125–2136.

Henson, R., Mattout, J., Phillips, C., & Friston, K. (2009). Selecting forward models for meg source-reconstruction using model-evidence. *NeuroImage*, *46*(1), 168–76. doi:10.1016/j.neuroimage.2009.01.062

Henson, R., Mattout, J., Singh, K., Barnes, G., Hillebrand, A., & Friston, K. (2007). Population-level inferences for distributed meg source localization under multiple constraints: application to face-evoked fields. *NeuroImage*, *38*(3), 422–38. doi:10.1016/j.neuroimage.2007.07.026

Henson, R. & Rugg, M. (2003). Neural response suppression, haemodynamic repetition effects, and behavioural priming. *Neuropsychologia*, *41*(3), 263–270.

Heywood, C., Cowey, A., & Rolls, E. (1992). The role of theface-cell'area in the discrimination and recognition of faces by monkeys [and discussion]. *Philosophical Transactions of the Royal Society of London. Series B: Biological Sciences*, *335*(1273), 31–38.

Hoerl, A. E. & Kennard, R. W. (1970). Ridge regression: biased estimation for nonorthogonal problems. *Technometrics*, *12*(1), 55–67.

Hoffman, K. L., Gothard, K. M., Schmid, M. C., & Logothetis, N. K. (2007). Facial-expression and gaze-selective responses in the monkey amygdala. *Current Biology*, *17*(9), 766–772.

Holm, S. (1979). A simple sequentially rejective multiple test procedure. *Scandinavian journal of statistics*, *6*(2), 65–70.

Holmes, A. P., Blair, R., Watson, G., & Ford, I. (1996). Nonparametric analysis of statistic images from functional mapping experiments. *Journal of Cerebral Blood Flow & Metabolism*, *16*(1), 7–22.

Hommel, B. (2011). The Simon effect as tool and heuristic. *ACTPSY*.

Humphrey, N. K. (1976). The social function of intellect. *Growing points in ethology*, 303–317.

Hyvärinen, A., Karhunen, J., & Oja, E. (2004). *Independent component analysis*. John Wiley & Sons.

Ikeda, H., Leyba, L., Bartolo, A., Wang, Y., & Okada, Y. C. (2002). Synchronized spikes of thalamocortical axonal terminals and cortical neurons are detectable outside the pig brain with meg. *Journal of neurophysiology*, *87*(1), 626–630.

Itier, R., Herdman, A., George, N., Cheyne, D., & Taylor, M. (2006). Inversion and contrast-reversal effects on face processing assessed by meg. *Brain research*, *NA*(1), 108–20. doi:10.1016/j.brainres.2006.07.072

Itier, R. J. & Taylor, M. J. (2004). Source analysis of the n170 to faces and objects. *Neuroreport*, *15*(8), 1261–1265.

Jabbi, M., Kohn, P., Nash, T., Ianni, A., Coutlee, C., Holroyd, T., ... Berman, K. (2014). Convergent bold and beta-band activity in superior temporal sulcus and frontolimbic circuitry underpins human emotion cognition. *Cerebral cortex (New York, N.Y. : 1991)*. doi:10.1093/cercor/bht427

Japee, S., Crocker, L., Carver, F., Pessoa, L., & Ungerleider, L. (2009). Individual differences in valence modulation of face-selective m170 response. *Emotion (Washington, D.C.) 9*(1), 59–69. doi:10.1037/a0014487

Jovicich, J., Czanner, S., Greve, D., Haley, E., van der Kouwe, A., Gollub, R., ... Dale, A. (2006). Reliability in multi-site structural mri studies: effects of gradient non-linearity correction on phantom and human data. *NeuroImage*, *30*(2), 436–443. doi:DOI:10.1016/j.neuroimage.2005.09.046

Kano, F. & Tomonaga, M. (2010). Face scanning in chimpanzees and humans: continuity and discontinuity. *Animal Behaviour*, *79*(1), 227–235.

Kawasaki, H., Tsuchiya, N., Kovach, C. K., Nourski, K. V., Oya, H., Howard, M. A., & Adolphs, R. (2012). Processing of facial emotion in the human fusiform gyrus. *Journal of cognitive neuroscience*, *24*(6), 1358–1370.

Kelly, Y. T., Webb, T. W., Meier, J. D., Arcaro, M. J., & Graziano, M. S. (2014). Attributing awareness to oneself and to others. *Proceedings of the National Academy of Sciences*, *111*(13), 5012–5017.

Keysers, C., Wicker, B., Gazzola, V., Anton, J.-L., Fogassi, L., & Gallese, V. (2004, April). A touching sight: SII/PV activation during the observation and experience of touch. *Neuron*, *42*(2), 335–46.

Khan, S., Gramfort, A., Shetty, N., Kitzbichler, M., Ganesan, S., Moran, J., ... Kenet, T. (2013). Local and long-range functional connectivity is reduced in concert in autism spectrum disorders. *Proceedings of the National Academy of Sciences of the United States of America*, *110*(8), 3107–12. doi:10.1073/pnas.1214533110

Kilner, J. M., Kiebel, S. J., & Friston, K. J. (2005). Applications of random field theory to electrophysiology. *Neuroscience letters*, *374*(3), 174–178.

Kobayashi, H. & Kohshima, S. (1997). Morphological uniqueness of human eyes and its adaptive meaning. *Nature*, *387*, 767–768.

Köymen, B., Lieven, E., Engemann, D. A., Rakoczy, H., Warneken, F., & Tomasello, M. (2014). Children's norm enforcement in their interactions with peers. *Child development*, *85*(3), 1108–1122.

Kuzmanovic, B., Georgescu, A., Eickhoff, S., Shah, N., Bente, G., Fink, G., & Vogeley, K. (2009). Duration matters: Dissociating neural correlates of detection and evaluation of social gaze. *NeuroImage*, *46*, 1154–1163.

Lachat, F., Farroni, T., & George, N. (2012). Watch out! magnetoencephalographic evidence for early modulation of attention orienting by fearful gaze cueing. *PloS one*, *7*(11), e50499. doi:10.1371/journal.pone.0050499

Larson, E. & Lee, A. K. C. (2012, September). The cortical dynamics underlying effective switching of auditory spatial attention. *NeuroImage*. PMID: 22974974. doi:10.1016/j.neuroimage.2012.09.006

Ledoit, O. & Wolf, M. (2004). A well-conditioned estimator for large-dimensional covariance matrices. *Journal of Multivariate Analysis*, *88*(2), 365–411. doi:http://dx.doi.org/10.1016/S0047-259X(03)00096-4

Lewis, S., Thoma, R. J., Lanoue, M. D., Miller, G. A., Heller, W., Edgar, C., ... Paulson, K., et al. (2003). Visual processing of facial affect. *Neuroreport*, *14*(14), 1841–1845.

Libet, B., Gleason, C. A., Wright, E. W., & Pearl, D. K. (1983). Time of conscious intention to act in relation to onset of cerebral activity (readiness-potential) the unconscious initiation of a freely voluntary act. *Brain*, *106*(3), 623–642.

Lieberman, M. D. (2006, September). Neural bases of situational context effects on social perception. *Social Cognitive and Affective Neuroscience*, *1*(2), 73–74. doi:10.1093/scan/nsl015

Lin, F. H., Witzel, T., Ahlfors, S. P., Stufflebeam, S. M., Belliveau, J. W., & Hamalainen, M. S. (2006). Assessing and improving the spatial accuracy in MEG source localization by depth-weighted minimum-norm estimates. *Neuroimage*, *31*(1), 160–71.

Lin, F., Belliveau, J., Dale, A., & Hamalainen, M. (2006). Distributed current estimates using cortical orientation constraints. *Human brain mapping*, *27*(1), 1–13. doi:10.1002/hbm.20155

Lin, F.-H., Witzel, T., Hämäläinen, M. S., Dale, A. M., Belliveau, J. W., & Stufflebeam, S. M. (2004). Spectral spatiotemporal imaging of cortical oscillations and interactions in the human brain. *Neuroimage*, *23*(2), 582–595.

Linkenkaer-Hansen, K., Palva, J., Sams, M., Hietanen, J., Aronen, H., & Ilmoniemi, R. (1998). Face-selective processing in human extrastriate cortex around 120 ms after stimulus onset revealed by magneto- and electroencephalography. *Neuroscience letters*, (3), 147–50.

Litvak, V., Mattout, J., Kiebel, S., Phillips, C., Henson, R., Kilner, J., ... Friston, K. (2011). Eeg and meg data analysis in spm8. *Computational Intelligence and Neuroscience*, *2011*. doi:10.1155/2011/852961

Liu, J., Harris, A., & Kanwisher, N. (2002). Stages of processing in face perception: an meg study. *Nature neuroscience*, *5*(9), 910–6. doi:10.1038/nn909

Liu, L. & Ioannides, A. (2006). Spatiotemporal dynamics and connectivity pattern differences between centrally and peripherally presented faces. *NeuroImage*, *31*(4), 1726–40. doi:10.1016/j.neuroimage.2006.02.009

Llinás, R. R. (1988). The intrinsic electrophysiological properties of mammalian neurons: insights into central nervous system function. *Science*, *242*(4886), 1654–1664.

Logothetis, N. K. (2008). What we can do and what we cannot do with fmri. *Nature*, *453*(7197), 869–878.

Logothetis, N. K., Pauls, J., Augath, M., Trinath, T., & Oeltermann, A. (2001). Neurophysiological investigation of the basis of the fmri signal. *Nature*, *412*(6843), 150–157.

Lu, Q., Jiang, H., Bi, K., Liu, C., & Yao, Z. (2014). Discriminative analysis with a limited number of meg trials in depression. *Journal of affective disorders*, *167*, 207–214. doi:10.1016/j.jad.2014.06.007

Lu, Q., Wang, Y., Luo, G., Li, H., & Yao, Z. (2013). Dynamic connectivity laterality of the amygdala under negative stimulus in depression: a meg study. *Neuroscience letters*, *547*, 42–7. doi:10.1016/j.neulet.2013.05.002

Macaluso, E. & Patria, F. (2007). Spatial re-orienting of visual attention along the horizontal or the vertical axis. *Experimental brain research*, *180*(1), 23–34.

Macaluso, E., Frith, C. D., & Driver, J. (2000). Modulation of human visual cortex by crossmodal spatial attention. *Science*, *289*(5482), 1206–1208.

Makeig, S., Westerfield, M., Jung, T.-P., Enghoff, S., Townsend, J., Courchesne, E., & Sejnowski, T. (2002). Dynamic brain sources of visual evoked responses. *Science*, *295*(5555), 690–694.

Maris, E. & Oostenveld, R. (2007, August). Nonparametric statistical testing of EEG- and MEG-data. *J Neurosci Methods*, *164*(1), 177?90. doi:10.1016/j.jneumeth.2007.03.024

Mars, R. B., Sallet, J., Neubert, F.-X., & Rushworth, M. F. (2013). Connectivity profiles reveal the relationship between brain areas for social cognition in human and monkey temporoparietal cortex. *Proceedings of the National Academy of Sciences*, *110*(26), 10806–10811.

Marsh, K. L., Richardson, M. J., & Schmidt, R. C. (2009, April). Social Connection Through Joint Action and Interpersonal Coordination. *Topics in Cognitive Science*, *1*(2), 320–339. doi:10.1111/j.1756-8765.2009.01022.x

Martinsson, P.-G., Rokhlin, V., & Tygert, M. (2011). A randomized algorithm for the decomposition of matrices. *Applied and Computational Harmonic Analysis*, *30*(1), 47–68. doi:http://dx.doi.org/10.1016/j.acha.2010.02.003

Mason, M. F., Tatkow, E. P., & Macrae, C. N. (2005, March). The look of love: gaze shifts and person perception. *Psychological science*, *16*(3), 236–9. doi:10.1111/j.0956-7976.2005.00809.x

Mazaheri, A. & Jensen, O. (2008). Asymmetric amplitude modulations of brain oscillations generate slow evoked responses. *The Journal of Neuroscience*, *28*(31), 7781–7787.

Mazaheri, A. & Jensen, O. (2010). Rhythmic pulsing: linking ongoing brain activity with evoked responses. *Frontiers in human neuroscience*, *4*.

McCall, C., Blascovich, J., Young, A., & Persky, S. (2009). Proxemic behaviors as predictors of aggression towards black (but not white) males in an immersive virtual environment. *Social Influence*, *4*(2), 138–154.

McPeek, R. M. & Keller, E. L. (2002). Superior colliculus activity related to concurrent processing of saccade goals in a visual search task. *Journal of Neurophysiology*, *87*(4), 1805–1815.

Meeren, H., de Gelder, B., Ahlfors, S., Hamalainen, M., & Hadjikhani, N. (2013). Different cortical dynamics in face and body perception: an meg study. *PloS one*, *NA*(9), e71408. doi:10.1371/journal.pone.0071408

Minka, T. P. (2000). Automatic choice of dimensionality for PCA. In *Nips* (Vol. 13, pp. 598–604).

Mnatsakanian, E. V. & Tarkka, I. M. (2004). Familiar-face recognition and comparison: source analysis of scalp-recorded event-related potentials. *Clinical neurophysiology*, *115*(4), 880–886.

Monroe, J., Griffin, M., Pinkham, A., Loughead, J., Gur, R., Roberts, T., & Christopher Edgar, J. (2013). The fusiform response to faces: explicit versus implicit processing of emotion. *Human brain mapping*, *34*(1), 1–11. doi:10.1002/hbm.21406

Morel, S., Ponz, A., Mercier, M., Vuilleumier, P., & George, N. (2009). Eeg-meg evidence for early differential repetition effects for fearful, happy and neutral faces. *Brain research*, *1254*(NA), 84–98. doi:10.1016/j.brainres.2008.11.079

Mosher, J. C., Leahy, R. M., & Lewis, P. S. (1999). Eeg and meg: forward solutions for inverse methods. *IEEE Trans Biomed Eng*, *46*(3), 245–59. 0018-9294 (Print) Journal Article.

Mosher, J. & Leahy, R. (1998, January). Recursive MUSIC: A framework for EEG and MEG source localization. *Biomedical Engineering, IEEE Transactions on*, *45*(11), 1342–1354.

Mundy, P., Sigman, M., & Kasari, C. (1990). A longitudinal study of joint attention and language development in autistic children. *Journal of Autism and developmental Disorders*, *20*(1), 115–128.

Murakami, S., Hirose, A., & Okada, Y. C. (2003). Contribution of ionic currents to magnetoencephalography (meg) and electroencephalography (eeg) signals generated by guinea-pig ca3 slices. *The Journal of physiology*, *553*(3), 975–985.

Murakami, S. & Okada, Y. (2006). Contributions of principal neocortical neurons to magnetoencephalography and electroencephalography signals. *The Journal of physiology*, *575*(3), 925–936.

Muthukumaraswamy, S. D. & Singh, K. D. (2009). Functional decoupling of bold and gamma-band amplitudes in human primary visual cortex. *Human brain mapping*, *30*(7), 2000–2007.

Myowa-Yamakoshi, M., Tomonaga, M., Tanaka, M., & Matsuzawa, T. (2003). Preference for human direct gaze in infant chimpanzees (pan troglodytes). *Cognition*, *89*(2), 113–124.

Nagarajan, S. S., Attias, H. T., Hild, K. E., & Sekihara, K. (2007). A probabilistic algorithm for robust interference suppression in bioelectromagnetic sensor data. *Statistics in medicine*, *26*(21), 3886–3910.

Nakamura, K., Chung, H., Graziano, M., & Gross, C. (1999). Dynamic representation of eye position in the parieto-occipital sulcus. *Journal of Neurophysiology*, *81*(5), 2374–2385.

Nichols, K. & Champness, B. (1971). Eye gaze and the gsr. *Journal of Experimental Social Psychology*, *7*(6), 623–626.

Nichols, T. E. & Holmes, A. P. (2002, January). Nonparametric permutation tests for functional neuroimaging: a primer with examples. *Human Brain Mapping*, *15*(1), 1–25. PMID: 11747097.

Nummenmaa, L. & Calder, A. J. (2009). Neural mechanisms of social attention. *Trends in cognitive sciences*, *13*(3), 135–143.

Nummenmaa, L., Glerean, E., Viinikainen, M., Jääskeläinen, I. P., Hari, R., & Sams, M. (2012). Emotions promote social interaction by synchronizing brain activity across individuals. *Proceedings of the National Academy of Sciences*, *109*(24), 9599–9604.

Nummenmaa, L., Passamonti, L., Rowe, J., Engell, A. D., & Calder, A. J. (2010). Connectivity analysis reveals a cortical network for eye gaze perception. *Cerebral Cortex*, *20*(1780-1787).

Ochiai, T., Grimault, S., Scavarda, D., Roch, G., Hori, T., Riviere, D., ... Régis, J. (2004). Sulcal pattern and morphology of the superior temporal sulcus. *Neuroimage*, *22*(2), 706–719.

Okazaki, Y., Abrahamyan, A., Stevens, C., & Ioannides, A. (2008). The timing of face selectivity and attentional modulation in visual processing. *Neuroscience*, *152*(4), 1130–1144.

Orban, G. A., Van Essen, D., & Vanduffel, W. (2004). Comparative mapping of higher visual areas in monkeys and humans. *Trends in cognitive sciences*, *8*(7), 315–324.

Pantazis, D., Nichols, T. E., Baillet, S., & Leahy, R. M. (2005, March). A comparison of random field theory and permutation methods for the statistical analysis of MEG data. *NeuroImage*, *25*(2), 383–394. doi:10.1016/j.neuroimage.2004.09.040

Pascual-Marqui, R. (2002). Standardized low resolution brain electromagnetic tomography (sLORETA): technical details. *Methods Find. Exp. Clin. Pharmacology*, *24*(500), 5–12.

Pedregosa, F., Varoquaux, G., Gramfort, A., Michel, V., Thirion, B., Grisel, O., ... Duchesnay, E. (2011). Scikit-learn: machine learning in Python. *Journal of Machine Learning Research*, *12*, 2825–2830.

Peirce, J. W. (2007). Psychopy—psychophysics software in python. *Journal of neuroscience methods*, *162*(1), 8–13.

Peirce, J. W. (2008). Generating stimuli for neuroscience using psychopy. *Frontiers in neuroinformatics*, *2*.

Perani, D., Cappa, S., Bettinardi, V., Bressi, S., Gorno-Tempini, M., Matarrese, M., & Fazio, F. (1995). Different neural systems for the recognition of animals and man-made tools. *Neuroreport*, *6*(12), 1637–1641.

Perrett, D., Smith, P., Potter, D., Mistlin, A., Head, A., Milner, A., & Jeeves, M. (1985). Visual cells in the temporal cortex sensitive to face view and gaze direction. *Proceedings of the Royal society of London. Series B. Biological sciences*, *223*(1232), 293–317.

Perry, G. & Singh, K. (2014). Localizing evoked and induced responses to faces using magnetoencephalography. *The European journal of neuroscience*, *39*(9), 1517–27. doi:10.1111/ejn.12520

Pfeiffer, U. J., Schilbach, L., Timmermans, B., Kuzmanovic, B., Georgescu, A. L., Bente, G., & Vogeley, K. (2014). Why we interact: on the functional role of the striatum in the subjective experience of social interaction. *NeuroImage*, *101*, 124–137. doi:http://dx.doi.org/10.1016/j.neuroimage.2014.06.061

Pfeiffer, U. J., Timmermans, B., Bente, G., Vogeley, K., & Schilbach, L. (2011, November). A Non-Verbal Turing Test: Differentiating Mind from Machine in Gaze-Based Social Interaction. *PloS one*, *6*(11), e27591.

Pfeiffer, U. J., Vogeley, K., & Schilbach, L. (2013). From gaze cueing to dual eye-tracking: novel approaches to investigate the neural correlates of gaze in social interaction. *Neuroscience & Biobehavioral Reviews*, *37*(10), 2516–2528.

Pfeiffer, U., Schilbach, L., Jording, M., Timmermans, B., Bente, G., & Vogeley, K. (2012). Eyes on the Mind: Investigating the Influence of Gaze Dynamics on the Perception of Others in Real-Time Social Interaction. *Frontiers in Psychology*, *3*.

Pizzagalli, D., Lehmann, D., Hendrick, A., Regard, M., Pascual-Marqui, R., & Davidson, R. (2002). Affective judgments of faces modulate early activity (approximately 160 ms) within the fusiform gyri. *NeuroImage*, *NA*(3 Pt 1), 663–77. doi:None

Posner, M. I. (1980). Orienting of attention. *Quarterly journal of experimental psychology*, *32*(1), 3–25.

Pourtois, G., Spinelli, L., Seeck, M., & Vuilleumier, P. (2010). Modulation of face processing by emotional expression and gaze direction during intracranial recordings in right fusiform cortex. *Journal of cognitive neuroscience*, *22*(9), 2086–2107.

Premack, D. & Woodruff, G. (1978). Does the chimpanzee have a theory of mind? *Behavioral and brain sciences*, *1*(04), 515–526.

R Core Team. (2014). *R: a language and environment for statistical computing*. R Foundation for Statistical Computing. Vienna, Austria.

Rakoczy, H. (2008). Taking fiction seriously: Young children understand the normative structure of joint pretence games. *Developmental Psychology*, *44*(4), 1195.

Ramoser, H., Müller-Gerking, J., & Pfurtscheller, G. (1998). Optimal spatial filtering of single trial EEG during imagined hand movement. *IEEE Trans. Rehab. Eng*, *8*, 441–446.

Redcay, E. & Carlson, T. (2014). Rapid neural discrimination of communicative gestures. *Social cognitive and affective neuroscience*, (NA), NA. doi:10.1093/scan/nsu089

Redcay, E., Dodell-Feder, D., Pearrow, M. J., Mavros, P. L., Kleiner, M., Gabrieli, J. D. E., & Saxe, R. (2010). Live face-to-face interaction during fMRI: a new tool for social cognitive neuroscience. *NeuroImage*, *50*(4), 1639–1647.

Reddy, V. (2003). On being the object of attention: implications for self–other consciousness. *Trends in cognitive sciences*, *7*(9), 397–402.

Reuter, M., Rosas, H. D., & Fischl, B. (2010). Highly accurate inverse consistent registration: a robust approach. *NeuroImage*, *53*(4), 1181–1196. doi:10.1016/j.neuroimage.2010.07.020

Reuter, M., Schmansky, N. J., Rosas, H. D., & Fischl, B. (2012). Within-subject template estimation for unbiased longitudinal image analysis. *NeuroImage*, *61*(4), 1402–1418. doi:10.1016/j.neuroimage.2012.02.084

Ribary, U., Ioannides, A., Singh, K., Hasson, R., Bolton, J., Lado, F., ... Llinas, R. (1991). Magnetic field tomography of coherent thalamocortical 40-hz oscillations in humans. *Proceedings of the National Academy of Sciences*, *88*(24), 11037–11041.

Ridgway, G. R., Litvak, V., Flandin, G., Friston, K. J., & Penny, W. D. (2012, February). The problem of low variance voxels in statistical parametric mapping; a new hat avoids a "haircut". *NeuroImage*, *59*(3), 2131–2141. doi:10.1016/j.neuroimage.2011.10.027

Rilling, J. K., Sanfey, A. G., Aronson, J. A., Nystrom, L. E., & Cohen, J. D. (2004). The neural correlates of theory of mind within interpersonal interactions. *Neuroimage*, *22*(4), 1694–1703.

Rizzolatti, G., Fadiga, L., Matelli, M., Bettinardi, V., Paulesu, E., Perani, D., & Fazio, F. (1996). Localization of grasp representations in humans by pet: 1. observation versus execution. *Experimental brain research*, *111*(2), 246–252.

Said, C. P., Moore, C. D., Engell, A. D., Todorov, A., & Haxby, J. V. (2010). Distributed representations of dynamic facial expressions in the superior temporal sulcus. *Journal of vision*, *10*(5), 11.

Saito, D. N., Tanabe, H. C., Izuma, K., Hayashi, M. J., Morito, Y., Komeda, H., ... Fujibayashi, Y., et al. (2010). "stay tuned": inter-individual neural synchronization during mutual gaze and joint attention. *Frontiers in integrative neuroscience*, *4*.

Salustri, C. & Kronberg, E. (2004). Language-related brain activity revealed by independent component analysis. *Clinical neurophysiology : official journal of the International Federation of Clinical Neurophysiology*, (2), 385–95. doi:None

Sams, M., Hietanen, J., Hari, R., Ilmoniemi, R., & Lounasmaa, O. (1997). Face-specific responses from the human inferior occipito-temporal cortex. *Neuroscience*, *NA*(1), 49–55. doi:None

Sato, N., Nakamura, K., Nakamura, A., Sugiura, M., Ito, K., Fukuda, H., & Kawashima, R. (1999). Different time course between scene processing and face processing: a meg study. *Neuroreport*, *NA*(17), 3633–7. doi:None

Sato, N. & Nakamura, K. (2001). Detection of directed gaze in rhesus monkeys (macaca mulatta). *Journal of Comparative Psychology*, *115*(2), 115.

Sato, W., Kochiyama, T., Uono, S., & Yoshikawa, S. (2008). Time course of superior temporal sulcus activity in response to eye gaze: a combined fmri and meg study. *Social cognitive and affective neuroscience*, *NA*(3), 224–32. doi:10.1093/scan/nsn016

Sauseng, P., Klimesch, W., Gruber, W., Hanslmayr, S., Freunberger, R., & Doppelmayr, M. (2007). Are event-related potential components generated by phase resetting of brain oscillations? a critical discussion. *Neuroscience*, *146*(4), 1435–1444.

Saxe, R. (2006). Uniquely human social cognition. *Current opinion in neurobiology*, *16*(2), 235–239.

Saxe, R. & Kanwisher, N. (2003). People thinking about thinking people. The role of the temporo-parietal junction in "theory of mind". *NeuroImage*.

Schilbach, L., Eickhoff, S. B., Cieslik, E., Shah, N. J., Fink, G. R., & Vogeley, K. (2010). Eyes on me: an fMRI study of the effects of social gaze on action control. *Social Cognitive and Affective Neuroscience*.

Schilbach, L. (2010, June). A second-person approach to other minds. *Nature reviews. Neuroscience*, *11*(6), 449. doi:10.1038/nrn2805-c1

Schilbach, L., Timmermans, B., Reddy, V., Costall, A., Bente, G., Schlicht, T., & Vogeley, K. (2013). Toward a second-person neuroscience. *Behavioral and Brain Sciences*, *36*(04), 393–414.

Schilbach, L., Wilms, M., Eickhoff, S. B., Romanzetti, S., Tepest, R., Bente, G., ... Vogeley, K. (2009). Minds Made for Sharing: Initiating Joint Attention Recruits Reward-related Neurocircuitry. *J Cogn Neurosci*, *3*(1), 37–50.

Schweinberger, S. R., Pickering, E. C., Jentzsch, I., Burton, A. M., & Kaufmann, J. M. (2002). Event-related brain potential evidence for a response of inferior temporal cortex to familiar face repetitions. *Cognitive Brain Research*, *14*(3), 398–409.

Sebanz, N. & Frith, C. (2004). Beyond simulation? neural mechanisms for predicting the actions of others. *Nature neuroscience*, *7*(1), 5–6.

Segonne, F., Dale, A. M., Busa, E., Glessner, M., Salat, D., Hahn, H. K., & Fischl, B. (2004). A hybrid approach to the skull stripping problem in mri. *NeuroImage*, *22*(3), 1060–1075. doi:DOI:10.1016/j.neuroimage.2004.03.032

Segonne, F., Pacheco, J., & Fischl, B. (2007). Geometrically accurate topology-correction of cortical surfaces using nonseparating loops. *IEEE Trans Med Imaging*, *26*, 518–529.

Senju, A. & Johnson, M. H. (2009). The eye contact effect: mechanisms and development. *Trends in cognitive sciences*, *13*(3), 127–134.

Shepherd, S. V. (2010). Following gaze: gaze-following behavior as a window into social cognition. *Frontiers in integrative neuroscience*, *4*.

Shipp, S., Blanton, M., & Zeki, S. (1998). A visuo-somatomotor pathway through superior parietal cortex in the macaque monkey: cortical connections of areas v6 and v6a. *European Journal of Neuroscience*, *10*(10), 3171–3193.

Singh, K. D., Barnes, G. R., Hillebrand, A., Forde, E. M., & Williams, A. L. (2002). Task-related changes in cortical synchronization are spatially coincident with the hemodynamic response. *Neuroimage*, *16*(1), 103–114.

Sled, J., Zijdenbos, A., & Evans, A. (1998). A nonparametric method for automatic correction of intensity nonuniformity in mri data. *IEEE Trans Med Imaging*, *17*, 87–97.

Snyder, L., Batista, A., & Andersen, R. (1997). Coding of intention in the posterior parietal cortex. *Nature*, *386*(6621), 167–170.

Sperber, D., Wilson, D., & Ziran. (1986). Relevance: communication and cognition.

Stefanics, G., Hangya, B., Hernádi, I., Winkler, I., Lakatos, P., & Ulbert, I. (2010). Phase entrainment of human delta oscillations can mediate the effects of expectation on reaction speed. *The Journal of neuroscience*, *30*(41), 13578–13585.

Supek, S. & Aine, C. J. (Eds.). (2014). *From signals to dynamic cortical networks*. Springer Berlin / Heidelberg.

Susac, A., Ilmoniemi, R., Ranken, D., & Supek, S. (2011). Face activated neurodynamic cortical networks. *Medical & biological engineering & computing*, *NA*(5), 531–43. doi:10.1007/s11517-011-0740-4

Tallon-Baudry, C. & Bertrand, O. (1999). Oscillatory gamma activity in humans and its role in object representation. *Trends Cogn Sci*, *3*(4), 151–162. 1364-6613 Journal article.

Tanaka, E., Inui, K., Kida, T., & Kakigi, R. (2009). Common cortical responses evoked by appearance, disappearance and change of the human face. *BMC neuroscience*, *10*(1), 38. doi:10.1186/1471-2202-10-38

Tarantola, A. (1987). *Inverse problem theory: methods for data fitting and model parameter estimation*. Elsevier Science Pub. Co. Inc., New York, NY.

Taulu, S., Simola, J., & Kajola, M. (2005). Applications of the signal space separation method. *Signal Processing, IEEE Transactions on*, *53*(9), 3359–3372.

Taylor, M., Bayless, S., Mills, T., & Pang, E. (2011). Recognising upright and inverted faces: meg source localisation. *Brain research*, *NA*(NA), 167–74. doi:10.1016/j.brainres.2010.12.083

Taylor, M., George, N., & Ducorps, A. (2001). Magnetoencephalographic evidence of early processing of direction of gaze in humans. *Neuroscience letters*, *316*(3), 173–7.

Thierry, G., Pegna, A. J., Dodds, C., Roberts, M., Basan, S., & Downing, P. (2006). An event-related potential component sensitive to images of the human body. *Neuroimage*, *32*(2), 871–879.

Tikhonov, A. & Arsenin, V. Y. (1977). Solutions of ill-posed problems. *WH Winston, Washington, DC*, *330*.

Tipping, M. E. & Bishop, C. M. (1999). Probabilistic principal component analysis. *Journal of the Royal Statistical Society: Series B (Statistical Methodology)*, *61*(3), 611–622.

Tomasello, M. (1999). *The cultural origins of human cognition*. Harvard University Press Cambridge, MA.

Tomasello, M. (2008). *Origins of human communication*. The MIT Press.

Tomasello, M., Carpenter, M., Call, J., Behne, T., & Moll, H. (2005). Understanding and sharing intentions: The origins of cultural cognition. *Behavioral and Brain Sciences*, *28*(05), 675–691.

Tomasello, M., Call, J., & Hare, B. (2003). Chimpanzees understand psychological states–the question is which ones and to what extent. *Trends in cognitive sciences*, *7*(4), 153–156.

Tomasello, M., Hare, B., Lehmann, H., & Call, J. (2007). Reliance on head versus eyes in the gaze following of great apes and human infants: the cooperative eye hypothesis. *Journal of Human Evolution*, *52*(3), 314–320.

Tomonaga, M., Tanaka, M., Matsuzawa, T., Myowa-Yamakoshi, M., Kosugi, D., Mizuno, Y., ... Bard, K. A. (2004). Development of social cognition in infant chimpanzees (pan troglodytes): face recognition, smiling, gaze, and the lack of triadic interactions1. *Japanese Psychological Research*, *46*(3), 227–235.

Tsao, D. Y., Moeller, S., & Freiwald, W. A. (2008). Comparing face patch systems in macaques and humans. *Proceedings of the National Academy of Sciences*, *105*(49), 19514–19519.

Tsao, D. & Freiwald, W. (2003). Faces and objects in macaque cerebral cortex. *Nature ... 6*(9), 989–995.

Tsao, D., Freiwald, W., Tootell, R., & Livingstone, M. (2006). A cortical region consisting entirely of face-selective cells. *Science*, *311*(5761), 670–674.

Ulloa, J., Puce, A., Hugueville, L., & George, N. (2014). Sustained neural activity to gaze and emotion perception in dynamic social scenes. *Social cognitive and affective neuroscience*, *9*(3), 350–7. doi:10.1093/scan/nss141

Umilta, M. A., Kohler, E., Gallese, V., Fogassi, L., Fadiga, L., Keysers, C., & Rizzolatti, G. (2001). I know what you are doing: a neurophysiological study. *Neuron*, *31*(1), 155–165.

Uusitalo, M. & Ilmoniemi, R. (1997). Signal-space projection method for separating MEG or EEG into components. *Medical and Biological Engineering and Computing*, *35*(2), 135–140.

Uutela, K., Hämäläinen, M., & Somersalo, E. (1999). Visualization of magnetoencephalographic data using minimum current estimates. *Neuroimage*, *10*, 173–180.

Van Essen, D. C. (2005). A population-average, landmark-and surface-based (pals) atlas of human cerebral cortex. *Neuroimage*, *28*(3), 635–662.

Van Essen, D. C. & Dierker, D. L. (2007). Surface-based and probabilistic atlases of primate cerebral cortex. *Neuron*, *56*(2), 209–225.

Vanni, S., Revonsuo, A., & Hari, R. (1997). Modulation of the parieto-occipital alpha rhythm during object detection. *The Journal of Neuroscience*, *17*(18), 7141–7147.

Veen, B. V., Drongelen, W. V., Yuchtman, M., & Suzuki, A. (1997, January). Localization of brain electrical activity via linearly constrained minimum variance spatial filtering. *Biomedical Engineering, IEEE Transactions on*, *44*(9), 867–880.

Vogeley, K. & Bente, G. (2010). "Artificial humans": Psychology and neuroscience perspectives on embodiment and nonverbal communication. *Neural networks : the official journal of the International Neural Network Society*, *23*(8-9), 1077–90. doi:10.1016/j.neunet.2010.06.003

Völlm, B. A., Taylor, A. N., Richardson, P., Corcoran, R., Stirling, J., McKie, S., ... Elliott, R. (2006). Neuronal correlates of theory of mind and empathy: a functional magnetic resonance imaging study in a nonverbal task. *Neuroimage*, *29*(1), 90–98.

von Grünau, M. & Anston, C. (1995). The detection of gaze direction: a stare-in-the-crowd effect. *Perception*, *24*(11), 1297–1313.

von Helmholtz, H. (1853). ÜBER einige Gesetze der Verteilung elektischer Ströme in körperlichen Leitern, mit Anwendung auf die thierisch-elektrischen Versuche. *Ann.Phys.Chem. 89*, 211–333, 353–377.

Vuilleumier, P. & Pourtois, G. (2007, January). Distributed and interactive brain mechanisms during emotion face perception: evidence from functional neuroimaging. *Neuropsychologia*, *45*(1), 174–94. doi:10.1016/j.neuropsychologia.2006.06.003

Wang, Y., Newport, R., & Hamilton, A. (2011). Eye contact enhances mimicry of intransitive hand movements. *Biology letters*, *7*(1), 7–10.

Wang, Y., Ramsey, R., & De C Hamilton, A. F. (2011). The control of mimicry by eye contact is mediated by medial prefrontal cortex. *Journal of Neuroscience*, *31*(33), 12001–12010.

Warneken, F., Chen, F., & Tomasello, M. (2006). Cooperative activities in young children and chimpanzees. *Child Development*, *77*(3), 640–663.

Watanabe, S., Kakigi, R., Koyama, S., & Kirino, E. (1999). It takes longer to recognize the eyes than the whole face in humans. *Neuroreport*, *10*(10), 2193–2198.

Watanabe, S., Kakigi, R., Miki, K., & Puce, A. (2006). Human mt/v5 activity on viewing eye gaze changes in others: a magnetoencephalographic study. *Brain research*, *NA*(1), 152–60. doi:10.1016/j.brainres.2006.03.091

Watanabe, S., Kakigi, R., & Puce, A. (2003). The spatiotemporal dynamics of the face inversion effect: a magneto-and electro-encephalographic study. *Neuroscience*, *116*(3), 879–895.

Watson, R., Latinus, M., Charest, I., Crabbe, F., & Belin, P. (2014). People-selectivity, audiovisual integration and heteromodality in the superior temporal sulcus. *cortex*, *50*, 125–136.

Wimmer, H. & Perner, J. (1983). Beliefs about beliefs: representation and constraining function of wrong beliefs in young children's understanding of deception. *Cognition*, *13*(1), 103–128.

Wolpert, D. H. (1996). The lack of a priori distinctions between learning algorithms. *Neural computation*, *8*(7), 1341–1390.

Woolrich, M., Hunt, L., Groves, A., & Barnes, G. (2011a, August). MEG beamforming using Bayesian PCA for adaptive data covariance matrix regularization. *NeuroImage*, *57*(4), 1466–1479.

Woolrich, M., Hunt, L., Groves, A., & Barnes, G. (2011b). MEG beamforming using Bayesian PCA for adaptive data covariance matrix regularization. *Neuroimage*, *57*(4), 1466–1479.

Xu, Y., Liu, J., & Kanwisher, N. (2005). The m170 is selective for faces, not for expertise. *Neuropsychologia*, *NA*(4), 588–97. doi:10.1016/j.neuropsychologia.2004.07.016

Yoshida, W., Dolan, R. J., & Friston, K. J. (2008). Game Theory of Mind. *PLoS Computational Biology*, *4*(12), e1000254.

Yovel, G. & Freiwald, W. A. (2013). Face recognition systems in monkey and human: are they the same thing? *F1000prime reports*, *5*, 10.

Zumer, J. M., Attias, H. T., Sekihara, K., & Nagarajan, S. S. (2007). A probabilistic algorithm integrating source localization and noise suppression for MEG and EEG data. *Neuroimage*, *37*(1), 102–115.

Zumer, J. M., Attias, H. T., Sekihara, K., & Nagarajan, S. S. (2008). Probabilistic algorithms for MEG/EEG source reconstruction using temporal basis functions learned from data. *Neuroimage*, *41*(3), 924–940.